THE ANALYSIS OF BIOLOGICAL MOLECULES BY ELECTROSPRAY IONISATION FOURIER TRANSFORM ION CYCLOTRON RESONANCE (ESI-FTICR) MASS SPECTROMETRY

by

James Ian Wallace B.Sc.

A thesis submitted in fulfilment of the requirements for the degree of

PhD in Analytical Chemistry

University of Warwick

1999

Declaration

I hereby declare that this thesis is my own work and that , to the best of my knowledge and belief, it contains no material previously published or written by another person, nor material which has been accepted for the award of any other degree or diploma of a University or Institute of Higher Education, except where due acknowledgement is made in the text.

James Ian Wallace B.Sc.

Abbreviations

CID	Collision induced dissociation
FT-ICR	Fourier transform ion cyclotron resonance mass spectrometry
ICR	Ion cyclotron resonance
MS	Mass spectrometry
TOF	Time-of-flight
MALDI	Matrix assisted laser desorption ionisation
ESI	Electrospray ionisation
GGYR	Tetra-peptide Glycine-Glycine-Tyrosine-Arginine
KAA	N_{α},N_{ε}-diacetyl-Lysine-d-Alanine-d-Alanine
CaM	Calmodulin
MLCK	Myosin light chain kinase
TCA	Tri-chloro acetic acid
HPLC	High pressure liquid chromatography
SDS	Sodium dodecyl-sulfate
EGTA	Ethylene glycol-bis(β-aminoethyl ether)-N,N,N',N'-tetra acetic acid

Acknowledgments

I would like to thank the following people for their help and advice, without which this thesis would not have been possible.

- My supervisor Professor Peter J Derrick for all his help and discussions.
- My colleagues Dr Daniel Lafitte, Dr Tessa Hill, Dr Helen Cooper, Mr Xidong Feng, Dr Albert Heck, Dr Jan Axelsson, Dr Tracey Shield (nee Rafferty), Mr Gary Shield and Dr Jackie Jarvis (nee Moseley), who have contributed both to my knowledge and the content of this thesis. Thanks everyone.
- Smith Kline-Beecham for their financial support throughout the course of my studies, with special thanks to Dr David Bell, Dr Andy Organ and Andrew West for their help.
- My fellow PhD students and friends, Andy "Jack" Smith, Alan Millar, Paul Myatt, Chris Edwards, Anne-Mette Hoberg, Mark Barrow, Phil Green, Liam McDonnell, Andrew Bottril, Ben Thomas, Saj Bashir and Mark Woodward.
- Thanks Mum and Dad for your love, support and encouragement.
- Last but not least my partner Kerry for her unshakable faith that I would finish, her support and encouragement and for just being there.

INDEX

1.0 Introduction

The objective of this thesis was to investigate the facility of electrospray ionisation Fourier transform ion cyclotron resonance (ESI-FT-ICR) mass spectrometry for the analysis of biological molecules. To this end, two different proteins were investigated by various mass spectrometric methods designed to study aspects of the individual proteins structure, conformation and function. The proteins investigated included calmodulin, a Ca^{2+} mediated protein involved in a variety of cellular processes and papain, a cysteine protease. The interactions of these proteins with peptides representing segments of their target molecules were successfully studied, and conformational changes of calmodulin induced by Ca^{2+} ions were also determined. These latter studies, involved both gas and solution phase hydrogen/deuterium exchange, and metal ion "titration" to investigate conformation changes of calmodulin. Conformational changes induced by Ca^{2+} ions were successfully monitored, with the superior resolution of FT-ICR mass spectrometry lending itself to unequivocal assignment of mass spectrometrically observed species. This has previously been difficult if not impossible with other types of mass spectrometric instrumentation such as electrospray ionisation combined with triple quadrupole instrumentation.

The first mass spectrometric evidence for calmodulin: peptide complexes without Ca^{2+} ions is also presented, the peptide in question being RS20. It was assumed before these experiments that four Ca^{2+} ions were necessary to activate calmodulin before any such interactions could occur. This evidence casts doubts on the established mechanism of calmodulin function, but it may also indicate that a second mechanism for calmodulin mediated cellular functions exists. A mechanism that could be much faster than that currently recognised.

1.1 The History of Mass Spectrometry

The foundations of modern mass spectrometry were laid by Joseph John Thomson (1856-1940), the physicist who discovered and demonstrated the existence of the electron and measured its mass-to-charge ratio (1897). He was also responsible for separating an ion beam into its constituent parts, each with their own specific *e/m* ratio. These latter experiments can be considered the basis of modern mass spectrometry.[1]

The experiments consisted of passing a narrow positive ion beam between two parallel brass plates. A magnetic and an electric field were applied orthogonal to these plates, thus deflecting the ion beam. The beam produced a spot at a particular point on a photographic plate, the position of which depended on the charge q and mass m of the particle. Thomson showed that if the ions were travelling in the x direction and the magnetic and electric fields were applied in the y direction, ions would be deflected in the yz plane forming a parabola. The shape of this parabola in the yz plane is described by the equation (1).

$$z^2 = k\frac{q}{m}y \qquad (1)$$

k is a constant depending on the dimensions of the apparatus used and the strengths of the fields. The length of the parabola was found to be indicative of the energy spread of the ions in the ion beam, with the ions of highest energy hitting the photographic plate closest to the origin.

Thomson also discovered that low pressures were needed, as the penetrative power of the positive ion beam was much lower than that for cathode rays. Initial experiments at relatively high pressures produced parabolas corresponding to the charged hydrogen and

helium atoms and the hydrogen molecule. Only at significantly lower pressures did the heavier atoms become observable. By examining the photographic plates Thomson realised (from faint lines joining the parabolas to the origin) that positive ions could be converted to neutrals by collision processes and vice versa. The dimensions of the parabolas also allowed the assignment of the atomic and/or molecular masses of the constituents of the analyte gas. Sensitivity could be improved by increasing the exposure time. Thomson realised, therefore, that this technique had distinct advantages over existing spectroscopy methodology, especially for the analysis of unknown gaseous samples.

Mass spectrometry as a field of study originated in the 1930's from work pioneered by the likes of Aston, Bainbridge, Dempster and Nier. It was Francis William Aston (1877-1945), who during this period, developed the forerunner of all modern double focusing-instruments. His instrument took Thomson's original idea, but put the electric and magnetic fields in series (the electric field first). Thus by varying the construction of the instrument it was possible to ensure that positive rays with the same *e/m* ratio but different velocities could be focused at exactly the same point. With this instrument Aston managed to prove conclusively that the stable elements had isotopes; radioactive elements had already been established to be isotopically diverse.[2]

Whereas Aston made use of a discharge bulb for the production of ions, Dempster in the Ryerson laboratory at the University of Chicago was using aluminium phosphate on a heated thin platinum strip and bombardment by electrons to produce positive ions. He accelerated the low-energy ions with an electric field, separated them in a 180° homogenous magnetic field and detected them with a quadrant electrometer. With this apparatus he identified $^{23}Na^{+}$ and $^{39}K^{+}$. An improved electron bombardment ion source

later allowed Dempster to report the abundances of ^{24}Mg, ^{25}Mg, ^{26}Mg and ^{39}K and ^{40}K. The elements Pt and Ir were successfully identified by Dempster in 1935.

A moving particle will have momentum, kinetic energy and velocity. The selection of one or more of these properties is the basis of all mass spectrometers. For example, a typical energy selector is a radial electric field, and a momentum selector would be a homogenous magnetic field. The relationships are expressed in the equations below:

$$mv = Bzer \qquad (2)$$

Magnetic-Sector Equations

$$zeV = \frac{mv^2}{2} \qquad (3)$$

Combining (2) and (3) where z is the number of charges on the ion, m is the mass of the ion, V is the accelerating potential, v is the velocity of the ion, B is the magnetic field strength and r is the radius of curvature through the magnetic field, gives the standard mass spectrometer equation.

$$\frac{m}{z} = \frac{B^2 r^2 e}{2V} \qquad (4)$$

Equation (4) thus shows that varying either B or V will allow ions of different m/z to be separated. In practice the exponential magnet scan is most commonly used, since it has the advantage over scanning V that it does not change the focus of the ion beam.

The equation for the case of the electric sector takes the form below:

$$\frac{mv^2}{R} = ezE \qquad (5) \quad \text{Electric-Sector Equation}$$

where E is the electrostatic field strength and R is the circular path that the ion takes such that the centrifugal force acting on it is balanced by the electrostatic force.

Dempster made use of the relationship in Eqn. 4 for his instrument, while Bainbridge used a velocity selector combined with a 180° magnetic field in his instrument[3]. The velocity selector in this case consisted of crossed electric and magnetic fields. Using this instrument Bainbridge made one of the first precise measurements of the masses of hydrogen and deuterium. Velocity selectors were used by several other workers in the field including Smythe and Mattauch at the California Institute of Technology. [2]

One of the most significant developments in mass spectrometry was the double focusing magnetic-sector analyser. In 1929 Bartky and Dempster provided the theory behind such an instrument consisting of a 90° and a 180° electric and magnetic sector respectively.[4] A double-focusing mass spectrometer allowed ions of the same mass but different translational energy to be focused at the same point, a feat impossible for existing instruments of the time and allowed greater resolution than was previously available. In the period between 1929 and 1951 a great many developments with this type of instrument were achieved. In 1951 Nier and Johnson developed and constructed a double-focusing instrument consisting of a 90° electric and a 60° magnetic sector. To this day such an instrument is said to be of a Nier-Johnson geometry; such instruments are still used for high-resolution organic mass spectrometry. So called reverse-geometry double focusing mass spectrometers are also common since the order of the sectors is not critical. A diagram of a Nier-Johnson instrument is shown below:

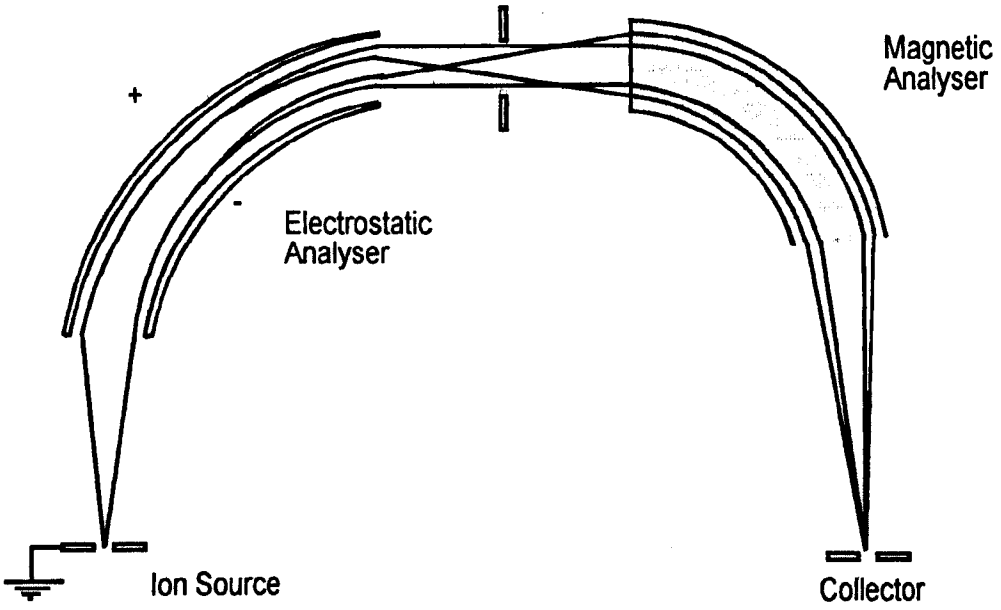

Figure 1 : Schematic diagram of a double-focusing sector instrument of Nier-Johnson geometry.

Other instruments were designed and built between 1929 and 1950, which did not rely on magnetic and electric sectors. These included the time-of-flight (TOF) analyser, the quadrupole and the Omegatron, the basis of the modern Fourier transform ion cyclotron resonance mass spectrometer (FT-ICR MS).

Time-of-flight (TOF) was suggested by Stephens in 1946[5] and an instrument was first built by Cameron and Eggers in 1948.[6] The first commercial instrument was marketed by the Bendix Corporation and was based on work carried out by Wiley and Mclaren in 1955. The advantages of TOF were the ability to observe alterations of reaction rates, and the speed at which spectra could be acquired.

The quadrupole mass filter was developed by Paul et al in 1958[7] and according to Paul had three main uses. These were as a filter for single ions, as a scanning device for producing a mass spectrum and as a device for selecting ions. The quadrupole has become

a significant part of mass spectrometric instrumentation. A basic quadrupole mass spectrometer is shown below.

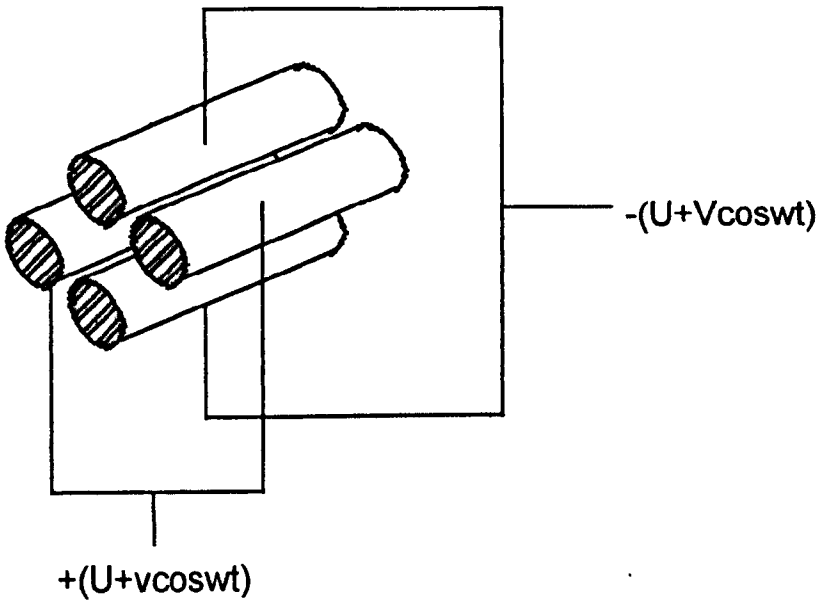

Figure 2 : A schematic of a quadrupole mass filter.

The Omegatron built in 1948 by Sommer et al[8, 9] was based on the velocity-selecting cyclotron principle. In this instrument the ever expanding orbits of resonant ions passed through a slit to an electron multiplier where the ions were detected; the instrument was mainly used for the detection of light ions. This apparatus was adapted and improved by Smith in his mass synchrometer. This instrument was originally used as a super-velocity selector, but became the most precise method for the determination of nuclidic masses due to the correlation between the mass of the ion and the precisely known frequency used to accelerate them.

Over the 45 years since this introduction, ICR mass spectrometry has been steadily improved until today it is one of the most sensitive and accurate techniques available for the determination of ion mass. The modern ICR mass spectrometer as we know it today has its roots in work by J. D. Baldeschwieler in collaboration with Peter Llewellyn in the

mid 1960's. This collaboration resulted in the Varian-Stanford ICR instrument that was the main scientific tool of this type during the late 1960's and early 1970's. These instruments were usually used for the investigation of gas-phase ion chemistry and some basic mass analysis.

It was not until 1974, however, when Fourier transform (FT) techniques were first applied to ICR[10-12] that the instrument became a viable analytical tool. FT increased speed, gave higher resolution and allowed more effective processing by computers of the data generated. During the late 1970's and early 1980's Nicolet and other companies started to manufacture the forerunners of todays FT mass spectrometers.

Throughout the 1980's until the present time FT-ICR instrumentation has been steadily developed. Cell design has been improved and virtually all ion sources have been successfully mounted outside the magnetic field. Thus source designs, that by necessity had to operate at atmospheric pressure, could now be used for FT-ICR with the aid of multiple stages of differential pumping. This allowed the electrospray ionisation source (ESI), an ion source of great use for the analysis of large fragile molecules such as proteins, to be used for the first time with FT-ICR and it is in this field that Fourier transform ion cyclotron resonance mass spectrometry (FT-ICR MS) excels.

1.2 Fourier Transform Ion Cyclotron Resonance : Instrumentation

The basic Fourier transform ion cyclotron resonance (FT-ICR) mass spectrometer can be considered to consist of four main parts. These are (i) the ion source (ii) the ion optics (iii) the magnet and (iv) the ion trap or cell. Each will be discussed in more detail in later sections, but for now a brief description of each part will suffice.

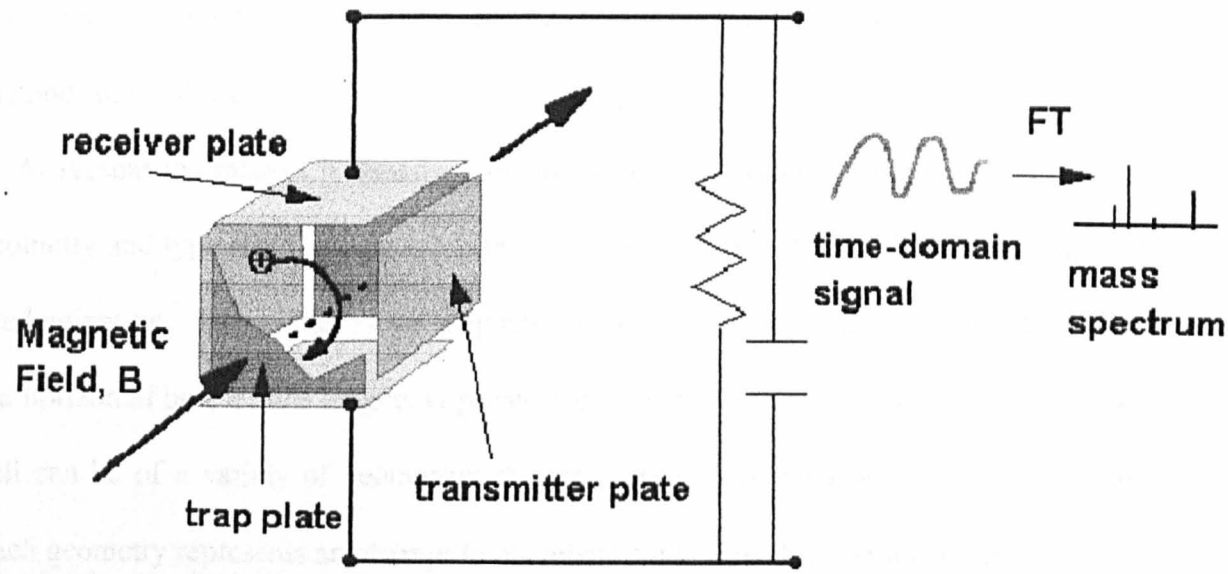

Figure 3 : Schematic of a cubic cell.

The ion source is, as its name implies, the region of the instrument where ions are formed. In mass spectrometry, and FT-ICR especially, ions are often produced in a region of higher pressure than that which is used for detection. It is usual for several stages of differential pumping to be employed to overcome this problem with cryo-, rotary and turbomolecular pumps being used for this purpose. Ion sources make use of a variety of phenomenon to ionise the sample molecules of interest. These include electrospray (ESI),

matrix-assisted laser desorption/ ionisation (MALDI), electron impact (EI) and chemical ionisation (CI). These are the most common ion sources for FT-ICR. Other sources have been successfully coupled with FT-ICR including fast atom bombardment (FAB) and atmospheric pressure chemical ionisation (APCI).

Ion sources were initially placed within the magnet field of FT-ICR mass spectrometers. However, as already mentioned with the advent of multiple stages of differential pumping and improvements in ion optics for the transfer of ions through the "magnetic mirror", ion sources were placed outside the magnetic field. This development allowed easier access to the ion sources for maintenance and sample introduction and also allowed new ionisation methods to be utilised.

At present the magnet is usually a supercooled superconducting magnet of solenoidal geometry and typically 1.0, 3.0, 4,7, 7.0, or 9.4 Tesla, with 3.0 and 4.7 Tesla instruments predominating. The greater is the magnetic field, the superior is the instrument. Within the horizontal bore of this magnet is placed the detection device: the ion trap or cell. The cell can be of a variety of geometries that have been developed over the last 45 years. Each geometry represents an attempt to overcome some flaw or imperfection pertaining to the detection of ions. For example, early cells were not ion traps at all but instead ions were allowed to drift from one end of the cell to the other as they were detected. McIver introduced the concept of the trapped ion cell for FT-ICR in 1970 [33] and this allowed greater detection efficiency and access to new ion-ion and ion-molecule reaction studies. As to the geometry of the cell, numerous shapes exist including cubic, rectangular (or elongated), hyperbolic, cylindrical and other trap designs such as shimmed cells (to reduce the radial component of the trapping field) and "infinity" cells. These developments will be discussed in detail in later sections. The most commonly used cell geometries are the

elongated and cylindrical cells since their dimensions (and advantages) are uniquely suited to FT-ICR mass spectrometry.

1.2.1 Cell

Penning type ion traps used in FT-ICR have been developed from Hipple *et al's* "Omegatron".[34] An ion trap that makes use of an axial magnetic field and a three dimensional (3-D) quadrupolar electrostatic trapping potential is known as a Penning trap, although it is now commonly used to refer to a trap using any electric potential in a magnetic field. Hipple *et al's* ion trap consisted of an arrangement of "guard rings" between two opposed plates. Ions within the volume of the trap were "excited" one at a time by the addition of a continuously applied uniform alternating electric field. The ions that were orbiting at a frequency in resonance with this field were excited to larger orbits, detected by a detector attached to one of the plates and measured by an electrometer. Thus the rf field was scanned across the entire mass range and the instrument detected a single m/z at a time. Modern instruments, with the introduction of Fourier Transform techniques, are capable of detecting the entire m/z range at once. This method of ion detection used by Hipple *et al* was however not very reliable, especially at the high pressures the "Omegatron" operated at. It thus found most use as a residual gas detector rather than a mass spectrometer.

Even with the obvious disadvantages of the "Omegatron", it still set several features of modern FT-ICR. These included the on-resonant excitation of ions to detectable radii, the confinement of ions within a magnetic field and 3-D axial quadrupolar electrostatic potential wells and the fact that m/z ratios are measured by determining the ICR frequencies of the individual ions.

Passing an electron beam through the cell along the magnetic field's central axis carried out ionisation in the "Omegatron". This electron beam was a significant problem in that its space charge shifted the measured ICR frequency with a resulting decrease in mass accuracy.

During the 1960's and 1970's further advances were made in the field. Most notably being Wobschall's introduction of an rf bridge circuit for detection in 1963 [20] , Llewellyn's ICR spectrometer with a cell split into three regions (ion source, ion analyser and ion collector) and McIver's trapped ion cell in 1970.[33] Llewellyn's design meant that the ionising electron beam no longer passed through the detection region and thus a greater mass accuracy was achieved, while McIver's trapped ion cell, as already mentioned, allowed ion generation, ion-molecule reactions and ion detection to be conducted in a single volume.

In McIver's design ionisation was attained by using an electron beam parallel to the magnetic field lines, but since the beam could be turned off before detection took place mass accuracy was retained. These instruments all scanned the magnetic field to measure the cyclotron frequency of individual ions; this was a relatively slow procedure. ICR as an analytical tool came into its own with the introduction of FT to the technique by Comisarow and Marshall in 1974.[10] This allowed the entire mass spectrum to be acquired within approximately a second, compared to half an hour by scanning the magnetic field. It also allowed greater magnetic field homogeneity since the magnet could now be fixed at a certain magnetic field strength. ICR performance was, therefore, no longer curtailed by the homogeneity of the magnet but was now greatly influenced by the shape of the electric field within the trap. Thus further developments in trap design have focused on creating the perfect field shape for ICR detection.

To continue this discussion, it must first be understood that ions in a static magnetic field are constrained only in the xy plane (if the magnetic field is taken to lie along the z-axis). An electric potential must be applied to two trap plates at either end of the cell to prevent z-axis ejection of ions from the cell. The electric field $\Phi(x,y,z)$ within an empty cell must therefore satisfy Laplace's equation.

$$\frac{\delta^2 V}{\delta x^2}+\frac{\delta^2 V}{\delta y^2}+\frac{\delta^2 V}{\delta z^2}=0 \qquad (6)$$

Thus the desired field must be produced from defined trap boundaries and voltages. This is essentially an inversion of the standard Laplace calculation; normally the potential generated within specified boundaries and voltages is calculated. This is quite a complex calculation but can be simplified if the required 3-D potential is projected onto a desired 2-D electrode surface. This allows the potential at any point in space to be calculated by applying the expected potential values to each point on the 2-D electrode surface. In theory calculating the desired electric potential within the cell is therefore relatively simple, but in practice producing such a potential is difficult. Two approaches exist for attaining the desired potential from a cell: (i) splitting a simple boundary shape into many different electrodes, to which a variety of voltages can be applied to produce the desired shape and (ii) limiting the number of electrodes and thus the potentials applied/ constructing electrodes that produce the desired field shape e.g. two hyperboloids of revolution can produce the desired potential shape.

Cells can be constructed in virtually any geometry when constructed of segmented electrodes to which potentials are applied. For example a cylindrical trap can be constructed from ring electrodes to produce a nearly perfect quadrupolar trapping

potential. The ring electrodes can either be all exactly the same size with different potentials that vary quadratically from the midplane, or the electrodes size can vary such that the potential increment from one electrode to another is constant. In either case the potential within the trap will approach a near perfect case as the number of electrodes approaches infinity.

The second approach using more complex electrodes to which a single potential is applied to generate the required potential is given by a cell constructed of a "ring" and two "end caps" of hyperboloid revolution. The finite size of these two electrodes unfortunately leads to distortion of the trapping potential. Correction can be obtained by adding electrodes for this purpose, increasing the distance between the end caps or by altering the angle between the end caps and the ring electrode.

These traps work perfectly until an azimuthal dipolar excitation field is applied to excite the ions to a detectable cyclotron radius and phase coherence. The quadrupolar trapping potential then changes shape due to the influence of this field. The combined field is now "saddle shaped" for a cubic trap with only the centre of the cell matching the pure quadrupolar trapping potential of the previous examples. As ions move from the centre of the cell/ trap, ion magnetron motion is no longer circular but for large magnetron radius approaches a "square" trajectory. The reduced cyclotron frequency (ω_-) also varies with the ion position inside the trap. The quadrupolar trapping potential produces an upper mass (or more accurately m/z) limit. It has a radial outward directed component so that there is a radially outward-directed force that counteracts the Lorentz force of the magnetic field. This causes frequency shifts and allows ions to lose magnetron potential energy by ion/ neutral collisions etc. which results in radial diffusion from the trap and the appearance of the upper mass limit mentioned.

Trap development has therefore tried either to increase the homogenous region in the centre of the cell or to remove the field lines due to the trapping potential from the detection area completely.

It can be shown for a cubic trap that ions of a critical mass-to-charge ratio (m/q) spiral outward and cannot be trapped.

$$\varpi_{+} \equiv \frac{\varpi_c}{2}\left[1+\sqrt{1-{(m/q)}/{(m/q)_{crit}}}\right] \tag{7}$$

where

$$(m/q)_{crit} = \frac{l^2 B^2}{4\alpha V_T} \tag{8}$$

ω_+ is the reduced cyclotron frequency and ω_c is the unperturbed cyclotron frequency.

This limit is due to the radial component of the trapping potential. Equation 3 shows that the upper mass-limit can be enlarged by increasing B and/ or l or by lowering V_T (the trap voltage) and/ or the trap geometric factor α (see table 1, section). B is fixed and V_T cannot be reduced too far otherwise the axial kinetic energy of the ions would mean they would escape from the cell. The only solution is, therefore, to alter the shape and/ or length of the cell to reduce α. Elongated cubic cells reduce the electric field near the centre of the cell by a factor of approximately 10^6 for a trap aspect of 6:1. (A perfect cube would have a trap aspect of 1:1.) A greater number of ions can also be trapped for an extended dynamic range.

Another design feature of ion traps that removes the radial component which causes ejection, is to remove trapping potential field lines from the main volume of the trap. Removing the potential altogether is not an option since the ions need to be constrained

within the trap during excitation and detection. Wang and Marshall [35] therefore introduced the screened ion trap. This design has grounded screens placed just inside the trapping plates that virtually eliminates the field within the trap. The region where ions can therefore be detected accurately and without problems associated with the radial component of the trapping field is greatly extended and so therefore is the amount of ions that the trap can hold at any one time. Typically a screened tetragonal trap of dimensions 6.35 x 5.08 x 5.08 cm^3 within a 3 Tesla magnet and with two 50 x 50 tungsten wire meshes exhibits a 100-fold smaller reduced cyclotron frequency ω_+ shift than that of a 5.08 cm^3 cubic trap.[35] Such a screened trap has also been used for trapping both positive and negative ions simultaneously.

Further developments in removing the radially outward directed electric field has involved the production of dynamic traps. These involve the use of an alternating voltage instead of the d.c. voltage normally used for trapping. If the alternating voltage is chosen carefully it is possible to produce a potential with zero time-average value.[36, 37] This can be modelled as a static electric "pseudopotential" and for ion-neutral collisions causes ions to be axialised, which therefore reduces radial diffusion.

Optimisation of the other two electric fields within an ion trap has also been examined. These electric fields originate from the dipolar excitation and detection events. In both cases shimming with guard rings/ wires or segmenting the relevant electrodes results in a more uniform distribution of the field lines in the trap.

It was noted by Huang et al [38] and Kofel et al [39] that axial motion was increased on application of the azimuthal (in a plane perpendicular to the magnetic field B_o) dipolar excitation electric field. It was Van der Hart *et al* [40] who showed that this was due to the non-uniformity of this electric field throughout the trap. Ion axial motion was found to be

excited by this applied field at frequencies other than $2\omega_z$ (ω_z is the trapping oscillation frequency), for example $2\omega_z \pm \omega_-$ and $\omega_+ \pm 2\omega_z$. This resulted in z-axis ejection of ions as their cyclotron radius was increased. Adding guard rings [41] increased the spatial uniformity of the field lines and thus considerably reduced z-axis ejection and improved the accuracy and reliability of relative peak heights in FT-ICR mass spectrometry over a broader mass range in relation to the unshimmed trap.

Improving dipolar detection in an ion trap has also been considered, in order to reduce side-bands and harmonics and improve signal strength. These are all factors affected by non-uniform fields within an ion trap. Problems exist for detection, since in reality only the centre of the trap has a spatially uniform electric field, and ions have to be excited to higher cyclotron radii for detection and thus away from this uniform region. Other ion motions are therefore instigated, which result especially with a large magnetron motion, in reduced-image current amplitude and as already mentioned side bands and harmonics. Again splitting the detection electrodes into segments allows uniform field lines to be obtained throughout more of the trap. Capacitively coupled segments are used in preference to resistively coupled segments to prevent loss of signal. However, capacitively coupled segmented electrodes do have drawbacks; they also result in a loss of detected signal. This can be overcome by detecting the signal using all six electrodes of the cubic ion trap.

It has been suggested that a so called "hypercube" [19] consisting of electrodes each of which is split into a 5 x 5 grid of smaller electrodes could be constructed. This would allow the potentials of these smaller electrodes to be adjusted to compensate for the non-uniformity of the field lines in the trap due to the trapping, detection and excitation electric fields. The complexity of such a trap may be too much to handle, since such a trap would

consist of 150 electrodes with each being available for individual adjustment.

1.2.2 Magnet and Field Strength

As previously mentioned the magnets used in FT-ICR usually take the form of a supercooled superconducting solenoidal geometry magnet and are available in a variety of field strengths. A number of factors in FT-ICR are directly dependent on field strength. The four performance factors which theoretically vary linearly with field strength, are mass resolving power, data acquisition speed, quadrupolar axialisation efficiency and the upper mass limit for peak coalescence. Of course other factors preventing a perfect linear relationship occuring for these parameters include inhomogenous electric and magnetic fields and collisions. Other performance factors which theoretically vary quadratically with magnetic field strength include the maximum number of ions that can be trapped inside the cell, the duration for which ions can be trapped within the cell, the maximum ion kinetic energy and the upper mass-limit arising from the trapping potential.

The strength of the magnetic field of the instrument therefore dictates the quality of the spectra obtained.

1.2.3 Sources and Transfer Optics

Most ionisation sources can be combined with FT-ICR to provide virtually unlimited areas of research. Nowadays electrospray ionisation (ESI) sources are most commonly combined with FT-ICR. The mechanism for ion formation by such a source will be discussed in a later section. Figure 4 below demonstrates a typical ESI source design. Sample molecules as wide ranging as proteins and synthetic polymers can be ionised by this method and little or no fragmentation is observed if the conditions are appropriate. The significant advantage for FT-ICR is that high-mass sample molecules are multiply charged and thus "folded" down to a lower position on the *m/z* scale.

Matrix-assisted laser desorption/ ionisation (MALDI) has been coupled to an FT-ICR both externally and internally. External sources utilised typically have a time-of-flight factor. The transfer optics used to pass the ions through the magnetic field are necessarily quite long (>1 metre), so that sources and pumps can be used outside the influence of strong magnetic fields. These long "flight tubes" and the fact that the cell is "gated" to allow ions to pass into it mean that timing is critical to achieve a good ion population within the cell. With polymer distributions, for example, it is necessary to realise that the "gate" time will affect the polymer distribution observed. This is one reason why it is usually found that MALDI is better suited to take place either within the cell or just outside. This internal ionisation presents complications for sample introduction since the source is within the confined magnet bore, but means that more ions are obtained within the cell and that there is no "time of flight" factor.

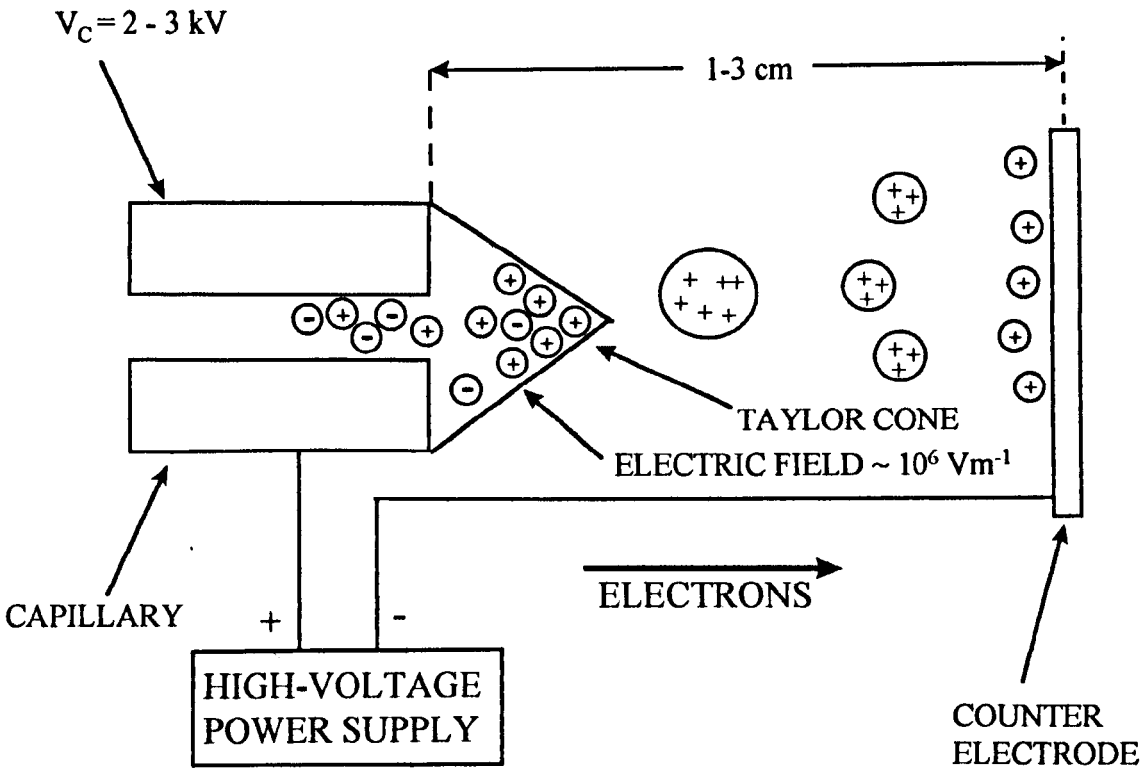

Figure 4 : A schematic of an ESI source.

The transfer of ions through the magnetic field into the cell has been achieved in a variety of ways that will be discussed below. Necessary complications that must be taken into account when designing such a system is the mirror-like effect of the magnetic field on the ions and the fact that the ion beam must be significantly reduced in velocity at the cell entrance to be trapped by the analyser cell. The latter factor is in direct contradiction to the fact that ions must have a notable axial velocity to pass through the "magnetic mirror".

Initial methods for the introduction of sample molecules through the magnetic field of an FT-ICR mass spectrometer used quadrupole rods to pass the ions through the "magnetic mirror". This was achieved by McIver et al [42] and the Finnigan corporation in the early 1980's, when they combined a Finnigan quadrupole instrument with a superconducting magnet. This allowed multiple stages of differential pumping to be used to reduce the

pressure between the source and the analyser. However, the oscillating quadrupolar fields within the quadrupole and the large magnetic field gradient combine to cause an acceleration of the ions any time a harmonic of the resonance frequency of the ion is reached. Thus the pathway of an ion within the quadrupole transfer rods will be extremely complex and the fact that a large velocity component perpendicular to the magnetic field is created by the rods means that the chance of the ion being reflected by the "magnetic mirror" is increased.

An alternative to the quadrupole ion guides is the use of electrostatic ion [67] and einzel lenses [43]. If a series of such lenses are used and the ions are confined to a narrow pathway along the magnetic axis, the magnet's effect on such a beam is limited to a spiral caused by cyclotron motion of the ion. An ion beam can be focused and decelerated in time for entrance into the cell, while keeping the ionisation source of choice clear of the troublesome magnetic field and the spatial constraints of the magnet bore. Such a system of lenses is used on the Bruker BioAPEX 94e FT-ICR mass spectrometer. Other methods of ion transfer from an external ion source include octupole ion guides [44].

1.3 Basics Of Fourier Transform Ion Cyclotron Resonance Mass Spectrometry

Fourier transform ion cyclotron resonance (FT-ICR) mass spectrometry is fundamentally different from other mass spectrometry techniques in that all the ions are excited and detected together in the detection region (the cell or trap). The ion masses can be assigned, due to the fact that each ion has a characteristic cyclotron frequency, which can be monitored in the detection region. This can be measured by monitoring the alternating electric field generated between a pair of detection plates as the ion first comes close to one and then the other. The resulting signal is complex and consists of information on the masses of all the ions present in the cell during the detection event. A mathematical procedure known as a Fourier transformation is used to "decode" the data into its separate parts and the resulting information is translated into the mass spectrum. The technique is non-destructive since the ions do not collide with a detector such as an electron multiplier, instead the ions, as has already been mentioned, induce an image current on a pair of detector plates.

The detector plates are an integral part of the cell, which is contained within the bore of a superconducting magnet and can be said to consist of three pairs of plates. These are the detection plates, the excitation plates and the trapping plates. The axis of the magnetic field is typically taken as the z-axis, and any ions entering or being formed in this region will automatically start to orbit this axis in the xy plane at a frequency characteristic of the ions m/z. It is this cyclotron frequency that is measured by the mass spectrometer since it is related to the ions mass by the equations below.

$$\varpi_c = \frac{qB_o}{m} \qquad \text{(SI Units)} \qquad (9)$$

where ω_c, q and m are the cyclotron frequency, the charge and the mass of the ion respectively and B_o is the strength of the magnetic field in Tesla.

The ions are constrained to move in a circular orbit around the z-axis due to the Lorentz force caused by the magnetic field. Without the influence of electric fields the ion will orbit in a perfectly circular orbit without any perturbations. Ion motion becomes more complicated when the influence of the electric fields, from the trapping plates for example, are taken into account. However, if for the moment the electric field are ignored, the balance of forces between the Lorentz force and the centrifugal force will give the following relationships.

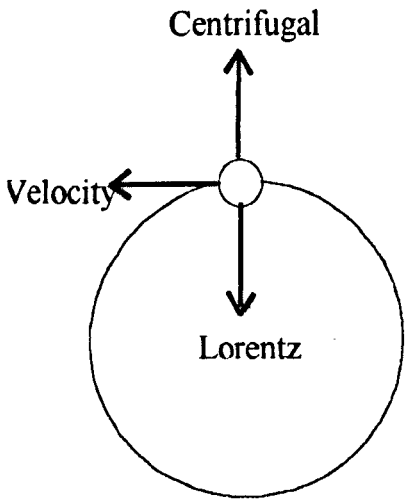

$$m\frac{d\mathbf{v}}{dt} = q\mathbf{v} \times \mathbf{B} \qquad (10)$$

where m, q and $\mathbf{v}$ are ionic mass, charge and velocity respectively. The vector cross product shows that the Lorentz force acts in a direction perpendicular to the magnetic field lines. If we let $v_{xy} = \sqrt{v_x^2 + v_y^2}$ in the xy plane, and note that angular acceleration is $\left|dv/dt\right| = v_{xy}^2/r$ then we can simplify equation (10) to the following expression.

$$qv_{xy}B = \frac{mv_{xy}^2}{r} \tag{11}$$

Thus by rearranging and simplifying this equation ($\omega = v_{xy}/r$) an expression equating the cyclotron frequency of an ion to the inverse mass to charge ratio is obtained.

$$\omega_c = \frac{qB_o}{m} \tag{12a}$$

$$\nu_c = \frac{\omega_c}{2\pi} = \frac{1.535611 \times 10^7 B_o}{(m/z)} \tag{12b}$$

where ν_c is in Hz, B_o is in Tesla, m is in Daltons and z is in multiples of elementary charge. Below is a graph that illustrates the range of ion cyclotron frequencies that singly charged ions of different m/z undergo at diverse magnetic field strengths.

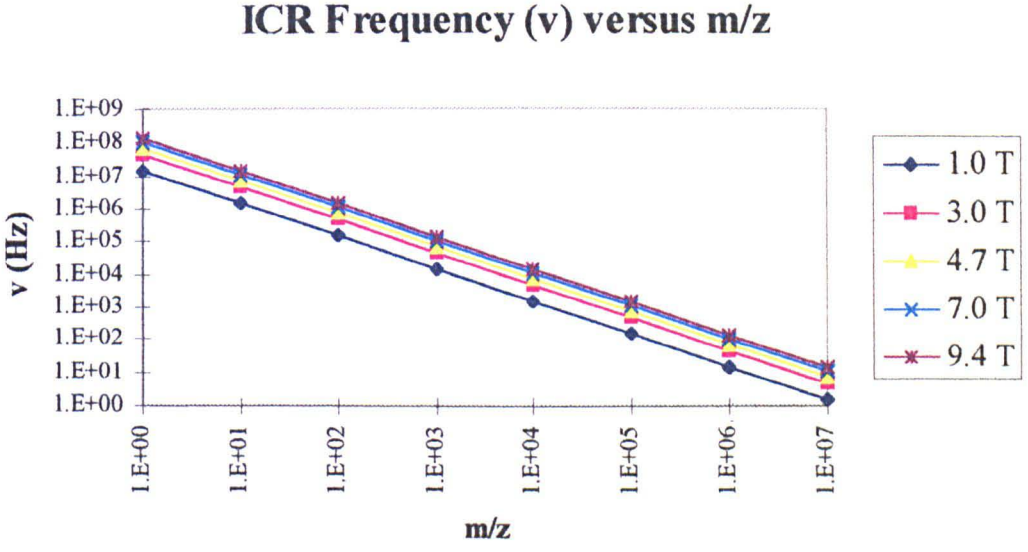

Figure 5: A plot of ICR frequency versus *m/z* ratio.

To be noted from equations 12a and 12b is the fact that all ions of the same mass to charge ratio have the same cyclotron frequency independent of their initial velocity.

By rearranging equation 11 an expression for the ion cyclotron orbital radius is attained.

$$r = \frac{1.036427 \times 10^{-8}(m/z)v_{xy}}{B_o} \tag{13}$$

since $mv_{xy}^2/2 \approx kT$, where r is in metres, m is in Daltons, T is in Kelvin and z is in multiples of elementary charge.

The velocity and translational energy of the excited ion can also be calculated by rearrangement of the previous equations.

$$v_{xy} = \frac{9.64853 \times 10^{7} B_o r}{(m/z)} \tag{14}$$

$$K.E. = \frac{4.824265 \times 10^{7} z^{2} B_{o}^{2} r^{2}}{m} \tag{15}$$

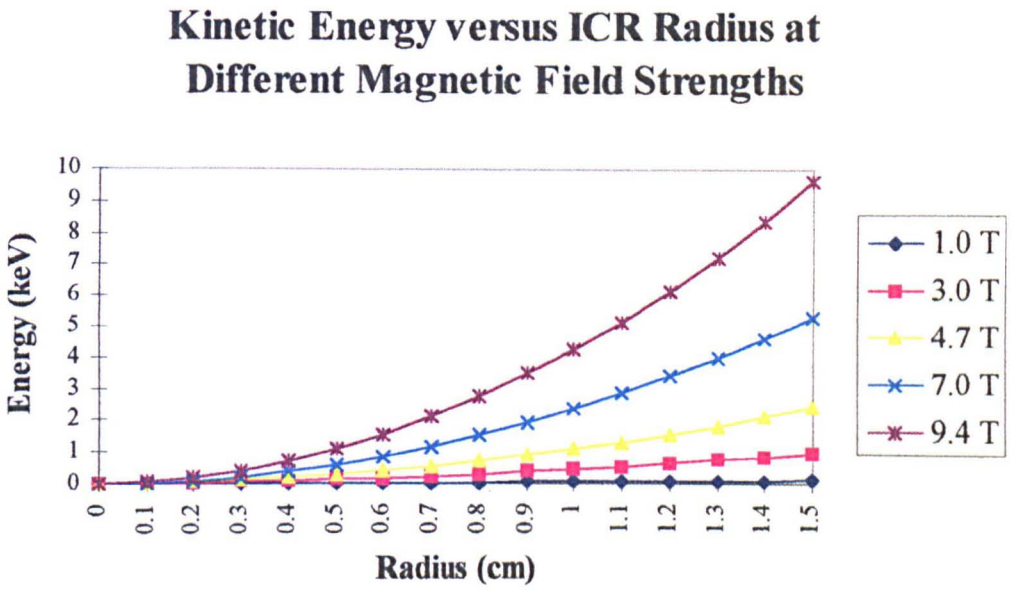

Figure 5: A plot of kinetic energy versus ICR orbital radius as a function of magnetic field strength.

The magnetic field only constrains the ions in the xy plane and two plates are placed at either end of the z-axis. These trapping plates have a small voltage applied to them, which forms a potential well, constraining the ions and preventing z-axis ejection. These trapping plates cause the ions to oscillate between them along the z-axis, and the frequency of such oscillations can be expressed as below. [66]

$$\nu_{z} = \frac{1}{2\pi}\sqrt{\frac{2qV_{trap}\alpha}{ma^{2}}} \tag{16a}$$

$$\nu_z = 2.21088 \times 10^3 \sqrt{\frac{zV_{trap}\alpha}{ma^2}} \qquad (16b)$$

However, Gauss' law of electrostatics states that an axially inward directed electric field has a radial outward component. This radial component opposes the magnetic force experienced by the ions, and therefore there is an effective reduction in the magnetic field strength on the ions.

The reduction in the magnetic field results in a reduced cyclotron frequency ω_+ and the introduction of two more modes of ion motion in the cell: magnetron and trapping motions. Magnetron motion (ω_-) is the slow precession of the centre of the cyclotron orbit in the xy plane while the trapping frequency as discussed above is represented by ω_z. These motions are all the result of the radial component of the trapping electric field, and numerous methods of reducing these fields within the cell area have been attempted, including screened cells and the infinity cell, discussed in section 1.7.

By again balancing the forces produced by the magnetic field, the electric field and centrifugal force, expressions can be obtained for ω_- and ω_+. This procedure will also assume a quadrupolar trapping potential. Thus;

$$Force = m\omega^2 r = qB_o\omega r - \frac{qV_{trap}\alpha}{a^2} r \qquad (17a)$$

or

$$\omega^2 - \frac{qB_o\omega}{m} + \frac{qV_{trap}\alpha}{ma^2} = 0 \qquad (17b)$$

where V_{trap} is the trap voltage along the z-axis (typically 1 Volt). The reduced cyclotron frequency ω_+ can then be stated as follows:

$$\omega_+ = \frac{\omega_c}{2} + \sqrt{\left(\frac{\omega_c}{2}\right)^2 - \frac{\omega_z^2}{2}} \qquad (18a)$$

and the magnetron motion ω_- as

$$\varpi_- = \frac{\omega_c}{2} - \sqrt{\left(\frac{\omega_c}{2}\right)^2 - \frac{\omega_z^2}{2}} \qquad (18b)$$

in which the trapping frequency is given by:

$$\omega_z = \sqrt{\frac{2qV_{trap}\alpha}{ma^2}} \qquad (18c)$$

and $\omega_c = \frac{qB_o}{m}$ is the unperturbed cyclotron frequency.

again V_{trap} is the trapping voltage, a the length of the cell (cubic or elongated geometry assumed) in metres and α is a factor of 1.3869 (see Table 1, section 1.3.3) for a cell of cubic geometry.

The displacement of the ion from the centre of the cell is periodic and is a combination of the reduced cyclotron and the magnetron frequencies.

$$\varpi_{radial} = \varpi_{+} - \varpi_{-} \tag{19}$$

Below is a diagram (Figure 6) that represents pictorially the motions that an ion undertakes.

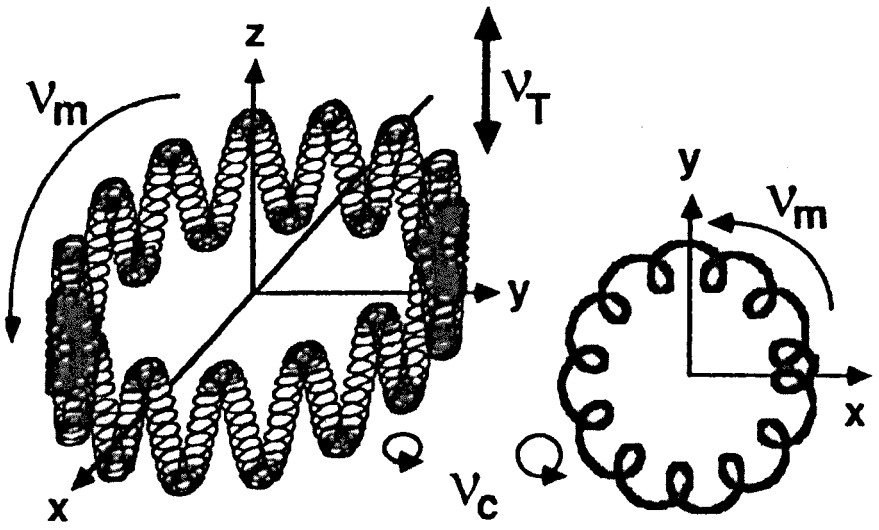

Figure 6: Schematic of ion motion in the FT-ICR ion trap kindly reproduced from Marshall *et al's* excellent primer [66]

It should be noted that the magnetron and trapping frequencies are usually much smaller than the cyclotron frequency of the ion and are generally not detected. Magnetron and trapping frequencies, if detected, are usually only seen as small side bands when the ion trap is misaligned with the magnet axis and/ or ion motional amplitudes approach the size of the trap. The diagram above accentuates the ion motion due to these effects for the purpose of clarity.

1.4 Excitation And Detection In Fourier Transform Ion Cyclotron Resonance Mass Spectrometry

1.4.1 Excitation

A useful signal cannot be obtained from an ion trap in FT-ICR without some form of excitation of the ions. Excitation not only excites the ions to a detectable radius, but also causes the ions to rotate in a coherent fashion.

For example, without excitation the ions will orbit at relatively small radii given by equation 13. They will rotate with all phases, so that there will be no coherent signal generated at the detection plates. Ions will be orbiting at the same frequency and radius, but because they have different phases the total signal will be effectively zero. For every ion there will be a corresponding ion orbiting exactly 180° out of phase. By exciting the ion with an on-resonant electric field, the ions orbital radius is increased and they will form a coherent ion packet. This allows an image current to be formed at the detection plates.

The excitation field is thus used for four reasons including those above. These are:

1) to accelerate ions to a higher orbital radius.
2) to form a coherent ion packet where all the ions are in phase.
3) to increase the ions kinetic energy for collision-induced dissociation and ion-molecule reaction experiments.
4) to eject the ions from the cell.

The simplest method of excitation is by making use of an azimuthal (in a plane perpendicular to the z-axis) dipolar single-frequency electric field. This field oscillates sinusoidally with time according to the vector relationship below.

$$\mathbf{E}(t) = E_o \cos \omega_c t \mathbf{j} \tag{20}$$

where ω_c is the unperturbed cyclotron frequency. **i, j** and **k** in these equations specify the direction of the vectors; since a vector quantity by definition has both magnitude and direction. If E_o is supposed to be produced by applying $+V_o$ and $-V_o$ volts to two infinitely long parallel plates with a separation of d meters then:

$$E_o = \frac{2V_o}{d} = \frac{V_{p-p}}{d} \tag{21}$$

V_{p-p} is the peak-to-peak voltage difference between the two plates. There are two solutions to this equation since the electric field may be split into two components $\mathbf{E}_L(t)$ and $\mathbf{E}_R(t)$, these are given below. The radio frequency (rf) electric field component rotating in the same direction as the ion and with the same frequency causes the ions orbital radius to be increased. The other component is so far off resonance that it has no effect on the ion.

$$\mathbf{E}_R(t) = \frac{E_o}{2} \cos \omega t \mathbf{j} + \frac{E_o}{2} \sin \omega t \mathbf{i} \tag{22a}$$

$$\mathbf{E}_L(t) = \frac{E_o}{2} \cos \omega t \mathbf{j} - \frac{E_o}{2} \sin \omega t \mathbf{i} \tag{22b}$$

where $\mathbf{E}(t) = \mathbf{E_L}(t) + \mathbf{E_R}(t)$. Thus $\mathbf{E_L}$ and $\mathbf{E_R}$ represent the components of the rf electric field in the two possible directions.

An ion absorbs power according to the dot product

$$A(t) = Force \cdot velocity = q\mathbf{E}(t) \cdot \mathbf{v}_{xy}$$

It can be shown that the radius after excitation by such an rf field is given by [66]:

$$r = \frac{V_{p-p} T_{excite}}{2dB_o} \qquad (23)$$

T_{excite} is the period of excitation and r is the post excitation radius.

Thus according to this equation, post-excitation ion cyclotron radius is independent of *m/z*. Thus by applying an rf electric field whose magnitude is constant with frequency it is possible to excite all ions of a certain *m/z* range to the same radius. An expression can also be developed for the kinetic energy of the ion after excitation by simply rearranging and substituting equation 11 into equation 23. This gives equation 24 below:

$$K.E._{post-excitation} = \frac{q^2 V_{p-p} \left(T_{excite}\right)^2}{8d^2 m} \qquad (24)$$

It is therefore relatively straightforward to produce ions of large kinetic energy after excitation allowing dissociation experiments to be implemented.

1.4.1.2 Broadband Excitation

Excitation discussed previously has consisted of a single-frequency resonant electric field. However, the simple procedure of turning such a field "on" or "off" results in other excitation at different frequencies. An expression for such a single-frequency excitation[18] that gives the time-domain spectrum $E(v)$ at excitation frequency ω_c used for $T_{excitation}$ seconds is given below:

$$E(v) = E_o \frac{\sin(2\pi v_c T_{excitation})}{2\pi v_c} \qquad (25)$$

E_o is the field strength.

Thus, even if the excitation field is matched exactly with the frequency of the ion of interest, the fact that the excitation field needs to be turned "on" and "off" results in excitation of other ions that have nearly identical frequencies. This is effectively a broadening of the range of the excitation to a bandwidth that is proportional to the reciprocal of $T_{excitation}$. Therefore the longer the time-domain signal duration the narrower is the corresponding frequency domain spectral width i.e. the greater the resolution of the excitation.

1.4.1.3 Quadrupolar Excitation

It can be shown [13] that a two-dimensional azimuthal quadrupolar rf potential with a frequency equal to the unperturbed cyclotron frequency will convert magnetron motion to cyclotron motion. Thus when ions are involved in collisions the ion cyclotron radius will decrease rapidly while the magnetron motion increases quite slowly. If the magnetron motion is therefore converted to cyclotron motion, the collisions will cause the cyclotron motion to rapidly fall to zero and the ions will relax to the centre axis of the cell. This technique has become known as quadrupolar axialisation and improves all aspects of FT-ICR mass spectrometry. It reduces an ion's internal energy, improves ion selection for MS/MS, CID efficiency, mass accuracy, mass resolution and ion remeasurement efficiency. Quadrupolar axialisation can therefore be used to improve the signal-to-noise ratio of a spectrum by making use of ion remeasurement experiments [14, 15]. The inter-conversion frequency [16] of magnetron to cyclotron frequency is given by

$$\varpi_{\text{interconvert}} = \frac{3(2.66667)qV_{quad}}{2md^2(\varpi_+ - \varpi_-)} \qquad (26)$$

where V_{quad} is the voltage applied to electrodes separated by d meters and 2.66667 is a scaling factor.

1.4.2 Detection

As previously mentioned, as they at first enter the ion trap, the ions are of random phase and their cyclotron radius at room temperature before excitation is very small. The signal generated by the ions is therefore undetectable. After excitation the ions are moved into a coherent phase and a larger cyclotron radius. If the ions in the ion trap are

considered to be a rotating monopole [17] when excited, then at certain points in time the ions will be closer to one detection plate than the other. Thus an alternating current will be induced in the detection circuit as the ion is first nearer one plate and then the other. The frequency of this alternating current will be proportional to the cyclotron frequency of the ions. For two infinitely extended parallel detection plates, the "image" charge (ΔQ) formed on the detection plates for an ion of charge q is given by the equation below:

$$\Delta Q = -\frac{2qy}{d} \qquad (27)$$

d is the distance between the two detection plates and y is the distance of the ion from the centre of the cell (where an ion at the centre of the cell would be $y=d/2$ along the y axis).

The expressions derived from this equation [17] disclose that the ICR signal is independent of B_o, increases linearly with post-excitation ion cyclotron radius and increases linearly with ion charge. This linearity is important for two reasons:

1) the ICR response at any frequency is proportional to the excitation spectral magnitude at that frequency.
2) simultaneous detection of the ions in a wide m/z range can be achieved, and a Fourier transform (FT) of the time domain ICR response gives the same absorption spectrum as would be achieved if the power absorption spectrum was measured by scanning infinitely slowly across the m/z range.

These points combine to produce the multichannel or Felgett advantage of FT-ICR mass spectrometry. This allows a spectrum of N data points to be acquired in $1/N$ the

time that would be required to acquire the data by scanning a channel at a time (as for a sector or quadrupole instrument).

1.4.2.1 Broadband Detection

A detection limit exists in an FT-ICR cell due to the resistance and capacitance of the receiver plates and their connecting wires. Under normal experimental conditions at typical ICR frequencies (>10kHz), using broadband chirp or SWIFT excitation , the signal-to-noise ratio of an experiment is independent of the cyclotron frequency. However, below these frequencies the signal-to-noise ratio varies directly with the frequency and is therefore a reflection of the relative current differential produced at the detection plates. The detection limit of a cell due to this capacitance and resistance can be calculated from the following equation:

$$N = \frac{CV_{d(p-p)}}{qA_1(r)} \qquad (28)$$

Where C is the capacitance of the detection circuit, $V_{d(p-p)}$ is the peak-to-peak amplitude of the detection voltage and $A_{1(r)}$ is a coefficient that is approximately proportional to r and can be determined graphically [18]. N is the minimum number (N) of ions that can be detected from an undamped signal in a single 1 second scan that can give a signal-to-noise ratio of 3:1. Thus a detection circuit with a capacitance of 60 picoFarads, a $V_{d(p-p)}$ of 3×10^{-7} V and an $A_{1(r)}$ of 0.5 has a detection limit of approximately 225 ions at an observed signal to noise ratio of 3:1.

1.4.3 Trap Size and Shape and its Effect on Dipolar and Two-Dimensional Excitation

Previous expressions for ion cyclotron radius r and translational energy following single-frequency resonant azimuthal dipolar excitation by a spatially uniform rf electric field have assumed an infinitely extended array of electrodes. This is obviously not the case within a typical FT-ICR instrument where the cell is of a fixed and finite geometry. However, equations 23 and 24 remain good approximations if a scaling factor β is included in the expressions. Thus the equations for a trap of finite size can be written as follows.

$$r = \frac{\beta_{dipolar} E_o T_{excite}}{2dB_o} \tag{29}$$

$$r = \frac{\beta_{dipolar} V_{p-p} \sqrt{1/sweeprate}}{2dB_o} \tag{30}$$

Equations 29 and 30 are for single frequency and broadband frequency-sweep dipolar excitation respectively.

$$K.E._{postexcitation} = \frac{1.20607x10^7 \beta_{dipolar}^2 z^2 V_{p-p}^2 (T_{excite})^2}{d^2 m} \tag{31}$$

$$K.E._{postexcitation} = \frac{1.20607x10^7 \beta_{dipolar}^2 z^2 V_{p-p}^2 \left(1/sweeprate\right)}{d^2 m} \tag{32}$$

$\beta_{dipolar}$ values for different geometries are shown below.

TABLE 1

Trap Shape	End Cap Separation	Excitation Electrode Separation	γ	α	$\beta_{dipolar}$	β_{quad}
Ideal	NA	NA	0.50000	4.00000	1.00000	2.66667
Cube	a	d=a	0.2787	2.8404	0.80818	2.77373
Infinity	a	d	0.2787	2.8404	~0.900[x]	NA[y]
Hyperbolic	a	$d = a/\sqrt{2}$	0.44403	4.0905	0.66483	2.6469

x : Approaches the value of $\beta_{dipolar}$ for an infinitely long cylindrical trap/ y : Cannot perform traditional 4 plate quadrupolar excitation therefore must use 2 plate quadrupolar excitation instead

Similarly the equation for the inter-conversion of magnetron motion to cyclotron motion via quadrupolar excitation can also be expressed with a scaling factor β.

$$\varpi_{\text{interconvert}} = \frac{3q\beta_{quad}V_{quad}}{2md^2(\varpi_+ - \varpi_-)} \qquad (33)$$

Ideal scaling factors can be produced for all three of these potentials by the "hypercube", which consists of a 5 x 5 grid of electrodes on each trap surface giving 150 individual electrodes which can be controlled separately. Thus a virtually perfect potential can be created within this trap that results in a $\beta_{dipolar}$ of approximately 1. Problems do exist however with such a trap since the large amount of electrodes necessarily mean an increase in capacitance and thus a decrease, to extremely low levels, in detection and excitation efficiency.[19]

1.5 Ion-Neutral Collisions, Mass Accuracy, Resolution and Resolving Power of FT-ICR MS

Collisions of the ions in an ICR cell with neutral molecules an important consideration when discussing factors that effect mass resolution. The most commonly used model for collisions in ion cyclotron resonance is to consider the effect of the collisions as a frictional damping force i.e. as represented as below:

$$m\frac{d\mathbf{v}}{dt} = q\mathbf{E} + q\mathbf{v} \times \mathbf{B} - f\mathbf{v} \qquad (34)$$

Such a theory depends on the rate of ion-molecule collisions. This is calculated by assuming[20]:

$$\frac{1}{\tau} = \frac{m_{neutral}}{m_{ion} + m_{neutral}} \nu_{collision} \qquad (35)$$

$\nu_{collision}$ is the number of ion-molecule collisions per second. This can be calculated by first determining the rate constant for ion-molecule collisions. An ion and a neutral can be said to interact through an ion-induced dipole potential ("Langevin model") at thermal velocity.[21] When the ion is modelled as a point charge then:

$$U_{(r)} = -\frac{\alpha' e^2}{2r^4} \qquad (36)$$

α is the isotropic polarisability of the neutral, e is the ion charge in statcoulombs or esu (e = 4.80653×10^{-10} statcoulombs) and r is the distance between the two particles. From equation 36 and the Langevin model the ion-neutral collision rate constant can be calculated:

$$k = \sqrt{\frac{4\pi^2 \alpha' e^2}{\mu}} \tag{37}$$

μ is the reduced mass of the ion or the molecule and α' is the isotropic polarisability of the neutral. This frictional damping model results in an exponential damping of the time-domain signal.

The previous model, although it offers a good description for room temperature ions, it is not an ideal description for the higher velocities of ions observed during a typical FT-ICR experiment.[67] It has been suggested that a hard sphere model[67], whose overall equation of motion is given below, would be more appropriate:

$$m\frac{d\mathbf{v}}{dt} = q\mathbf{E} + q\mathbf{v} \times \mathbf{B} - f\mathbf{v}^2 \tag{38}$$

Thus instead of exponential damping of the ion velocity with time as for the Langevin model the ion velocity is now given by

$$v(t) = \frac{v_o}{1 + v_o\left(m_{neutral} / m_{neutral} + m_{ion}\right) N \sigma_{hardsphere} t} \tag{39}$$

N is the neutral ion density, $m_{neutral}$ and m_{ion} are the masses of the neutrals and ions respectivley, $\sigma_{hardsphere}$ is the collision cross section of the hard-sphere. This can be transformed numerically to give a frequency-domain spectrum. This spectrum is narrow at half-maximum peak height but extended at the base. This broadness (due to the fact that the time-domain signal is not infinitely long) can be overcome experimentally by making use of apodisation to produce better signal-to-noise and removal of the side bands, which make up the broad base of the peak. Apodisation can be thought of as a method of smoothly reducing the time-domain signal from its maximum to zero at the point of signal truncation. It is a method of "weighting" the time-domain function before Fourier transformation to remove the unwanted artefacts from either side of the main peak. Unfortunately, apodisation on the one hand reduces the intensity of the side bands, but on the other broadens the peak resulting in poor resolution.

The relationship between cyclotron frequency and mass resolution can be obtained from equation 3a by calculating the first derivative giving :

$$\frac{\varpi_c}{d\varpi_c} = -\frac{m}{dm} \qquad (40)$$

This demonstrates the relationship between frequency resolving power and mass resolving power; apart from a minus sign the two are identical. Thus due to the fact that frequency can be measured with an accuracy of up to 9 decimal places, mass accuracy is exceptional in FT-ICR MS. Mass spectrometry makes use of the convention of defining mass resolution as the peak width at half-maximum peak height i.e. $\Delta m_{50\%}$. Thus the resolving power is defined as $m/\Delta m_{50\%}$ and experimental mass resolution can be expressed as:

$$\frac{m}{\Delta m_{50\%}} = -\frac{qB_o}{m\Delta\varpi_{50\%}} \tag{41}$$

It should be noted that the time-domain signal damps to zero at the high pressure limit but is continuous for the low pressure limit. Thus resolving power in the low pressure limit is independent of *m/z* but peaks will be closer together due to ICR frequency varying inversely with *m/z*. This latter reason is why mass resolving power varies inversely with *m/z*.

1.6 Upper Limits of FT-ICR MS

A variety of factors affect the upper mass and energy limits of a typical ion trap. These include space charge effects, non-uniform electric fields, ion potential energy limits and the actual physical dimensions of the trap itself. For example, ions whose cyclotron radius exceeds the trap dimensions (or cell radius) will be lost from the cell due to collisions with the cell walls. Thus the upper mass limit for ions at thermal equilibrium can be computed from the following equation:

$$m_{upper} = \frac{q^2 B_o^2 r_{max}^2}{2kT} \qquad (42)$$

Thus for a singly charged ion at room temperature in a cell of radius 3 cm in a magnetic field of 9.4 Tesla the upper mass limit is approximately 14.9 mega Daltons. However , this does not take into account the fact that ions must start with a much smaller cyclotron radius in order to be excited to a coherent and detectable ion signal. The upper mass limit is therefore much reduced.

Other constraints on the upper limit of FT-ICR include the loss of ions with a potential energy larger than the voltage applied to the trap plates, ion-ion repulsion of like charge and mass ions to different regions of the cell, which due to the finite size of the cell will necessarily contain regions of different electric potential, resulting in peak broadening.

Equation 35 above is only valid when there are no electric fields within the trap. It has been shown by Ledford *et al* [22] that the reduced cyclotron and magnetron frequencies coalesce to a common value m_{crit} such that when an ion of $m/z > m_{crit}$ is present in the trap it becomes unstable and is lost.

1.7 Mass Spectrometry/ Mass Spectrometry (MS/MS)

FT-ICR MS has advantages over other mass spectrometry techniques in this area due to its ability to achieve MS^n experiments. If desired it is possible to produce MS/ MS spectra on a parent from the initial ion population and then an MS/MS spectrum from the previous stage. With care this can be extended to multiple stages of dissociation giving detailed information on the molecule that is impossible to obtain from other mass spectrometers.

Several techniques exist in FT-ICR MS for dissociation of molecule ions including collision induced dissociation (CID)[23], surface induced dissociation (SID)[24, 25], blackbody infrared radiative dissociation (BIRD)[26] and infrared multiple photon dissociation (IRMPD) [27, 28]. Each technique has its own distinct advantages.

CID can be split into two regions of interest. These are sustained off-resonance irradiation (SORI) [29, 30]and on-resonance irradiation. SORI is a "softer" method of excitation of molecule ions for dissociation since it deposits less energy into the ion population of interest compared with on-resonance excitation. SORI influences the ion population of interest by making use of an rf electric field that is applied so that it is just out of resonance with the effective cyclotron motion (ω_{eff}) of the ion. This causes the ion population to fluctuate between being in phase and out of phase with the rf field according to a periodicity of $2\pi/\varpi_o - \varpi_{eff}$ where ω_o is the frequency of the off-resonance rf field.[66] The ion population is therefore alternatively excited and de-excited causing a build up of energy (after consecutive collisions) in the ions until it reaches its dissociation threshold.. SORI overcomes one of the major problems involved in MS/MS in FT-ICR, that of radial diffusion of the ions away from the centre of the cell due to collisions with the neutral collision gas. This results in a situation where ions are detected at a point removed from

the centre of the cell and therefore below maximum efficiency and resolution. SORI, due to the low energy imparted to the parent ions, maintains the ions near the centre of the cell.

The strength, and the position off-resonance, of the applied field to the parent ion frequency can be adjusted so that the desired amount of fragmentation can be observed i.e. the amount of energy imparted to the parent ion population can be controlled. Other techniques such as very low-energy (VLE)[31] and multiple excitation collisional activation (MECA) [32] operate under a similar principle, although SORI is most commonly realised in FT-ICR MS due to its ease of use and simple implementation.

IRMPD makes use of an IR (10.6 μm) laser to "heat" the ions. MS/MS results in similar spectra as those seen by SORI/CID. However, IRMPD has an advantage over collision induced dissociation in that the cell pressure can be maintained at extremely low pressures giving ultra high resolution of the daughter ions produced. The necessary gas pulse for CID means that the resolution is reduced and experimental duration is increased due to an obligatory pump down period.

A further method for MS/MS takes advantage of the black body radiation produced in a heated cell in a vacuum. This technique, known as BIRD, requires the parent ion to be confined in the trap for 10-1000 seconds. This allows the ion structures temperature dependent features to "interact" with the black body radiation. Since the ion cloud assumes a Boltzmann distribution within the cell a known and controllable energy distribution, then not only is the fragmentation pattern produced indicative of the ions structure but information on the dissociation energetics and mechanisms can be elucidated from the temperature dependence of the unimolecular dissociation rate constants.

Surface induced dissociation provides high energy deposition in the parent ion and a narrow distribution of this energy. The method, however, produces very little new

structural information and due to the high energy of the daughter ions, the confinement of these ions is extremely difficult.

1.8 Ionisation Techniques

1.8.1 Electron Impact Ionisation and Chemical Ionisation

Electron impact (EI) ionisation is the established ionisation method in organic mass spectrometry. In its simplest form, a volatile sample passes through an electron beam. The collision of the electron beam with the volatile sample can cause an electron to be removed from the sample molecule and thus causes the analyte to be ionised. The EI source is operated at relatively high pressures to maintain sensitivity and is typically relatively gas tight (apart from the small holes for the introduction of the electron beam and the exit slit for the ions). EI as an ionisation technique is now mainly used for the analysis of small organic and inorganic molecules.

The electron beam in electron impact ionisation is generally formed by heating a tungsten or ruthenium filament, the electrons being accelerated away from the filament by the application of an acceleration voltage somewhere between 5 and 100 volts. A magnetic field of a few hundred gauss is also applied across this region to confine the electrons to a tight helical path. Total electron (ionising) beam current can be monitored by feedback control from the current reaching the trap plate at the opposite end of the electron beam. Ions are created by collisions with the electrons and are thrust into the mass spectrometer by an applied repelling field, although only something like 1 in 1000 molecules attendant in the source are ionised. Ionisation efficiency tends to be at a maximum at an electron beam energy between 50 and 100 eV with nowadays almost all spectra being acquired at a standard electron energy of 70 eV, due to the sensitivity in this region being close to maximum and fragmentation being unaffected by small changes in electron energy. (EI mass spectral libraries typically consist of spectra obtained at this

energy.) EI mass spectra typically consist of several fragments and the technique is thus quite "harsh".

In 1966 Munson and Field introduced a new technique for sample ionisation, this was chemical ionisation (CI). [45] In this technique ions are generated by ion-molecule reactions rather than collisions with an energetic electron beam. CI is achieved by producing an ionised beam of reagent gas which is reactive with the analyte of interest. The reagent gas (e.g. methane) is maintained at a pressure of about 1 Torr while the analyte is typically at a partial pressure 0.001% that of the reagent gas.

The technique's wide applicability to less robust samples is due to the lower excess energy in the sample molecule compared with EI (i.e. perhaps 10 eV above ionisation energy for EI but, depending on the experiment, only 5 eV for CI) and the higher stability of protonated molecules compared with odd-electron ions.

Take as an example the common reagent gas methane. The predominant reagent ions formed under electron impact are CH_5^+ and $C_2H_5^+$:

$$CH_4 \rightarrow CH_4^{+\cdot}, CH_3^{+\cdot}, CH_2^{+\cdot}$$

$$CH_4^{+\cdot} + CH_4 \rightarrow CH_5^+ + CH_3^{\cdot}$$

$$CH_3^+ + CH_4 \rightarrow C_2H_5^+ + H_2$$

Other reactions that are less important include:

$$CH_2^{+\cdot} + CH_4 \rightarrow C_2H_3^+ + H_2 + H^{\cdot}$$

$$C_2H_3^+ + CH_4 \rightarrow C_3H_5^+ + H_2$$

Subsequent reactions between sample molecules and the reagent ions result in protonated molecules. Reactions between sample and reagent ions can be placed into four categories:

Proton transfer	$M + BH^+ \rightarrow MH^+ + B$
Charge exchange	$M + X^{+\cdot} \rightarrow M^{+\cdot} + X$
Electrophilic addition	$M + X^+ \rightarrow MX^+$
Anion abstraction	$AB + X^+ \rightarrow B^+ + AX$

The main reagent ions formed from methane produce molecules predominantly by proton transfer reactions.

1.8.2 Fast Atom Bombardment (FAB) Ionisation

FAB was once the method of choice for the analysis of labile molecules such as small peptides. The technique makes use of an incident beam of neutral Ar or Xe (usually Ar) which strikes a probe tip coated with the analyte of interest. This produces a beam of analyte ions that can be detected with a mass spectrometer.

Later workers introduced the idea of an ion beam rather than a neutral beam to cause ionisation.[46] This technique, since it now involved the use of an ion beam for ionisation became known as liquid secondary ion mass spectrometry (LSIMS). The problem which exists with this type of ion generation is that sample is rapidly lost from the area of the probe tip struck by the primary beam. This problem can be overcome by making use of a liquid matrix, such as glycerol, with which the sample is mixed. The liquid matrix in this

technique allows fresh sample to flow into the region that has been depleted. A continuous secondary ion beam is thus produced, for a minimum of 20 minutes in some cases, which allows better use of scanning instrumentation such as magnetic or electric sectors. An upper mass limit of approximately 24, 000 Daltons with a 35 keV caesium ion beam was established at the time FAB was widely used.[47]

Preliminary investigations made use of a neutral primary beam to overcome problems stemming from the high voltages required in the source of a magnetic-sector mass spectrometer. Extensive investigations subsequently showed that whether the primary beam was charged or neutral made little difference to the quality of the spectra obtained, although it was noted that increasing the size of the particles in the primary beam increases the yield of molecule ions in the secondary ion beam.[48] For organic analytes it was also noted that there was an increase in secondary ion yield if the primary beam was changed from atomic to molecular ions.[49]

The ionisation mechanism for FAB/ LSIMS is complex and incompletely understood. The mechanism has been considered to involve desorption of ions pre-formed in the sample into the gas phase by the incident primary beam. These ions would then undergo ion-molecule reactions in the region of dense gas just above the surface. These pre-formed ions have been found to be desorbed in preference to other methods of ionisation, however, spectra show that this is not the main process leading to formation of the secondary ion beam. A collision cascade is initiated when the primary ion beam strikes the surface of the probe tip, which causes extensive ionisation within the matrix. There is also a fast transition from the liquid to the gas phase that leaves the sample ions essentially matrix free. The resulting spectra are thus a result of all these processes.

The extremely fast expansion of the plume that occurs when the primary ion beam strikes the sample target offers an explanation on why labile molecules can survive intact during this ionisation process. The extremely short period of time during which the ions are at a temperature sufficient to cause fragmentation means that only uni-molecular dissociations are sufficiently fast to produce fragments. Thus the labile molecules remain intact to provide molecule-mass information in the mass spectra.

1.8.3 Plasma Desorption (PD)

Prior to the introduction of MALDI and ESI, plasma desorption mass spectrometry was applied to the analysis of larger biomolecules, since LSIMS/ FAB was restricted to the lower masses. The ability of PDMS to analyse these larger molecules presumably related to the fact that the overall ionisation process in PDMS is much more energetic (typically 100 MeV compared with the keV range of LSIMS/ FAB). This high energy is due to ionisation in PDMS being prompted by the fission products of Cf_{252} striking the backside of an aluminium or aluminised polyester foil plate on which the sample is deposited. These fission fragments are able to pass through the foil and cause desorption of the sample ions. A so-called fission track is formed on the solid surface as the fission products of Cf_{252} strike the foil. This area of damage is thought to be associated with desorption of cations, protons and small molecular ions such as CH_3^+. Intact molecular ion species of the sample of interest are thought to be desorbed from the edges of this region, with energy being transferred as a shockwave or an expansion of the lattice surrounding this fission track. This energy is just enough to break the bonds holding the sample to the surface but insufficient to break the non-covalent bonds of which the sample is made up.

Even though there is an extended mass range in PDMS compared with LSIMS/ FAB, the range of PDMS does not extend to extremely large proteins. ESI and MALDI have replaced them as the methods of choice for the ionisation of these types of samples.

1.8.4 Field Desorption

This was first investigated by Muller [50] in 1951 and made use of a strong electrostatic field to produce ions from a sample substrate under vacuum; it was adapted to mass spectrometric analysis by Inghram and Gomer.[51] This allowed molecular ions to be formed from involatile and thermally unstable analytes.

The ionisation process in mass spectrometry occurs from a metallic wire anode coated with dendrites of small radius of curvature (~ 3 Angstroms). These dendrites act as a coating of extremely fine points at whose tip there is an extremely strong electrostatic field of between 10^7 and 10^8 Vcm^{-1}. The sample to be ionised is applied to the emitter and the sample desorbed by the intense electrostatic field.

The electric field at the tip of the dendrite is given by the following expression where α is a shape factor, V is the applied voltage, r is the radius of curvature and d is the distance to the counter-electrode.

$$F = V\left\{(1-\alpha)\left[0.5r\ln\left(\frac{4d}{r}\right)\right]^{-1} + \alpha r^{-1}\right\} \qquad (43)$$

There are thought to be three main processes involved in the production of ions via field desorption. These would be the following.

1) *Proton or cation attachment.* Sample ions may already be present as ions in the solid or liquid phase due to the presence of salts or acids or the fact that the sample is an electrolyte. Such samples will thus desorb ions at a lower field (10^6 Vcm^{-1}) compared with other processes involved in the field desorption of ions.
2) *Electron tunnelling.* At the maximum electric field induced in field desorption an electron from the sample molecule can tunnel into the metallic emitter leaving a molecular ion $M^{+\cdot}$. These strong electric fields are present only at the dendrite tips.
3) *Thermal mechanisms.* Many samples require heating of the emitter, which may cause thermal fragmentation of the sample and may lead to ionisation.

Emitter preparation is complex and takes several hours and usually consists of the formation of a carbonaceous dendrite from, for example, benzonitrile on a tungsten wire of 10 μm diameter. Temperature and current applied to the emitters as they are grown must be closely monitored throughout to allow sufficiently large but fine dendritic needles to form on the tungsten wire. The process is usually automated to allow accurate control of these parameters as the growth is extremely sensitive. The prepared emitters are either dipped into the sample molecule or the sample is introduced to the emitter via a microlitre syringe.

1.8.5 Laser Desorption and Matrix-Assisted Laser Desorption Ionisation (MALDI) Mass Spectrometry

Initial experiments involving lasers to ionise molecules focused on the use of both ultraviolet (UV) and infrared (IR) lasers to desorb directly and ionise the sample of interest. This so called laser desorption had an upper mass limit of approximately 1000 Da above which molecules were susceptible to degradation rather than ionisation. It was not until Tanaka *et al* [52] and Hillenkamp *et al* [53] demonstrated the advantages of a "matrix" in 1987 to allow absorption of the laser energy and thence transfer of this energy to the sample molecule of interest, that the use of lasers for ionisation in mass spectrometry became commonplace.

Previously the laser wavelength had to be "tuned" to the sample molecule of interest for efficient vaporisation and ionisation. Now, however, the matrix could be selected that absorbed the laser energy at a certain fixed wavelength so that a single laser could be used to ionise all samples. The laser of choice in most MALDI instruments today is the nitrogen UV laser operating at a wavelength of 314 ηm, although at the time of writing there is great interest in IR lasers for ionisation.

There are many different types of matrix depending on the sample to be analysed. For example, a protein/ peptide sample would typically be mixed with matrices such as 2,5-dihydroxybenzoic acid and cinnamic acid derivatives. Other classes of sample such as polymers would make use of other matrices, specific matrices giving better ionisation for certain samples. These matrices efficiently absorb the UV laser energy and pass it onto the analyte of interest. Typical sample preparations include the analyte at low concentrations with the matrix of choice at a molar ratio of 1:1000. The analyte embedded in such a

sample is shielded from any excess energy that might cause fragmentation and is separated by the matrix molecules thus preventing aggregation.

MALDI is typically combined with time-of-flight due to the pulsed and extremely focused nature of ion formation and the fact that the energy distribution of ions formed is uniquely suited to this method of analysis. The low cost and ease of use of such instruments, as well as the large mass range, mean that the two methods are particularly suited for most applications.

When the laser strikes the sample/ matrix mixture at the start of the experiment a plume of matrix and analyte leaves the surface of the sample probe. The MALDI mechanism of ion formation is not well understood and there is some debate over whether the ionisation of the sample molecule takes place in this plume or within the solid sample deposited on the sample probe.

Ions are commonly thought to be formed in the plume by protonation/ deprotonation or cationisation. Typical molecule ion peaks thus consist of $[M+H]^+$ or $[M+X]^{n+}$ where X is a cation and n is the relevant charge; little or no fragmentation is seen in a typical MALDI experiment. This factor means that MALDI is well suited for the analysis of biomolecules and as such MALDI has brought about a large growth in this area of mass spectrometry.

1.8.6 Electrospray Ionisation

Electrospray ionisation [54] in its simplest from, takes a sample in an aqueous medium (typically a 50:50 mixture of water and a dipolar solvent with a few percent of acid), and passes the solution through a fine needle to which a potential of 2-3 kV is applied. As the liquid emerges from the needle it breaks up into small charged droplets, which will eventually form the ions of interest.

The electrospray process is not fully understood however, due to there being no one mechanism for ion formation that successfully incorporates all the experimental evidence and allows predictions to be made on the outcome of an experiment. Several mechanisms have been proposed and these include one mechanism proposed by Dole [55] and another by Iribarne and Thomson [56]. Both mechanisms are considered to be an incomplete description of the electrospray process. To start, a more detailed explanation of droplet formation is required.

The aqueous medium containing the sample of interest, at a concentration of between 10^{-4} and 10^{-6} Molar, is sprayed through a needle at a potential of approximately 3 kV. The needle dimensions is typically 0.2 mm o.d. and 0.1 mm i.d. and is located approximately 1-3 cm from a planar counter electrode through which there is an orifice that leads to the mass spectrometer. The electric field at the tip of such a needle is extremely high at about 10^6 Vm^{-1}. This can be calculated for a needle of radius r_c at a potential V_c and located a distance d from the planar counter electrode using the equation below.

$$E_c = \frac{2V_c}{r_c \ln\left(4d/r_c\right)} \qquad (44)$$

Geometrically r_c is the most important parameter with E_c being inversely proportional to r_c. The intense electric field at the needle tip is of immense importance in producing charged droplets. The field partially penetrates the liquid surface causing the ions within the bulk solution to separate into two layers. The positive ions migrate to the surface of the liquid while the negative ions remain in the bulk of the solution (if the needle is held at a positive potential); this negates the field produced by the needle within the solution. The positive ions at the surface of the liquid are attracted downfield towards the counter electrode and this stretches the solution into a Taylor cone. This cone is a balance between the surface tension of the solution and the electric field at the needle tip. As the electric field at the tip is increased the cone becomes unstable and a liquid filament of a few micrometers across is produced. As the voltage is raised further, the cone tip is eventually replaced by a multispray condition, where four or more liquid filaments are produced from the needles rim. These filaments in turn break up into charged droplets some distance downfield, and since the solution is essentially an electric bilayer, with the surface enriched with positive ions, the droplets will have a surface that is positively charged with few counter ions in the droplet bulk.

The electrophoretic mechanism described above is favourable on experimental and energetic grounds. Experimental data (mass spectra) of solutions containing known electrolytes at concentrations of 10^{-5} to 10^{-3} Molar, show only those electrolytes known to be in the solution. Also, energetically the electric double layer prevents ionisation by other methods such as field ionisation. Deionising the solution results in an intermittent and

weak signal, thus providing further evidence for the electrophoretic mechanism of droplet formation.

The charge carriers in the electrospray mechanism have only recently been considered, mainly by mass spectrometrists to whom the nature of these charge carriers are of great importance. Pfeiffer *et al* [57] were the first to propose the electrophoretic mechanism, while Hayati *et al* [58] expanded the theory.

However, it was left to Smith [59] to consider the mechanism from the position of the mass spectrometrist. He provided a useful equation [54] that predicts the electric field at which the electrophoretic mechanism would be initiated for different solutions.

$$V_{on} \approx 2x10^{-5}(\gamma.r_c)^{1/2} \ln\left(4d/r_c\right) \qquad (45)$$

γ is the surface tension, r_c is the capillary radius and d is the distance between the capillary and the counter electrode. V_{on} is predicted and observed experimentally to increase with the surface tension of the solution, so that water, with the highest surface tension, also has the highest onset voltage for droplet formation. A few hundred volts higher than V_{on} is usually required for stable electrospray operation, although, at higher electric fields, corona discharge becomes a problem, resulting in protonated solvent clusters such as $H_3O^+(H_2O)_n$ in the positive ion mode, and a drop in the efficiency of the electrospray process. Electron scavenging gases such as O_2 and SF_6 can be used to prevent this discharge. It should be noted that air contains enough oxygen to prevent corona discharge for all but extremely high electric fields, and since the electrospray ionisation source in

mass spectrometry is typically utilised at atmospheric pressure, then for most experiments O_2 and SF_6 do not need to be added.

It has been observed that the droplets formed by the electrophoretic mechanism undergo evaporation of the bulk solvent and coulombic explosions that result in the formation of smaller and smaller droplets [54] ; the transition from droplet to ion however, cannot be observed, and it is the mechanism of this transition that is still debated.

The droplets have been found to "explode" at a point when the surface charge overcomes the surface tension of the solution. Thus the charge Q overcomes the surface tension γ at a point known as the Rayleigh limit, according to the equation below.

$$Q_R^2 = 64\pi^2\varepsilon_o\gamma R_R^3 \qquad (46)$$

ε_o is the permitivity of vacuum, γ is the surface tension and R_R is the radius of the droplet. The initial charge of the droplet has been found to be approximately 10^{-14} Coulombs by Gomez and Tang [60] which corresponds to only 50 % of the Rayleigh limit for a droplet of 1.5 μm. Droplets within the micrometer range are known to retain their charge and not emit gas phase ions. Such droplets are reduced in size by evaporation until they come close to the Rayleigh limit where they fission into smaller droplets. (Experiments carried out in the early 1990's showed that fission occurred at approximately 80 % of the Rayleigh limit for droplets in the 1 μm range.[60] It has also been found in studies of the charge-to-volume ratio that larger droplets come closer to the Rayleigh limit. Droplets will thus undergo successive evaporation and fission until the droplets are small enough for ions to be produced.

The droplets maintain a constant charge Q_o while the solvent evaporates, until the charge on the droplet surface exceeds the surface tension of the liquid[60]. The droplet then cleaves into several much smaller daughter droplets and a larger parent, and the process starts all over again, with successive fissions producing smaller and smaller droplets.

The droplet itself typically does not cleave into two equally sized daughter droplets, but instead it has been observed that the parent droplets vibrate between oblate and prolate shapes forming a tail. This breaks up into a larger parent droplet and several (~20) daughter droplets. These daughter droplets, which are of uniform size and shape, carry away approximately 15 % of the charge and 2 % of the mass of the parent, resulting in daughter droplets that are enriched with positive charge. This can be thought of as "uneven" fission while a cleavage that results in two evenly sized parent droplets can be considered to be an "even" fission. Figure 7 represents the mechanism of "uneven" droplet formation.

The times for the fissions to occur can be calculated by using expressions for the rate of solvent evaporation from small droplets given below. [54]

$$R = R_O - {\alpha \bar{v} p^o M}/{4 \rho R_g T} \qquad (47)$$

Where $\bar{v}$ is the average molecular velocity of the solvent gas, p^o is the vapour pressure of the solvent at the temperature of the droplet, M is the molar mass of the solvent molecules, ρ is the density of the solvent, R_g is the gas constant and T is the temperature of the droplet. The condensation coefficient α is ~0.04 for both ethanol and water.

The results in diagram 4 are calculated from more complex equations and are calculated for a methanol droplet of 1.5 μm, charge $Q_o=8x10^{-15}$ Coulombs and at an ambient temperature of 35 °C. It is expected that the daughter droplets of radius ≈ 0.08μm and approximately N=280 elementary charges will also undergo solvent evaporation and successive coulomb explosions until eventually gas phase ions are formed.

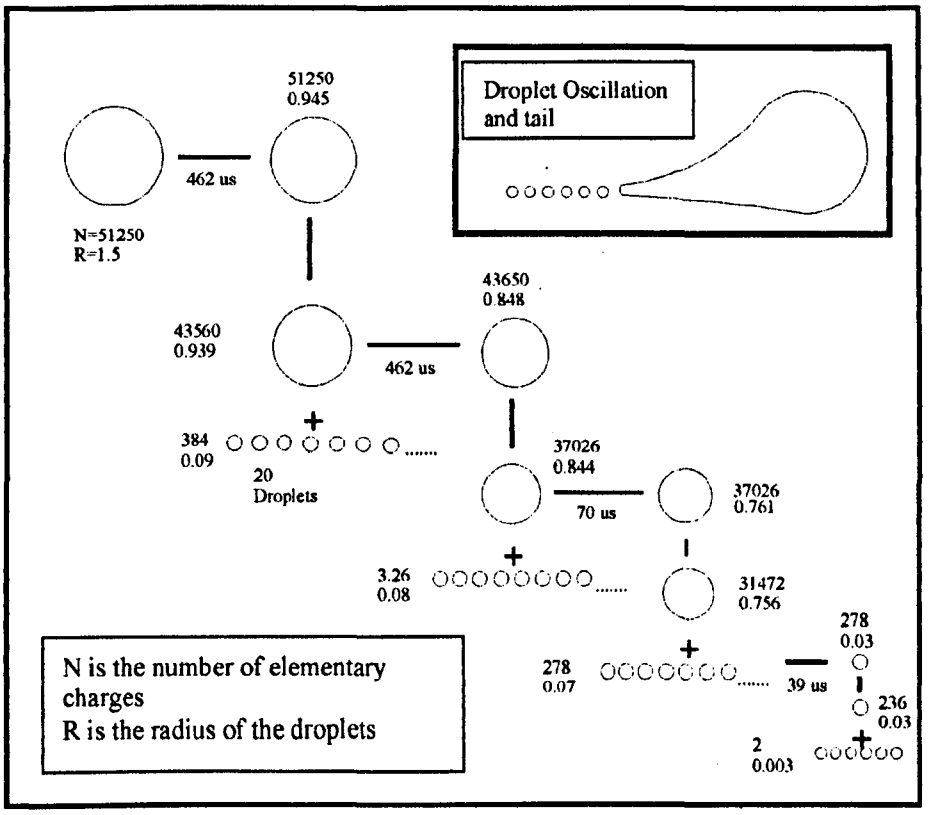

Figure 7: Illustration of the droplet fission process.

Figure 7 illustrates the fact that the time scale for this droplet shrinkage to ions is in the order of hundreds of microseconds, roughly the amount of time that the droplets are present in the source region. Therefore, theory agrees with experiment in this respect.

A difficulty arises, since the droplets are so small, the type of fission they undergo is unobservable. Thus these droplets may undergo the "uneven" fission as described above or the "even" fission mechanism. Whether the droplets undergo "uneven" or "even"

fission is of interest since it determines the number of excess positive charges on the surface compared to the charge-paired ions in the droplet bulk.

If the mechanism of droplet fission is taken to be even then there will be no net increase in charge on the surface compared to the bulk charge-pairs. However, uneven fission would lead to an increase if it is assumed that when the daughter droplet is formed the surface charge is transferred but the ion pair concentration in the bulk remains the same as the parent. This would lead to a factor of seven increase in the excess charge on the surface of the droplet, with successive fissions increasing by a factor of seven each time. A second generation would therefore have 49 times as much excess positive charge on the surface (compared to the bulk) compared to the parent droplet. It could therefore be argued that "uneven" fission is an essential process in forming electrospray ions.

There are two proposed mechanisms of ion formation from these daughter droplets. These were mentioned earlier and consist of Iribarne and Thomsons ion emission mechanism [56] (field desorption mechanism) and Doles single ion in droplet theory (SIDT) [55].

The latter depends on the formation of extremely small ($R \approx 1\eta m$) droplets containing only one ion. Solvent evaporation from such a droplet would leave a bare gas phase ion. The former theory predicts ion emission becoming competitive with Rayleigh fission at a droplet radius of $8\eta m$ and with a charge of $\approx 10^{-17}$ Coulombs. This ion emission is maintained by solvent evaporation, allowing R to decrease and thus retaining the high charge to droplet bulk ratio needed. Since the ion emission mechanism does not require the formation of droplets containing a single ion, ions can be produced in the gas phase from droplets that contain other solutes.

This difference was initially thought to be sufficient to prove one mechanism over the other. For example if a solution is made containing NaCl in various concentrations, then at the higher concentrations if SIDT held (and with the "even" fission mechanism) the mass spectra should show not just Na^+ ions but clusters of $Na^+(NaCl)_n$. This is because at higher concentrations some of the small SIDT droplets should contain NaCl charge pairs. However, experiments showed a complete absence of these clusters and at the time this was taken as evidence for the ion emission mechanism. If "uneven" fission is assumed, however, the results then validate the SIDT mechanism since the droplets may be depleted of NaCl ion pairs after several generations.

1.8.6.1 The Ion Emission (Iribarne And Thomson) Theory

The Iribarne or ion emission theory is based on transition state theory. The rate constant k_I for emission of ions from a droplet is given by the following relationship:

$$k_I = \frac{kT}{h}\exp\left(-\Delta G^{\#}/RT\right) \qquad (48)$$

where k is the Boltzmann constant, h is the Planck constant, T is the temperature of the droplet and $\Delta G^{\#}$ is the free energy of activation.

The ion emission mechanism has an advantage over the SIDT theory (as stated previously) in that it predicts the different gas-phase ion intensities seen for different ions at the same concentration in solution. That is it predicts the rate of ion emission depending on the ion's chemical properties. (If SIDT takes into account the surface activity of the ions as an adapted Iribarne and Thomson mechanism does later in this section, then this will account for the selectivity of the electrospray mechanism. Since the

ions that are enriched on the surface will be those that will preferentially form gas phase ions). The transition state is assumed to be a "late" transition state, whereby we mean that it has more in common with the products of the reaction than the reactants. The transition state for Iribarnes mechanism shows the ion surrounded by a solvation shell outside the droplet bulk. The energy of such a transition state can be calculated using classical electrostatics and thermodynamics. The barrier in this transition state is due to the opposing electrostatic forces. The repulsion of the escaping ion by the other charges in the droplet bulk and the attraction between the escaping ion and the droplet because of the polarizability of the solvent medium gives rise to this electrostatic barrier. One must remember, however, that if the ion with its solvation shell is formed at any other point in time then the ion emission mechanism is invalidated.

The free energy of activation in the previous equation was found to depend on four parameters. These were N the number of charges on the droplet, R the radius of the droplet, the ion cluster solvation energy and d the distance of the ion charges from the surface of the droplet.[61] k_I increases with N and decreases with R. These parameters are identical for any ion formed under the same conditions while the other two parameters express individual characteristics of the ions themselves. Ions with a solvation shell are emitted from the droplet bulk. They are not emitted as bare ions, therefore the larger the solvation energy the higher the rate of emission from the droplet bulk. For example the naked Na^+ ion needs approximately 98 kcal mol^{-1} to transfer the ion from solution to the gas phase, while the solvated ion $Na^+(H_2O)_7$ requires only about 56 kcal mol^{-1}.

The charges on the droplet cannot be on the droplet surface where their energy would be minimised since this would disrupt the solvation shells of the ions; the ion charges must thus reside just within the droplet bulk allowing their solvation shells to

remain intact. Thus ions such as Li^+ which are strongly solvated have a greater d (distance of the ion charges from the droplet surface). Iribarne and Thomson have provided calculations of k_I for most of the alkali cations [61] which show a downward trend in value as the group is descended.

Ion intensities in electrospray ionisation depend on the total concentration of the electrolytes present in the solution. In a typical electrospray sample analyte and impurities exist together, the impurities originating from the solvents used in sample preparation and from sources such as high pressure liquid chromatography (HPLC). The analyte solution is therefore never a single electrolyte system. The impurities usually consist of alkali metal ions such as Na^+, Li^+ and other ions commonly present in the solvents used such as NH_4^+. These impurities are important because at analyte concentrations below approximately 10^{-5} Molar the electrospray process would cease to function without their presence in the solution.

Experimental data continually reveals similar relationships between analyte concentration and ion intensity. A plot of ion intensity versus concentration for the analyte shows a linear section of slope approximately 1 from 10^{-8} to 10^{-6} Molar followed by "saturation" and a small drop in intensity at concentrations below 10^{-3} Molar. A similar curve for the impurities present in the solution is observed with the minimum at approximately 10^{-3} Molar rising to a maximum at 10^{-7} molar, while the total ion intensity shows a gradual increase as the total concentration of both impurity and analyte increases.

At low concentrations of analyte the capillary current is carried mainly by the impurities which are at a constant concentration; above an analyte concentration of about 10^{-5} Molar the analyte begins to dominate. Since there is an increase in the electrolyte concentration in the solution at this concentration of analyte the total capillary current

increases. At the same time there is a noticeable drop in the intensity of the current due to the impurity, this is because there is a competition between the electrolytes present in the solution for the conversion to gas phase ions. There is thus a reduction in the impurity ion intensity as the analyte concentration is increased. A simple relationship exists for a two-electrolyte system such that the ion intensity for the analyte can be calculated. If the analyte has a concentration of $[A^+]$ and the impurity $[B^+]$ with respective ion intensities I_A and I_B the relationship is as follows.

$$I_A = fp\frac{k_A[A^+]}{k_A[A^+]+k_B[B^+]}I \qquad (49)$$

fp is a factor that depends on f the fraction of charges on the droplet that are converted to gas-phase ions and p the ion-sampling efficiency. It has been found experimentally that the factor fp is constant up to a total concentration of 5×10^{-4} Molar.[54] From this relationship it should be apparent that the intensity of the analyte ions I_A is dependent on the ratio of k_A to k_B. This ratio is the yield ratio of gas phase ions A^+ and B^+ comparable with the solution concentrations. k_A and k_B are the Iribarne rate constants for the analyte ions A and B.

Solutions for the yield ratio were initially determined experimentally by keeping the concentration of the electrolytes equal in the analyte solution. [56]This can be considered to be a special case in equation 6a and 6b which when applied to I_A and I_B leads to the expressions below.

$$\frac{I_A}{I_B} = \frac{k_A[A^+]}{k_B[B^+]} \qquad (50)$$

$$\frac{I_A}{I_B} = \frac{k_A}{k_B} \quad \text{for } [A^+]=[B^+] \tag{51}$$

The relationship between I_A and I_B and solution concentrations is thought to be indirect. A more useful measurement would be the number N_A and N_B of charges due to analyte and impurity ions at the surface of the droplets and the number n_A and n_B of charge-paired ions. This latest relationship (Equation 50) can be used to provide information on the concentrations of analyte and impurity corresponding to the number of ions in the droplet by its deviation from, or agreement with, experimental results.

For a three-electrolyte system, that is two analyte electrolytes and the impurities present in the solution, a more complex relationship exists as expected. This is shown below:

$$I_A = fp\frac{k_A[A^+]}{k_A[A^+]+k_B[B^+]+k_C[C^+]}I \tag{52}$$

With this system, experimental results and theory show a reduction in one analyte signal as the other is increased. Thus if one analyte electrolyte is taken to be the buffer in the system, then as the buffer concentration is increased the analyte signal decreases. The loss of ion intensity is proportional to that analytes value of k_A, thus for example Bu_4N^+ has a higher k_A than Cs^+ [54] and therefore sees less of a decrease in the ion intensity. The previous equation also predicts that the loss of intensity of the analyte signal will be proportional to k_B, the Iribarne rate constant for ion formation of the buffer. Thus in

practical terms this means that a buffer with a low Iribarne rate constant would be desirable.

Experiments where the concentration of the analyte pairs remain at $[A^+]=[B^+]$ have been carried out with the observation that in general a fit for equations 50 and 51 cannot be obtained throughout the total concentration range (10^{-8} to 10^{-3} Molar) for a constant yield ratio (k_A/k_B). To explain some of these results the Iribarne mechanism was extended to allow the introduction of surface activity to the theory. Results show that when $k_A=k_B$, the yield ratio remains the same over the total concentration range.

The high k_A/k_B at high concentrations of A^+ is thought to be due to a higher Iribarne rate constant for A^+ than for B^+ or because of a higher surface activity. The greater differential surface energy results in an increase in the ratio of surface charges above that expected on the concentration ratios alone. Thus ion emission would be higher for an ion with greater surface activity, since ion emission is proportional to the number of surface charges, even if the Iribarne rate constants were identical.

The decrease in the yield ratio at low concentrations in these experiments was ascribed to the depletion of the ion A^+ because of its higher evaporation rate. At higher concentrations new A^+ is supplied to the droplet surface from the bulk solution, however, at the lower concentrations (where the yield ratio was observed to decrease) there is less A^+ in the droplet bulk and this leads to an overall depletion of this ion. The emission of this ion is therefore reduced and the yield ratio therefore decreases at the lower concentrations.

So far only ions formed from the alkali metal ions and other simple analytes have been discussed. How do multiply charged macro-ions form in the electrospray mechanism? This is one of the most important areas for study by electrospray ionisation.

A model has been suggested by Fenn [62] that states that in the initial state the polyprotonated macromolecule is situated inside the small charged droplet with all the charges neutralised by counterions. Due to Brownian motion a segment of the macromolecule can approach the droplets surface, as it does so some of the charge on the macro-ion replaces the charge that was already present on the droplets surface. As more of the charges on the macro-ion replace the charges on the surface of the droplet the macro-ion slowly leaves the droplet a charge site at a time. This process may be facilitated by thermal activation. Thus repulsion between the charge on the macro-ion and the charge on the droplet results in more and more of the macro-ion being introduced to the gas phase. This process is similar to the activation step postulated for the alkali metal ions previously. Eventually the whole ion will enter the gas phase.

Alternatively as the droplet shrinks in size due to the fissions mentioned previously there will come a point when the droplets diameter is significantly smaller than the length of the macro-ion. Eventually the macro-ion will be "wrapped" several times around the droplet with some of the charge sites, of necessity, being on the surface of the droplet. As the droplet oscillates then more charge sites from the macro-ion will be introduced to the surface of the droplet and eventually the ion may split off from the main droplet bulk as virtually a gas phase ion. By this it is meant that only a few molecules of solvent will be still attached to the macro-ion and thus after a little more solvent evaporation the macro-ion will be left as the bare gas phase macro-ion. The distinction between these two models for macromolecule ion formation is that the activation is thermal in the former mechanism and due to elastic deformation of the solvent making up the droplet in the latter.

From this discussion it is obvious that there is no compelling reason for one mechanism to be preferred over the other. As one mechanism is expanded, the other

seems to benefit. For example the "uneven" fission and "even" fission debate and the surface activity introduced into the ion emission mechanism gave support in turn to the SIDT mechanism of ion formation. More detailed work seems to have been carried out on the ion emission mechanism than for SIDT and at the present time this seems to be the preferred explanation for the formation of gas phase ions via electrospray ionisation.

1.9 Non-covalent interactions and investigation of biomolecules by mass spectrometry

1.9.1 Protein Structure

Proteins consist of a polyamino-acid chain (naturally occurring proteins and peptides being constructed of 20 naturally occurring amino acids), which is known as the primary structure of the peptide or protein. This chain is in turn folded and contorted into the protein's active structure. Thus the so called secondary structure consists of the folding of the protein into e.g. α-helixes and β–pleated sheets that are held together by hydrogen bonds, while the tertiary structure is the folding of the primary and secondary structure itself and is dependent on disulfide bonds and non-bonding interactions. Thus a protein can be folded into globular or open structures depending on the tertiary structure.

The final "layer" of structure is the quaternary structure that consists of the interactions of two peptide chains together. Non-covalent and covalent interactions of proteins fall under this last category. Thus insulin, for example, consists of two chains the α and the β chains held together by two disulfide bonds and myoglobin consists of four identical proteins bound together with a heme structure at the centre.

1.9.2 Mass Spectrometry For The Analysis Of Biological Samples

The relatively new mass spectrometry techniques of MALDI and electrospray (ESI) are being used to investigate these non-covalent interactions and protein structure. The ability of mass spectrometry to give quick, easy determination of physical constants of a protein, such as its molecular mass; and structural information, is a valuable tool for those interested in biological samples and provides a challenge to the mass spectrometrist.

ESI with its unique ability to form multiply charged ions from solution without significant fragmentation is of fundamental importance for the study of biological and other large fragile molecules by mass spectrometry. Techniques such as H/D exchange combined with ESI (which will be discussed in more detail in a later section) and the observation of different charge-state distributions in electrospray spectra give important information on protein conformations in the gas phase. This is thought to represent the conformation of the analyte molecule in the solution and as such allows relatively quick and easy investigations of non-covalent interactions and conformational studies of proteins by mass spectrometry.

MALDI meanwhile is finding a niche for the analysis of complex mixtures, and applications in proteolysis and chemical modification schemes designed to obtain information on the proteins structure and function. Mass spectrometry is fast providing information on protein structure that is complementary to other methods such as circular dichroism (CD), nuclear magnetic resonance (NMR), calorimetry and fluorescence spectroscopies.

Mass spectrometry in general is useful for the analysis of biological molecules and their primary, secondary and tertiary structures due to its sensitivity, speed and specificity. Low femto- and atto- molar sample concentrations can be used via nanospray and a typical

experiment may take as little as 30 minutes from preparing sample to getting a spectrum. Mass spectrometry with MS/MS can also provide information on relative binding affinities and the primary structure of the biological molecule of interest.

The direct measurement of the molecular mass of the complex also gives information on the stoichiometry of the complex, which is often important for the biological activity of a protein. The mass accuracy of these measurements means that it is possible to obtain details about the active biological sample including whether the sample is multi-meric, or the number and type of co-factors that are needed for its activity.

1.9.3 Electrospray Ionisation for the Analysis of Biological Molecules

Proteins and peptides can be ionised from a variety of solvents via electrospray including solvents that are known to allow them to retain their natural conformations. Such solvents include buffers such as ammonium acetate, ammonium sulfate and ammonium citrate and pure water.

Protein-ligand interactions can therefore be initiated in the solution phase and directly analysed in the gas-phase by the mass spectrometer. A more detailed discussion of the pros and cons of mass spectrometry for the analysis of these interactions will be given in chapter 4. Other mass spectrometric techniques such as MALDI are also useful for the analysis of biomolecules but the low resolution of such instruments (typically time of flight) and the fact that the MALDI process produces predominantly singly charged ions means that larger biomolecule-ligand interactions cannot be investigated with much accuracy. The multiple charging of the electrospray technique means that even large molecules can be observed at high resolution since the mass is effectively "folded" down to a region on the m/z scale that has the highest resolution and mass accuracy.

Electrospray can therefore take advantage of the high resolution and mass accuracy inherent in FT-ICR mass spectrometry.

Arguments still rage over the validity of results obtained by electrospray on such complexes. The fact that solution phase chemistry and gas phase chemistry are involved leads to a question on whether solution phase chemistry is mirrored by gas phase chemistry i.e. does a gas phase measurement give us information on a solution phase problem?

Published data has characteristically been in direct correlation with results obtained by solution phase methodology.[63-65] Some argue, however, that results that do not show expected non-covalent interactions or non-covalent interactions where none are expected, are not reported. The nature of this argument means that it is hard to prove, while experiments are consistently being published that provide direct correlation with results reported from solution phase experiments. Investigations where the ligands are in much greater concentration than the protein i.e. competitive conditions, show relative abundances of complexes in the mass spectra are consistent with their relative binding constants in solution and multi-meric complexes that are known to be biologically active are also observed under "natured" conditions. There may be, however, a correlation between those interactions that are achieved and the type of non-covalent interaction of which the complex makes use. Changing from solution to gaseous phases may cause some types to be strengthened while others are weakened. It is still undetermined whether such is the case but it is worth considering.

References

[1] I. W. Griffiths, *Rapid. Comms. 11* (1997) 2.

[2] H. J. Svec, *Int. J. Mass Spectrom. Ion Proc. 66* (1985) 3.

[3] K. T. Bainbridge, *J. Franklin Inst. 212* (1931) 317.

[4] W. Bartky, A. J. Dempster, *Phys. Rev. 33* (1929) 1019.

[5] W. E. Stephens, *Phys. Rev. 69* (1946) 691.

[6] A. E. Cameron, D. F. Eggers, *Rev. Sci. Instrum. 19* (1948) 605.

[7] W. Paul, H. P. Reinhard, U. v. Zahn, *Phys. 152* (1958) 143.

[8] H. Sommer, H. A. Thomas, J. A. Hipple, *Phys. Rev. 76* (1949) 1877.

[9] H. Sommer, H. A. Thomas, J. A. Hipple, *Phys. Rev. 82* (1951) 697.

[10] M. B. Comisarow, A. G. Marshall, *Chem. Phys. Lett. 25* (1974) 282.

[11] M. B. Comisarow, A. G. Marshall, *Chem. Phys. Letters. 26* (1974) 489.

[12] M. B. Comisarow, A. G. Marshall, *Chem. Phys. Lett. 26* (1974) 489.

[13] G. Bollen, R. B. Moore, G. Savard, H. Stolzenberg, *Appl. Phys. 68* (1990) 4355.

[14] E. R. Williams, F. W. McLafferty, *J. Am. Chem. Soc. 112* (1990) 6157.

[15] J. P. Speir, G. S. Gormann, C. C. Pitsenberger, C. A. Turner, P. P. Wang, I. J. Amster, *Anal. Chem. 1993* (1993) 1746.

[16] S. Guan, H. S. Kim, A. G. Marshall, M. C. Wahl, T. D. Wood, X. Xiang, *Chem. Rev. 8* (1994) 2161.

[17] M. B. Comisarow, *Chem. Phys. 69* (1978) 4097.

[18] A. G. Marshall, F. R. Verdunn, *FT in NMR, Optical and mass spectrometry:a users handbook*, Elsevier, Amsterdam 1990.

[19] S. Guan, A. G. Marshal, *Int. J. Mass Spectrom. Ion Phys. 146/147* (1995) 261.

[20] D. Wobschall, J. R. Graham, D. P. Malone, *Phy. Rev. 131* (1963) 1565.

[21] J. I. Steinfeld, J. S. Francisco, W. L. Hase, *Chemical Kinetics and Dynamics*, Prentice Hall 1989.

[22] E. B. Ledford, D. L. Rempel, M. L. Gross, *Anal. Chem. 56* (1984) 2744.

[23] R. B. Cody, R. C. Burnier, B. S. Freiser, *Anal. Chem. 54* (1982) 96.

[24] J. A. Castoro, L. M. Nuwaysir, C. F. Ijames, C. L. Wilkins, *Anal. Chem. 64* (1992) 2238.

[25] C. F. Ijames, C. L. Wilkins, *Anal. Chem. 62* (1990) 1295.

[26] W. D. Price, P. D. Schnier, E. R. Williams, *Anal. Chem. 68* (1996) 859.

[27] D. P. Little, J. P. Speir, M. W. Senko, P. B. O'Cornnor, F. W. McLafferty, *Anal. Chem. 66* (1994) 2809.

[28] R. L. Woodlin, D. S. Bomse, J. L. Beauchamp, *J. Am. Chem. Soc. 100* (1978) 3248.

[29] J. W. Gauthier, T. R. Trautman, D. B. Jacobson, *Anal. Chim. Acta. 246* (1991) 211.

[30] A. J. R. Heck, L. J. deKoning, F. A. Pinkse, N. M. M. Nibbering, *Rapid. Comms. 5* (1991) 406.

[31] K. A. Boering, J. Rolfe, J. I. Braumann, *Rapid. Comms. 6* (1992) 303.

[32] S. A. Lee, C. Q. Jiao, Y. Huang, B. S. Freiser, *Rapid. Comms. 7* (1993) 819.

[33] R. T. McIver, *Rev. Sci. Instrum. 41* (1970) 555.

[34] J. A. Hipple, H. Sommer, H. A. Thomas, *Phys. Rev. 76* (1949) 1877.

[35] M. Wang, A. G. Marshall, *Anal. Chem. 61* (1989) 1288.

[36] D. L. Rempel, M. L. Gross, *J. Am. Soc. Mass Spectrom. 3* (1992) 590.

[37] C. B. Jacoby, C. L. Holliman, D. L. Rempel, M. L. Gross, *J. Am. Soc. Mass Spectrom. 4* (1993) 186.

[38] S. K. Huang, D. L. Rempel, M. L. Gross, *J. Am. Soc. Mass Spectrom. 4* (1993) 186.

[39] P. Kofel, M. Allemann, H. P. Kellerhals, K. P. Wanczek, *Int. J. Mass Spectrom. Ion Proc. 74* (1986) 1.

[40] W. J. V. d. Hart, W. J. V. d. Guchte, *Int. J. Mass Spectrom. Ion Proc. 82* (1988) 17.

[41] M. Wang, A. G. Marshall, *Anal. Chem. 62* (1990) 515.

[42] R. T. McIver, R. L. Hunter, W. D. Bowers, *Int. J. Mass Spectrom. Ion Proc. 64* (1985) 67.

[43] P. Kofel, M. Allemann, H. Kellerhals, K. P. Wancek, *Int. J. Mass Spectrom. Ion Processes. 65* (1985) 97.

[44] S. Campbell, E. M. Marzluff, M. T. Rodgers, J. L. Beauchamp, M. E. Rempe, K. F. Schwink, D. L. Lichtenberger, *J. Am. Chem. Soc. 116* (1994) 5257.

[45] M. S. B. Munson, F. H. Field, *J. Am. Chem. Soc. 88* (1966) 2621.

[46] W. Aberth, K. M. Straub, A. L. Burlingame, *Anal. Chem. 54* (1982) 2029.

[47] M. Barber, B. N. Green, *Rapid. Comms. 1* (1987) 80.

[48] C. J. McNeal, *Anal. Chem. 54* (1982) 33A.

[49] M. G. Blain, S. Della-Negra, H. Joret, Y. LeBeyec, E. A. Schweikhart, *Phys. Rev. Lett. 63* (1989) 1625.

[50] E. W. Muller, *Z. Phys. 131* (1951) 136.

[51] M. G. Inghram, R. Gomer, *J. Chem. Phys. 22* (1954) 1279.

[52] K. Tanaka, *Rapid Comms. 2* (1988) 151.

[53] M. Karas, D. Bachmann, U. Bahr, F. Hillenkamp, *Int. J. Mass Spectrom.Ion Proc. 78* (1987) 53.

[54] P. Kebarle, L. Tang, *Anal.Chem. 65* (1993) 972A.

[55] M. Dole, L. D. Ferguson, L. L. Mack, R. L. Hines, R. C. Mobley, M. B. Alice, *J. Chem. Phys 49* (1968) 2240.

[56] J. V. Iribarne, B. A. Thomson, *J. Chem. Phys. 64* (1976) 2287.

[57] R. J. Pfeifer, C. D. Hendricks, *AIAAJ 6* (1968) 496.

[58] I. Hayati, A. I. Bailey, T. F. Tadros, *J. Colloid Interface Sci. 117* (1987) 205.

[59] D. P. H. Smith, *IEEE Trans. Ind. Appl. 1A-22* (1986) 527.

[60] A. Gomez, K. Q. Tang, *Physics of Fluids 6* (1994) 404.

[61] B. A. Thomson, J. V. Iribarne, *J. Chem. Phys. 71* (1979) 4451.

[62] J. B. Fenn, *J. Am. Soc. Mass Spectrom. 4* (1993) 524.

[63] O. V. O. Loo, D. R. Goodlett, R. D. Smith, J. A. Loo, *J. Am. Chem. Soc. 115* (1993) 4391.

[64] C. V. Robinson, E. W. Chung, B. B. Kragelund, J. Knudsen, R. T. Aplin, F. M. Poulsen, C. M. Dobson, *J. Am. Chem. Soc. 118* (1996) 8646.

[65] O. V. Nemirovskiy, R. Ramanathan, M. L. Gross, *J. Am. Soc. Mass Spectrom. 8* (1997) 809.

[66] A. G. Marshall, C. L. Hendrickson, G. S. Jackson, *Mass Spectrom. Rev.* (1998)

[67] P Kofel, M Allemann, H Kellerhals, K P Wancek, *Int. J. Mass Spectrom. Ion Processes.* 65 (1985) 97

[68] S. Guan, G. Z. Li, A. G. Marshall, *Int. J. Mass Spectrom. Ion Processes. (1997)*

2.0 Instrumentation

A Bruker Daltonics BioAPEX 94e Fourier transform ion cyclotron resonance mass spectrometer (Billerica, USA) with a Magnex Scientific (Abingdon, Oxford) 9.4 Tesla superconducting, horizontal bore magnet, has been employed in the work reported in this thesis. The following section will give details of this instrument.

The Bruker BioAPEX instrument consists of an ion source, in these experiments typically electrospray ionisation, connected to the ion trap via a series of differentially pumped electrostatic lenses. As already mentioned the superconducting magnet has a field of 9.4 Tesla and is therefore passively shielded to prevent strong magnetic fields interfering with apparatus within the laboratory and to allow safer maintenance of the instruments components. The ions are trapped within an infinity cell/ trap of diameter 6 cm the details and merits of such a design having been discussed in section 1.7.1. Data analysis was achieved by making use of a Silicon Graphics Indy workstation running Bruker XMASS software for instrument control and data analysis.

2.1 Electrospray Ionisation Source

In the experiments featured within this thesis the ion source utilised was the Analytica (Brandford, USA) electrospray ionisation source typically operating at a voltage of 2-3.5 kV. A schematic of the sample introduction region is shown below:

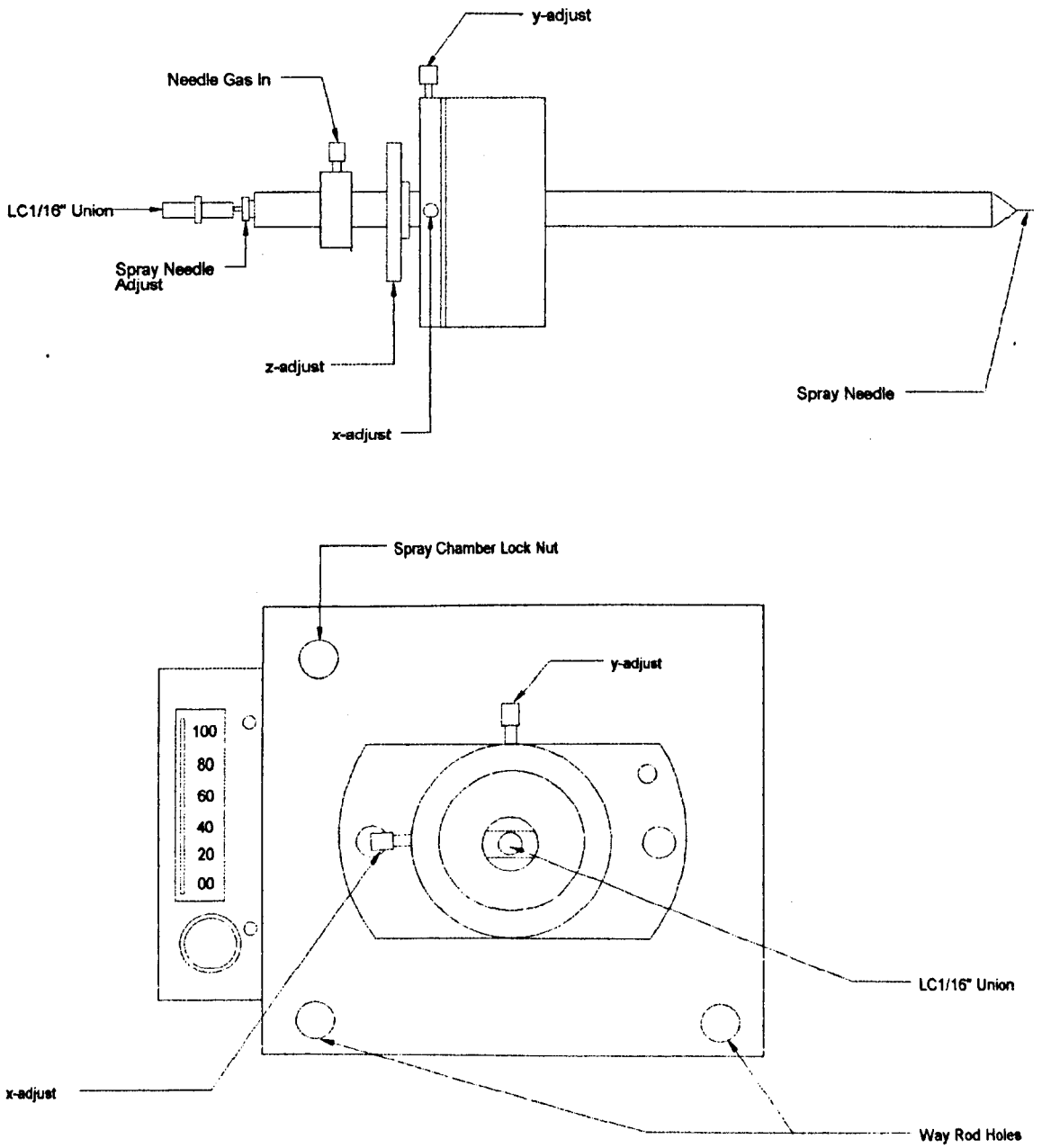

Figure 1: Schematic of the Analytica electrospray source

Figure 1 shows that the ESI sample introduction region is easily moved in the x, y and z directions by making use of fine attitude adjustment screws. The sample was pumped from a 100 μL Hamilton gas tight syringe using a Cole-Palmer programmable syringe pump at flow rates between 0.5 and 1.5 μL min^{-1}. The analyte solution passes through a small length (to minimise dead volume) of HPLC PEEK tubing into the narrow stainless steel capillary from which the solution is electrosprayed. This initial analyte introduction region is earthed for safety reasons, with the positive potential necessary for positive electrospray being generated by applying the equivalent negative voltage to the counter-electrodes (see Figure 2).

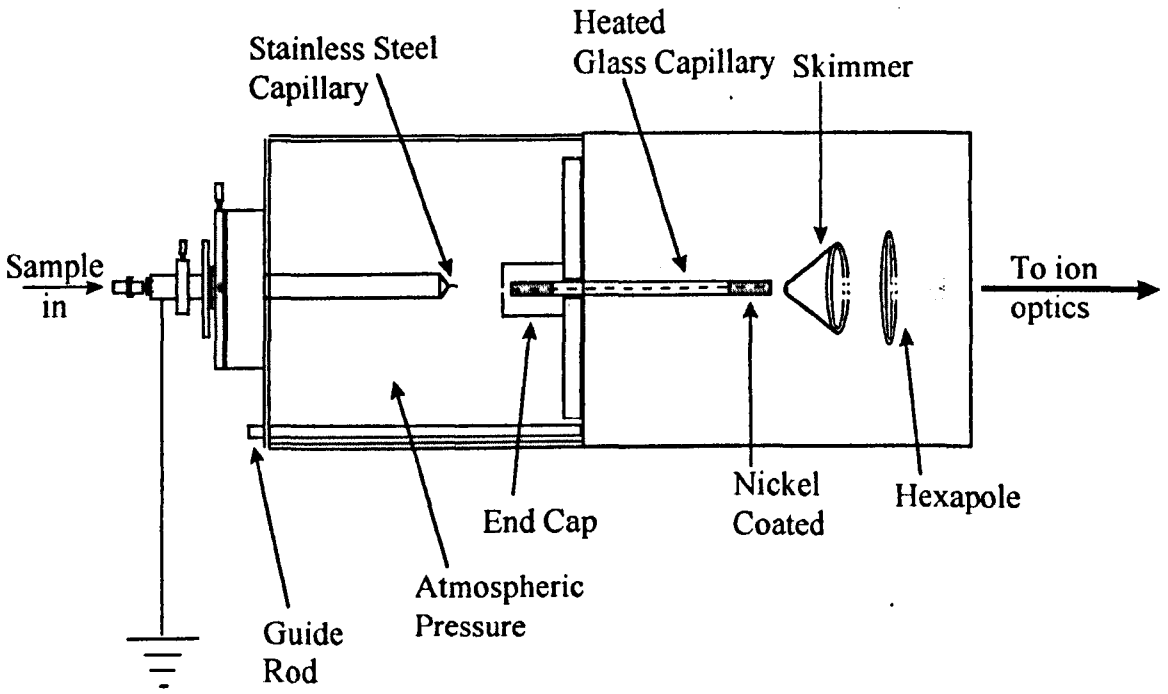

Figure 2: Schematic of the Analytica ESI source in its entirety.

The droplets formed in the region between the stainless steel capillary and the remainder of the instrument are dried using a counter-current flow of either CO_2 or N_2 gas flowing around the glass capillary and out through the hole in the end cap. This serves two purposes: (1) it prevents significant amounts of the liquid phase from entering the main

instrument and thus adversely affecting the low pressures needed for mass analysis (2) the gas heated to a temperature of between 50 and 150 ^{0}C heats the initial stages of the glass capillary as well as the air within the first stage of the source therefore increasing the efficiency of gas phase ion formation.

Any remaining solvent phase immediately after the glass capillary is removed as the ions pass through the skimmer which allows only the analyte ions that are travelling along the correct axis to enter the next stage of the source. Ions that are off-axis and any solvent that is left in the ion beam are removed by the narrow entrance (~ 1 mm) to the skimmer cone and its focusing nature. Placed immediately after the skimmer is a small hexapole (frequency 5.3 MHz and peak to peak voltage of 100V) which temporarily traps and bunches the ions exiting the source. Due to the pulsed nature of the FT-ICR technique i.e. the intermittent opening of the analyser cell for detection, the continuous ion production of a normal ESI source would result in a vast majority of the ions produced being wasted as they "bounced" off the first trap plate. The ions are therefore delayed by the hexapole for anywhere between 0.25 and 6 seconds and during this time the experimental sequence has completed a cycle and the newly produced ions can be introduced into the cell. This hexapole delay leads to greater efficiency and therefore sensitivity and also allows analyte solutions that do not easily produce gas phase ions to be investigated. For example, a typical experiment in water/ methanol + 1% acetic acid would need a hexapole delay of 0.5 - 2 secs, while a protein in a buffer solution such as ammonium acetate would need approximately 3 - 4 times this. This builds up an ion population prior to introduction to the cell, in the hexapole.

Since this region of the electrospray source is at a pressure of approximately 2 x 10 $^{-7}$ mbar, it can also be used to increase the amount of fragmentation seen in capillary-skimmer collision induced dissociation experiments. Increasing the hexapole delay gives

the molecule ions more chance of colliding with neutrals and other ions, and fragmenting, than if the ions were introduced directly into the cell. The ions within the hexapole are still relatively energetic, and the fact that the pressure within the hexapole is quite high compared with the analyser cell means that there is greater fragmentation information after longer delays. The region containing the glass capillary and the hexapole is pumped using a combination of an Edwards Rotary pump and a turbo-molecular pump.

2.2 Ion Transfer Optics

The diagram below is simplified representation of the electrostatic lenses that are required to pass the ions from the ion source into the cell through the "mirror" effect of the magnetic field.

This transfer region is differentially pumped by Edwards cryo-pumps. These gradually reduce the pressure from atmosphere in the electrospray source to around 2-5 x 10^{-10} mbar in the infinity cell. The cryo-pumps are backed by Edwards mechanical rotary pumps that are used to reduce the pressure in the transfer region from atmosphere to around 5 x 10^{-3} mbar prior to the cryo-pumps being started. This prevents a build up of impurities from the air on the charcoal adsorbers within the cryo-pumps. Pressures in the different regions of the instrument are monitored using a variety of Piranni and cold ion gauges. The cold ion gauges are used to monitor the lowest pressures, for instance in the cell of the FT-ICR mass spectrometer.

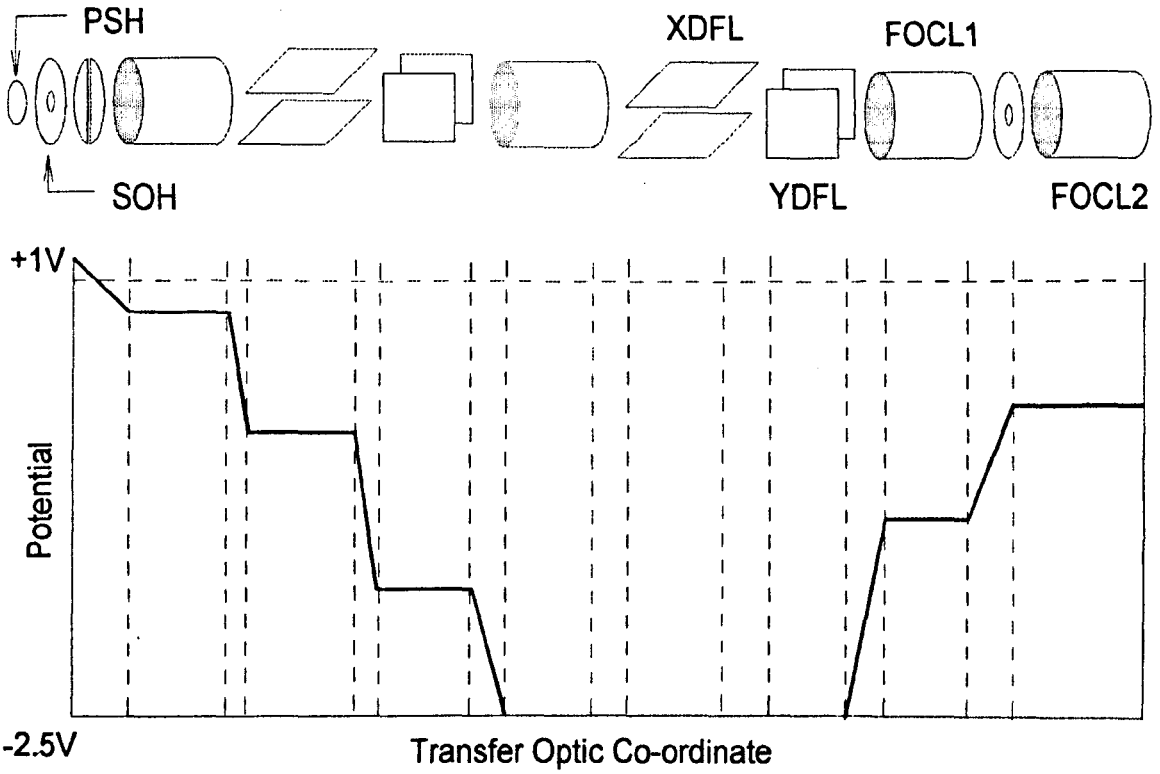
PSH
SOH
XDFL
YDFL
FOCL1
FOCL2
+1V
-2.5V
Potential
Transfer Optic Co-ordinate

3.0 Electrospray Ionisation of Papain and Calmodulin

3.1 Introduction

Electrospray ionisation (ESI) is the most important ionisation method in use today for the study of biological non-covalent interactions by mass spectrometry. It is an extremely "soft" method of ionisation in that the analysis of large and small biomolecules is possible without excessive fragmentation. Non-covalent interactions can thus be observed after ionisation and important information on stoichiometry and relative binding constants can be evaluated. [1, 2]

Proteins and peptides can be ionised from a variety of solvents via electrospray including solvents that are known to allow them to retain their natural conformations. Such solvents include buffers such as ammonium acetate, ammonium sulfate and ammonium citrate. These solvents do have some disadvantages, including a reduction in sensitivity compared with typical ESI solvent systems such as methanol/ water (1:1) or acetonitrile/ water (1:1). ESI of these buffered systems results in ions with lower charge state which has implications for particularly large biomolecules being analysed on limited mass-range instruments. Such reductions in charge state have been attributed to the fact that the proteins are in a folded "natural" conformation. [3-5]This means that there are fewer accessible sites available for ionisation due to the more compact conformation of the protein in its natural state.

Denaturing solvent systems such as methanol/ water plus 1% formic acid are useful in electrospray ionisation, since they allow a large distribution of charge states to be detected: the typical bell shaped distribution of electrospray. From this distribution it is possible to calculate an accurate molecular mass for the analyte molecule, due to the numerous measurements of the same value obtainable from the charge distribution of the

electrospray spectrum. These solvent systems can also be useful, since they can break up parts of the tertiary structure of the protein, allowing greater sequence information to be acquired from experiments such as collision-induced dissociation (CID) compared with similar experiments involving buffer systems. Again this can be explained by the fact that organic solvents "open up" the structure of the analyte protein. The table below gives physical parameters of the proteins used in this study.

Papain	
Molecular Weight (Average)	23,421.34 Da
Molecular Weight (Mono)	23,406.52 Da
Iso-electric point	8.75
Extinction coefficient (280 nm)	53610
Sequence	IPEYVDWRQKGAVTPVKNQGSCGSCWAFSAVVTIEGIIKIR TGNLNEYSEQELLDCDRRSYGCNGGYPWSALQLVAQYGI HYRNTYPYEGVQRYCRSREKGPYAAKTDGVRQVQPYNE GALLYSIANQPVSVVLEAAGKDFQLYRGGIFVGPCGNKVD HAVAAVGYGPNYILIKNSWGTGWGENGYIRIKRGTGNSY GVCGLYTSSFYPVKN
Calmodulin	
Molecular Weight (Average)	16,616.821 Da
Molecular Weight (Mono)	
Iso-electric point	4
Extinction coefficient (280 nm)	1280
Extinction coefficient (276.5 nm)	1560
Sequence	ADQLTDEQIAEFKEAFSLFDKDGDGTITTKELGTVMRSLG QNPTEAELQDMINEVDADGNGTIDFPEFLNLMARKMKDT DSEEELKEAFRVFDKDGNGFISAAELRHVMTNLGEKLTDE EVDEMIREADVDGDGQVNYEEFVQVMMAK

3.2 Experimental

3.2.1 Calmodulin Synthesis and Purification

DNA-encoded calmodulin was produced by Dr. Daniel Lafitte *et al* and purified by column chromatography. [6, 7]The purity of the protein, which was found to be greater than 99%, was checked by SDS polyacrylamide gel and high-pressure capillary

electrophoresis. ESI FT-ICR mass spectrometry experiments were carried out using ultra-pure water (Elga system) and plastic laboratory equipment to minimise unwanted salt contamination such as sodium and magnesium ions. Before introduction to the instrument calmodulin was further purified by desalting the sample using a Pharmacia Biotech Sephadex (Uppsala, Sweden) PD 10 column. This entailed equilibrating the column using the solvent system of choice, in this case ammonium acetate (5mM, pH 5.8) or water, and then dissolving 2-3 mg of calmodulin in 2.5 mL ammonium acetate or water. This was introduced to the column, the protein "washed" through the column with buffer and approximately 10 fractions (1 mL each) were collected. The protein content of each of these fractions was tested by placing a small aliquot of the fraction into a separate vial and then introducing an equivalent aliquot of Bradford Reagent. It was usually found that fractions 3-6 contained calmodulin, but to minimise unwanted salt contamination only fractions 4 and 5 were used. The concentrations of these aliquots were determined by UV absorption on a Jasco V-550 spectrophotometer. The molar extinction coefficient used for these experiments was ε_{276nm}=1560 $M^{-1}cm^{-1}$ [11]and the concentrations of the fractions were found to be between 20 and 25 μM.

3.2.2 Papain Sample Preparation

Initially papain was obtained as a lyopholised powder from Sigma (Poole, UK). This presented many problems, especially due to impurities contained in the sample. Primary investigations revealed a great difficulty in observing this particularly large protein by electrospray ionisation (ESI), even when dissolved in standard (and non-standard) solvent systems such as methanol/water + 1-3 % formic acid. These problems were blamed on the high concentration of salt in the sample. Methods for desalting the sample were

investigated including tri-chloroacetic acid (TCA) precipitations, "mini" HPLC, HPLC and other chromatographic methods. Initial experiments with TCA precipitations and HPLC were unsuccessful. The ESI signal was intermittent and of very low quality. Experiments making use of the Pharmacia Biotech PD 10 Sephadex gel chromatography columns were the most successful, with samples made up in solvent systems consisting of methanol/ water + 3% formic acid (Figures 6a) and ammonium acetate (5mM, pH 4.6-5.8) (Figures 6b). This however, still produced low quality spectra. A variety of papain samples were then purchased from Sigma (Poole, UK), and all were purified by each of the methods mentioned. The best quality spectra were found to be obtained from a sample consisting of a papain suspension in sodium acetate + 1% thymol purified using the Pharmacia Biotech PD 10 Sephadex gel chromatography columns.

3.2.2.1 Tri-chloroacetic acid precipitations

This procedure involved precipitating the protein from solution which with the judicious use of a centrifuge allowed the impurities to be removed.

The following steps were followed to clean up the protein sample purchased as a lyopholised powder:

1) Make up 1 g of tri-chloroacetic acid in 1 ml of water. (Solution 1)

2) Add approximately 2 mg of protein to 1 ml of water. (Solution 2)

3) Add 33 µl of solution 1 to solution 2 and mix well.

4) Centrifuge for half a minute.

5) Discard liquid and retain the pellet at the bottom of the micro-centrifuge tube.

6) Centrifuge again and discard the remaining liquid.

7) Add 1 mL of water to the pellet and add 0.1 µL aliquots of ammonia to the solution until the solution turns clear.

8) Repeat steps three to seven approximately three times.

9) Reconstitute the solution in the solvent system of choice for electrospray.

3.2.2.2 "Mini" HPLC

This method consisted of making use of a small HPLC column (1 x 10 mm), interior volume 5 µl produced by Michrom BioResources. This was held in a holder which was connected in line with a small pump and a rheodyne. The column was initially washed with 80% acetonitrile/ 20% water and 0.1% formic acid. 25 µl of a sample (concentration no greater than 20 µg/ 5 µl) were injected via the rheodyne and the salt washed away with a solution of 98% water/2% acetonitrile + 0.1% formic acid. The column was then

reversed in its holder and the sample eluted with 10 µl aliquots of a solution made up of 98% acetonitrile/ 2% water. The resulting aliquots were checked for pure protein using a Micromass TOFSpec (a time-of flight instrument) with MALDI source. Both the lyopholised powder and the crystallised suspension of papain were purified and analysed using this process.

The matrix chosen for the experiment was 2,4-dihydroxybenzoic acid (DHB) made up as 10 mg/ml in acetonitrile/ water (1:1). 20 µl of this was mixed with a 10 µl aliquot of the previously purified protein. No signal was observed for papain on the TOFSpec instrument after desalting with this method. The method was checked for effectiveness using cytochrome C and insulin with positive results for these proteins.

3.2.2.3 High-Pressure Liquid Chromatography (HPLC)

The HPLC system used for this procedure was the Hewlett Packard 1100 series with a Waters Symmetry C_{18} column (2.1 x 150mm, 5µm i.d.). Solvent systems were 0.1% tri-fluoroacetic acid (TFA) in HPLC grade water and 0.1% tri-fluoroacetic acid (TFA) in 80% HPLC grade acetonitrile/ 20 % HPLC grade water with a flow of 0.2 ml min^{-1}. (Figure 1)

1 mg of protein was dissolved in 1 mL of water and 50 µl aliquots were injected into the system. The resulting fractions were collected, combined and fast freeze dried using a GeneVac SF60 VacStop vacuum centrifuge system. The protein purity of the sample after this desalting process was again checked using a Micromass TOFSpec with MALDI source at Smith-Kline Beechams Laboratories in Harlow, Essex. Matrix and sample conditions were the same as those used for the "mini" HPLC purification procedure. The TOFSpec spectra obtained contain only low mass fragments for papain and this is

postulated to be the result of the protein degrading during the freeze drying process (see Figures 2 and 3).

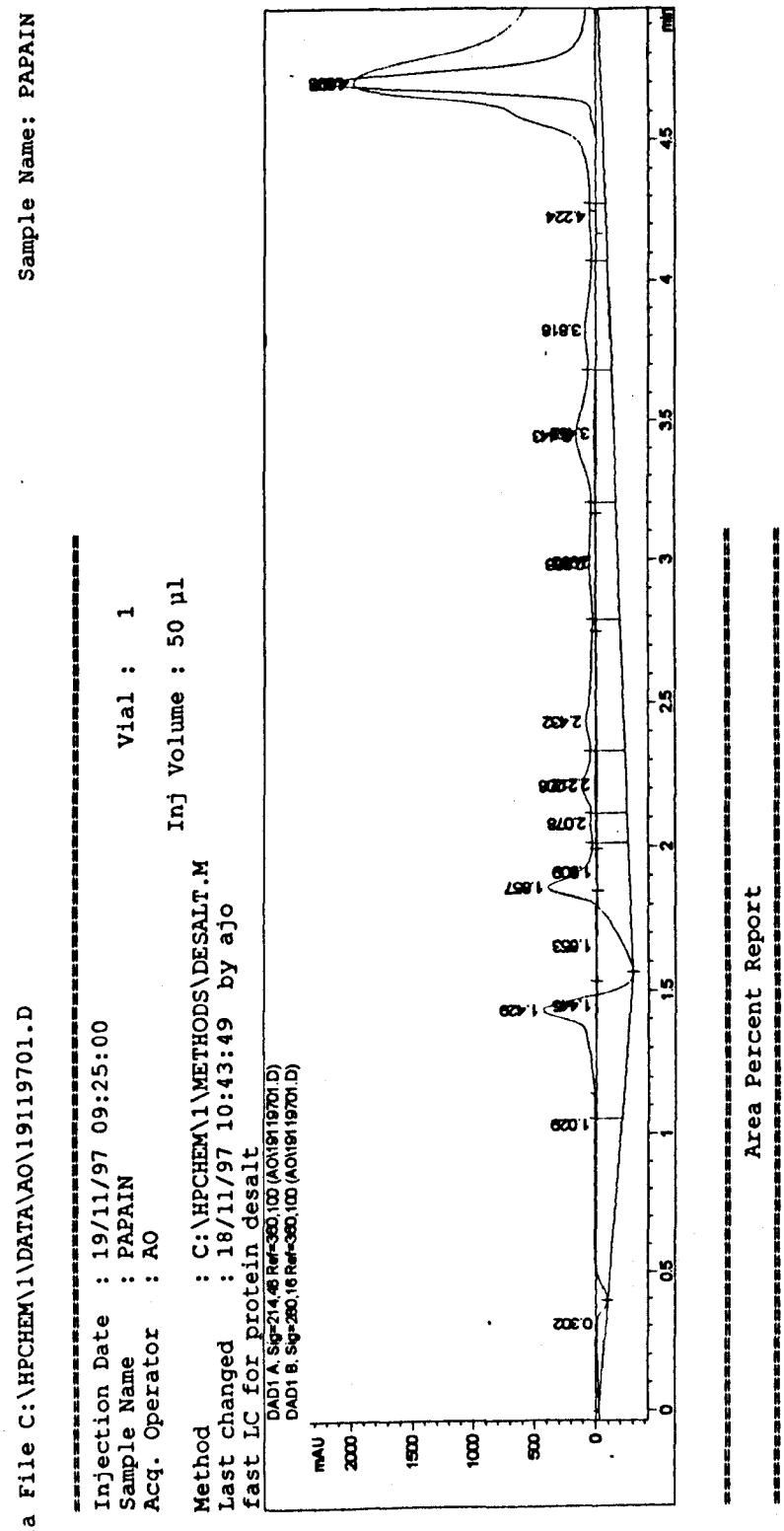

Figure 1: HPLC plot of papain using Hewlett Packard 1100 series system.

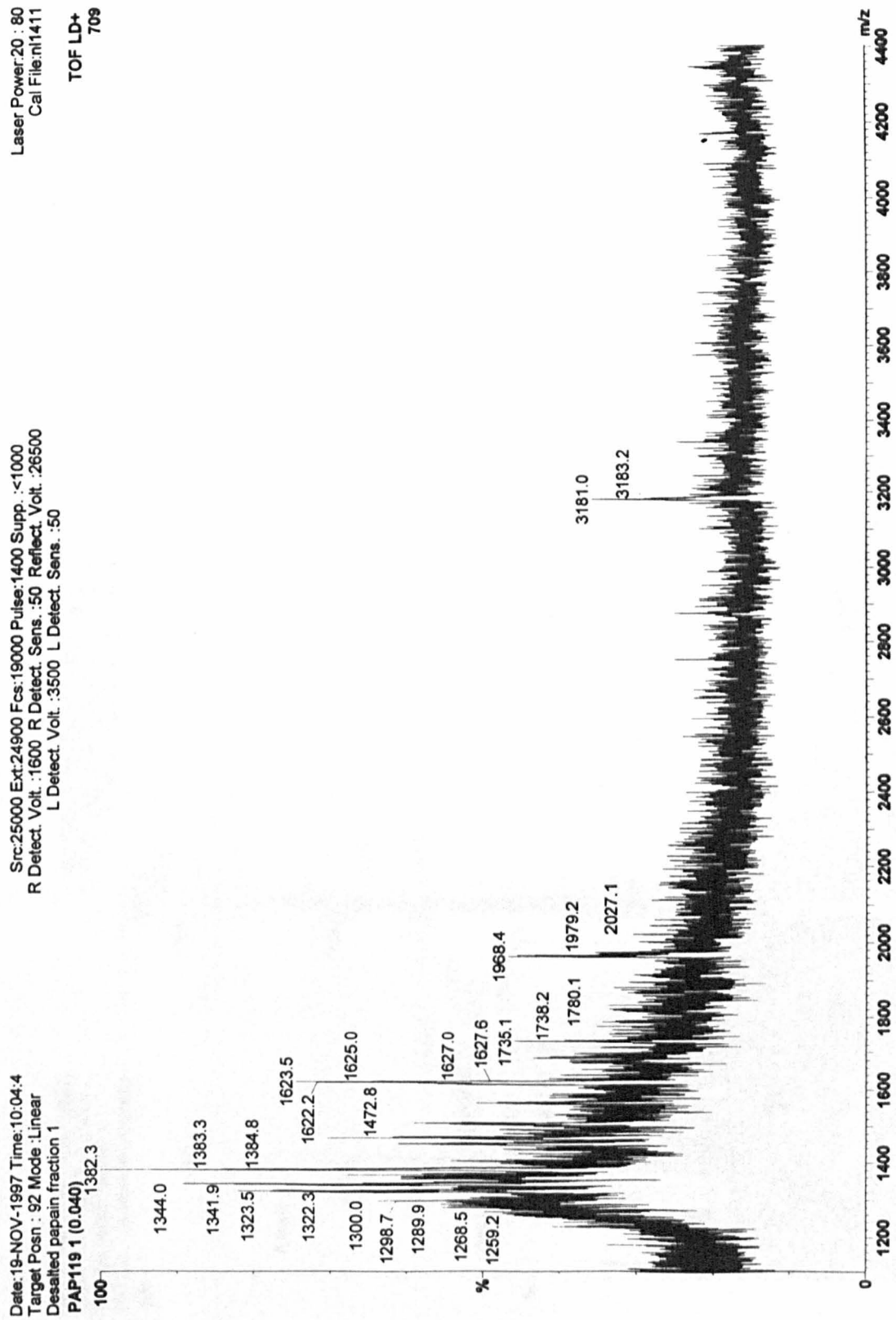

Figure 2: Micromass TOFSpec MALD/I mass spectra of papain (low mass range).

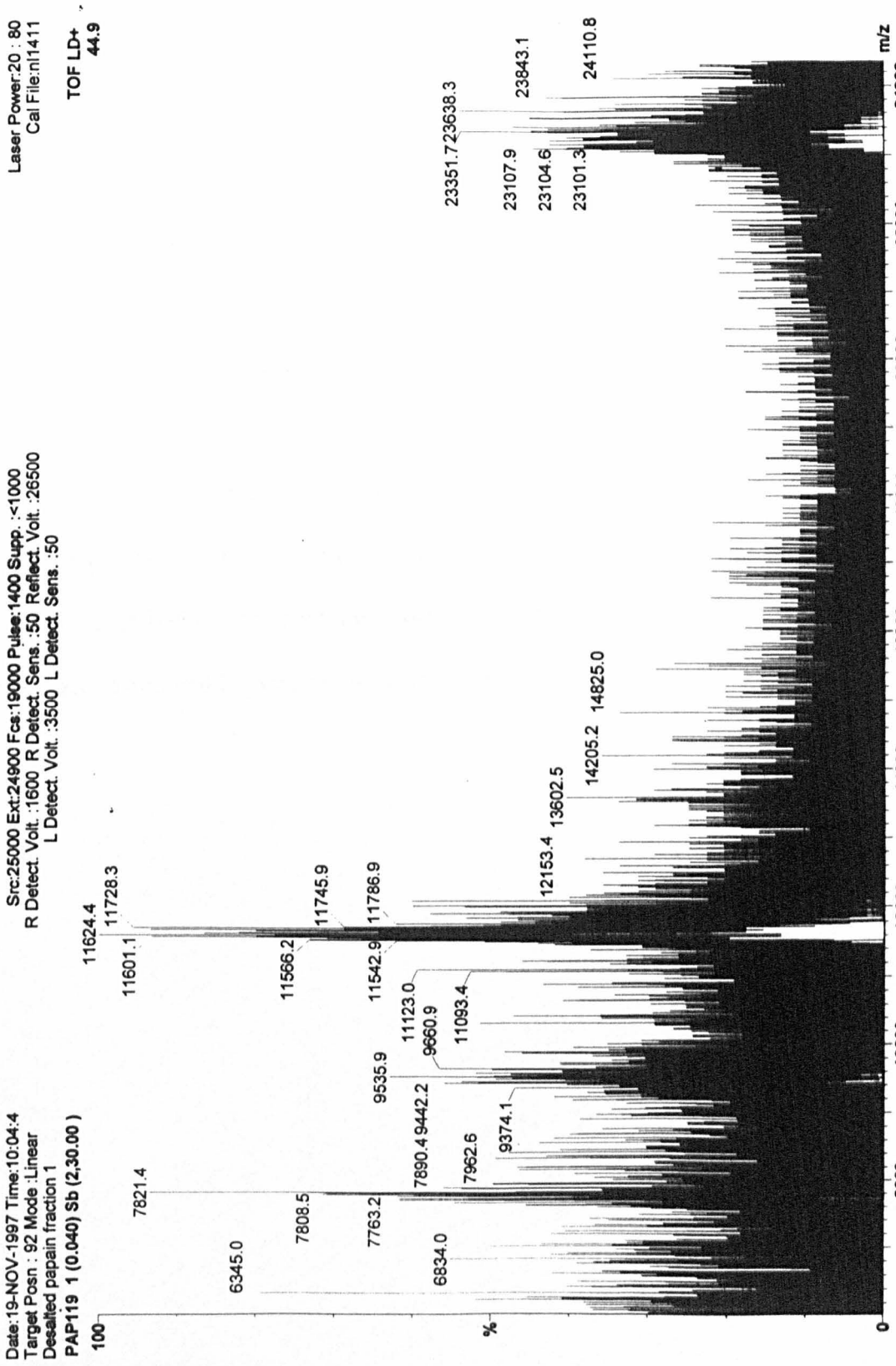

Figure 3: Micromass TOFSpec MALD/I mass spectra of papain showing poor molecule ion.

TOFSpec experiments where sample was directly spotted onto the MALDI slide after HPLC purification showed some small peaks of very poor quality corresponding to the molecule ion (see Figure 3 above).

The desalted sample was also evaluated using a Micromass Q-Tof instrument, a quadrupole-orthogonal time-of-flight (TOF) instrument with Z-spray™ nano-electrospray source. The spectra were acquired in methanol/ water + 1% acetic acid and also in ammonium acetate (5mM, pH4.6) . Again signal was observed immediately after the HPLC desalting process, but not at all after freeze drying (see Figures 4 and 5). It may be possible that papain, being a cysteine protease was undergoing auto-digestion during the relativley long period of time for the freeze drying process. The spectra of the sample immediately after HPLC, still contained many impurities with adducts complicating the acquired spectra and making interpretation difficult.

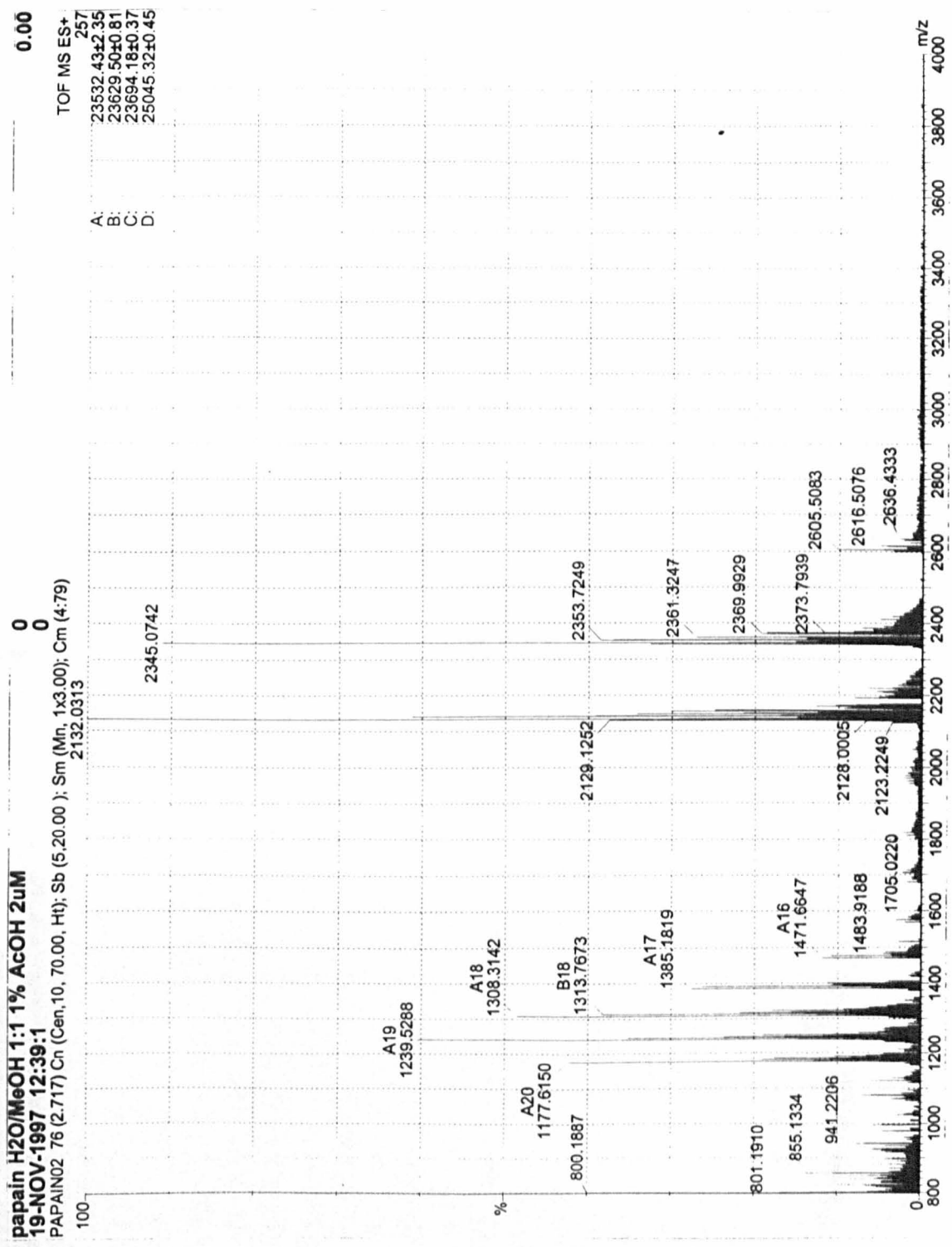

Figure 4: ESI mass spectra of papain in water/methanol + 1% acetic acid from Micromass Q-Tof instrumentation.

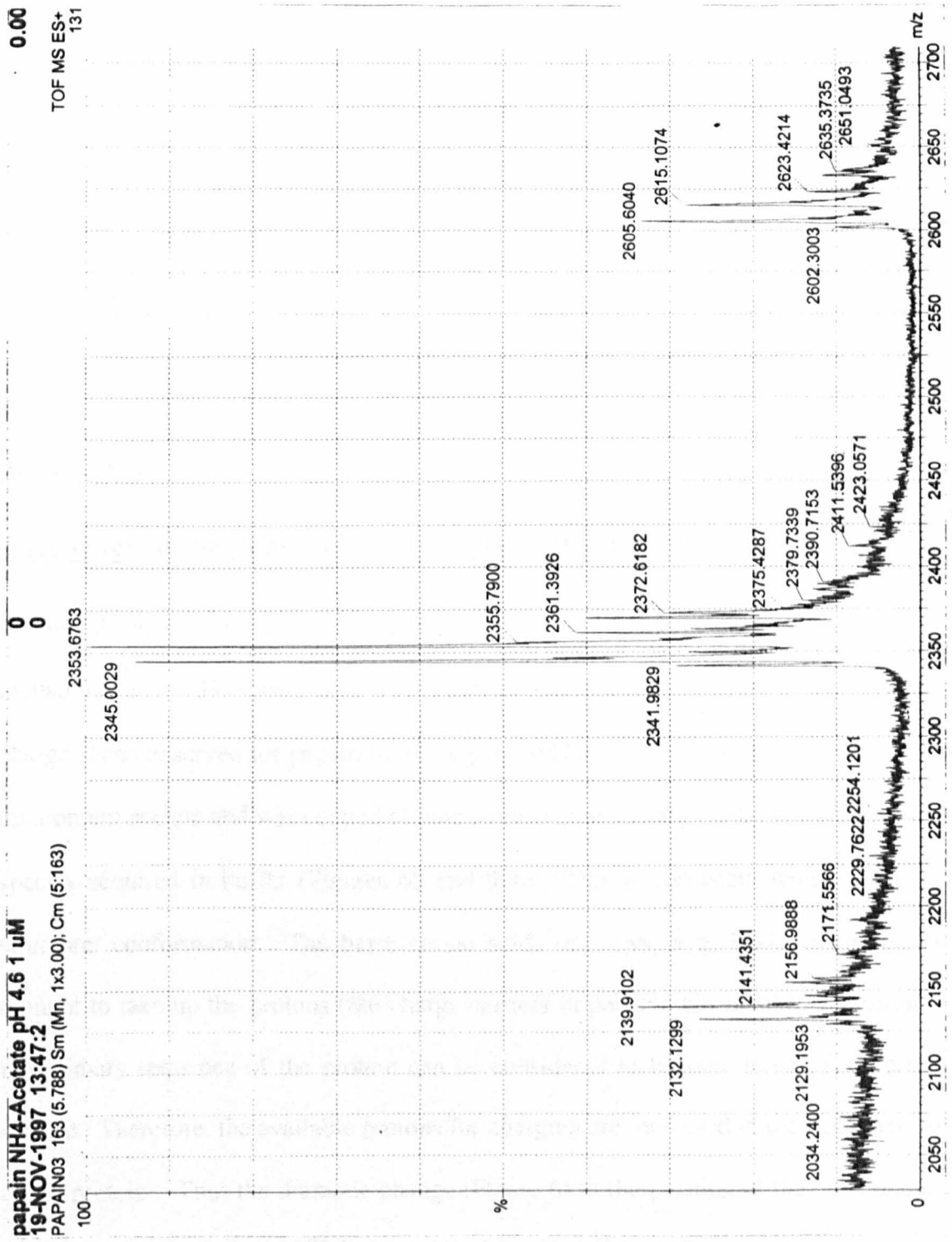

Figure 5: ESI mass spectra of papain in ammonium acetate (5mM, pH4.6) from Micromass Q-Tof instrumentation.

3.2.2.4 Electrospray Ionisation Fourier Transform Ion Cyclotron Resonance Mass Spectrometry Of Papain

Papain was obtained as a crystallised suspension in sodium acetate and 1% Thymol from Sigma (Poole, UK). This was desalted prior to electrospray ionisation using the same method as for calmodulin (see section 3.2.1), with ammonium acetate buffer (5mM, pH 4.6) as analyte solvent. This buffer pH was found to be optimum for the observation of papain: peptide complexes in electrospray ionisation FT-ICR mass spectrometry.

3.3 Results

3.3.1 Effect of Solvent on Electrospray Ionisation Mass Spectra

The difference between the proteins in 5 mM ammonium acetate, and in methanol/water + 3% formic acid was readily apparent (Figures 6 and 9). The number of charge states observed for papain in the organic solvent system was much greater than in ammonium acetate and was centred around a much higher charge state in comparison with spectra acquired in buffer (Figures 6b and 9 b). This is consistent with a more open structure/ conformation. The basic amino acids (e.g. Lys, Arg, His), which are those thought to take up the protons (the charge carriers in positive electrospray ionisation), in the primary sequence of the protein can be considered to become more exposed to the solvent. Therefore, the available protons for charging are increased in the denatured form of the protein . Thus the dramatic change (Figure 6) in the position of the most abundant charge state from $[M+18H]^{18+}$ in organic solvent and $[M+10H]^{10+}$ in ammonium acetate for papain is taken to indicate that the higher order structure was retained in ammonium acetate, whilst the organic solvent caused the protein to unfold/ become denatured.

Similar behaviour (Figure 9) was observed for apo-calmodulin with the most abundant charge state shifting from $[M+14H]^{14+}$ to $[M+8H]^{8+}$. This conclusion is consistent with ion mobility experiments conducted by Hudgins *et al*[8], Shelimov *et al*[9] and Valentine *et al*[10]. These experiments, utilising an electrospray source coupled with an ion mobility drift tube, showed that for the lower charge states produced for cytochrome C ions by electrospray ionisation in un-acidified aqueous solutions (cf. buffer solution) the natural conformation was predominant.

The ions observed for papain in organic solvent spanned the range from $[M+11H]^{11+}$ to $[M+24H]^{24+}$. The molecule ion in each of these charge states corresponded to the oxidised form of papain; very small peaks for the unoxidised ion were present (see Figure 7). The most abundant ion in each charge state corresponded to the oxidised form of papain plus a serine residue (+87 Da). Further peaks corresponded to phosphorylation plus water (+98 Da). Phosphorylation is a common modification of the amino acids serine, threonine and tyrosine. Figure 7 shows the molecule ions present in ammonium acetate ESI. The oxidised form of papain was predominant again, but this time a peak corresponding to the addition of water to the primary molecule ion was also observed. The difference between Figure 7 and Figure 8 might have been due to the solvent conditions, or the purity of the initial papain sample, more likely the latter. Figure 7 was obtained from the crystallised suspension, while Figure 8 was from the lyophilised powder. It was known that phosphate buffers had been used in the purification of this latter sample and this may explain the phosphorylation seen.

A similar change in charge state distribution was seen for apo-calmodulin, but in this case the spectra obtained from the solvent ammonium acetate showed a bimodal distribution. The most abundant charge state was still a lot lower than that from the

organic solvent system. The presence of the smaller distribution of higher charge states in the ammonium acetate spectrum showed that the protein was present in more than one conformation in the gas phase. The major conformation however, was the active or "natural" dumbbell shape. (see section 4.3)

Figures 10 and 11 show enlargements of the most abundant charge states in ammonium acetate and organic solvent respectively. As can be seen in Figure 10, it was difficult to completely remove all calcium from the analyte solution especially when using buffer as solvent. However, with great care the calcium adducts could be limited to just one. In both Figures 10 and 11 sodium adducts and water loss were observed.

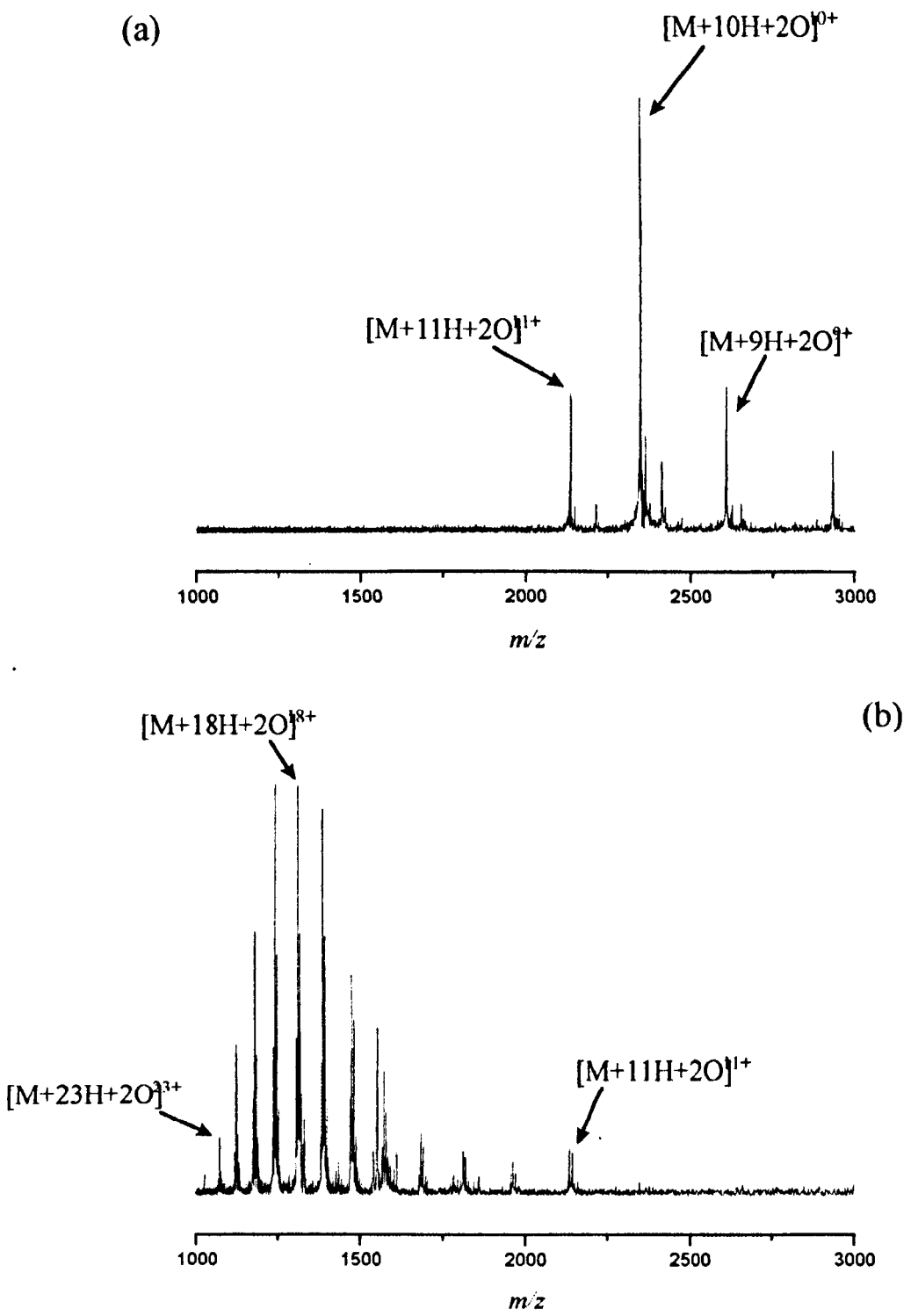

Figure 6: Comparison of the spectra acquired for papain in (a) ammonium acetate (pH4.6, 5mM) and (b) methanol/ water (1:1) + 3% formic acid.

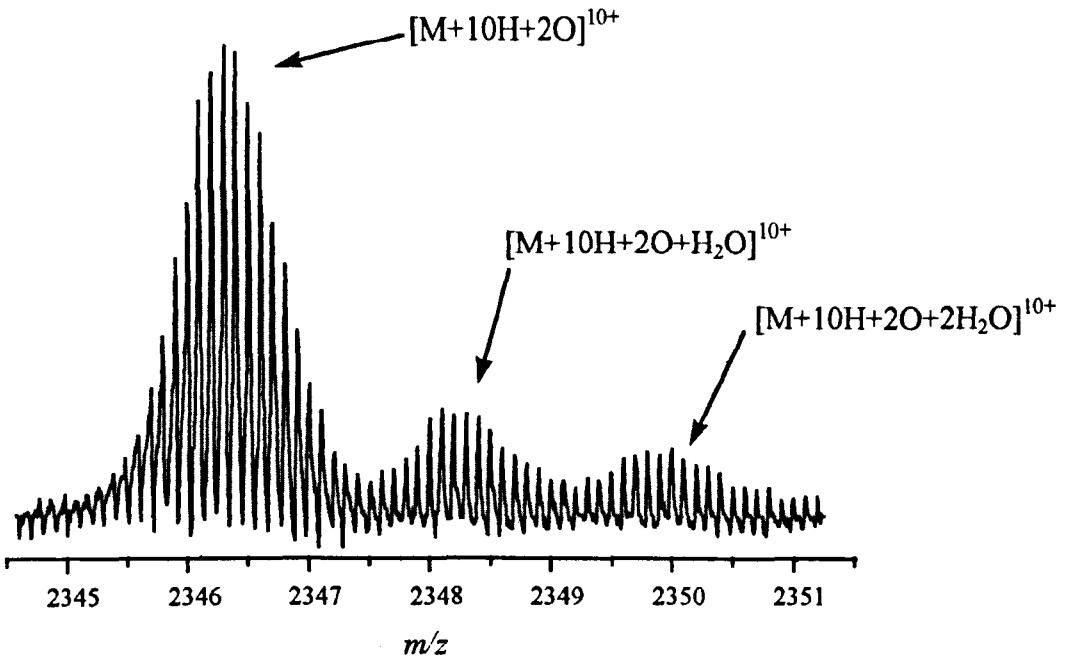

Figure 7: Close up of the 10^+ charge state of papain in ammonium acetate (5 mM, pH 4.6).

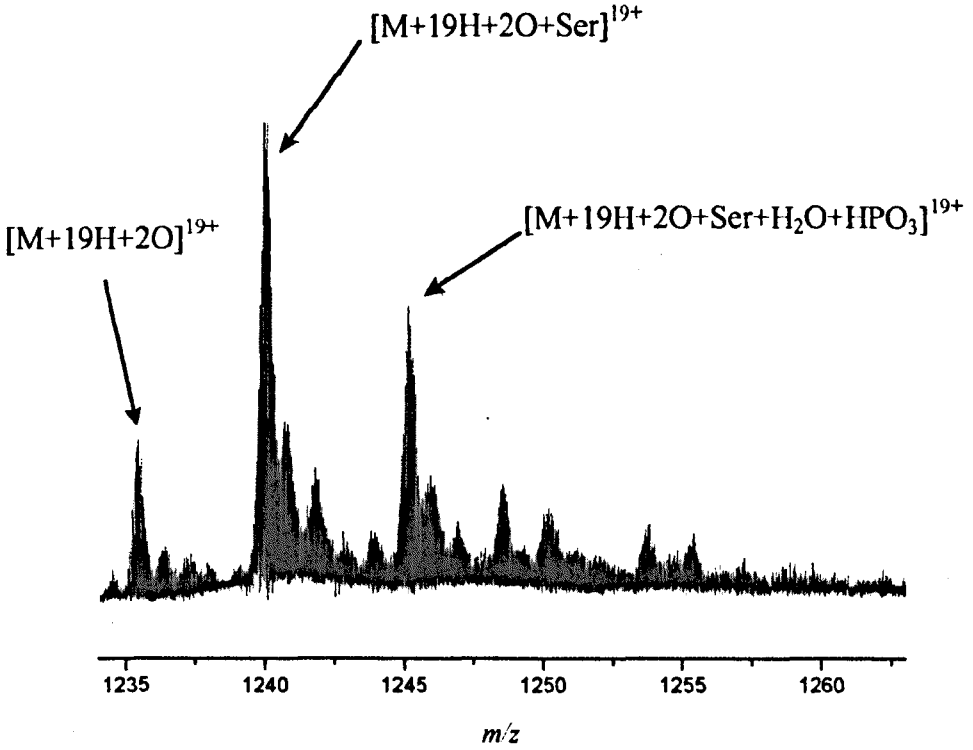

Figure 8: A close up of the 19^+ charge state of papain in methanol/ water + 3% formic acid.

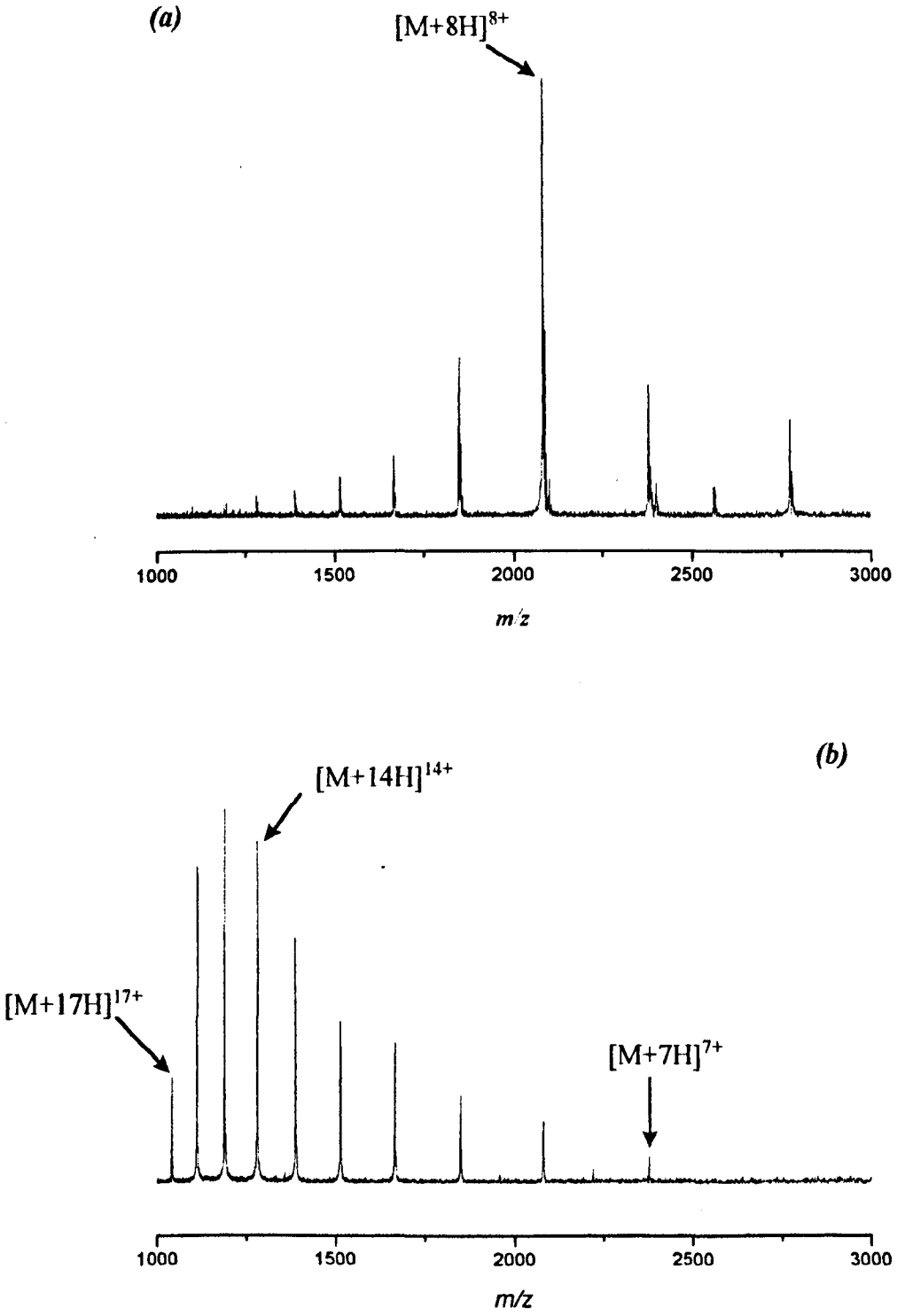

Figure 9: Comparison of the spectra acquired of calmodulin in (a) ammonium acetate (pH 5.8, 5mM) and (b) acetonitrile/ water (1:1) + 1% formic acid.

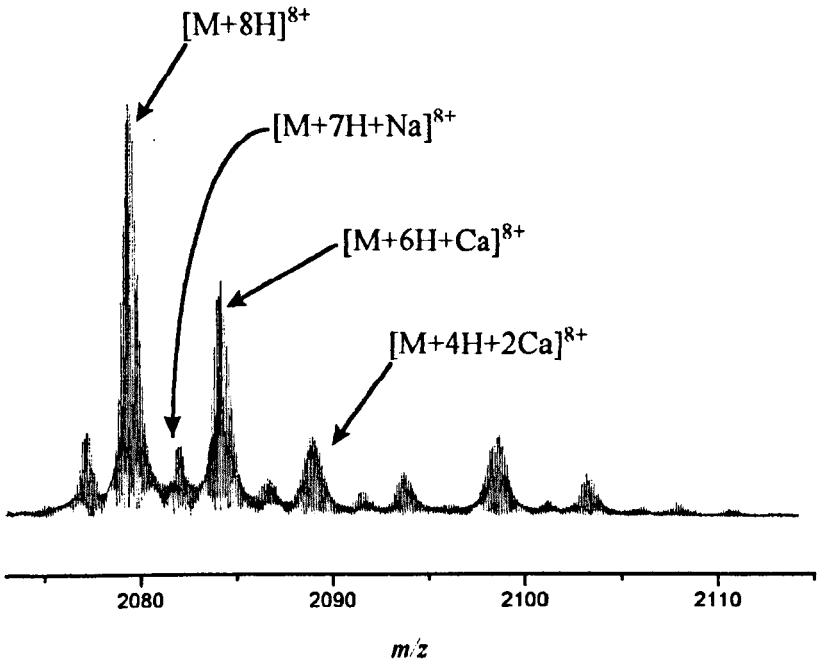

Figure 10: Close up of the 8^+ charge state of calmodulin in ammonium acetate (5mM, pH 5.8). Note the calcium.

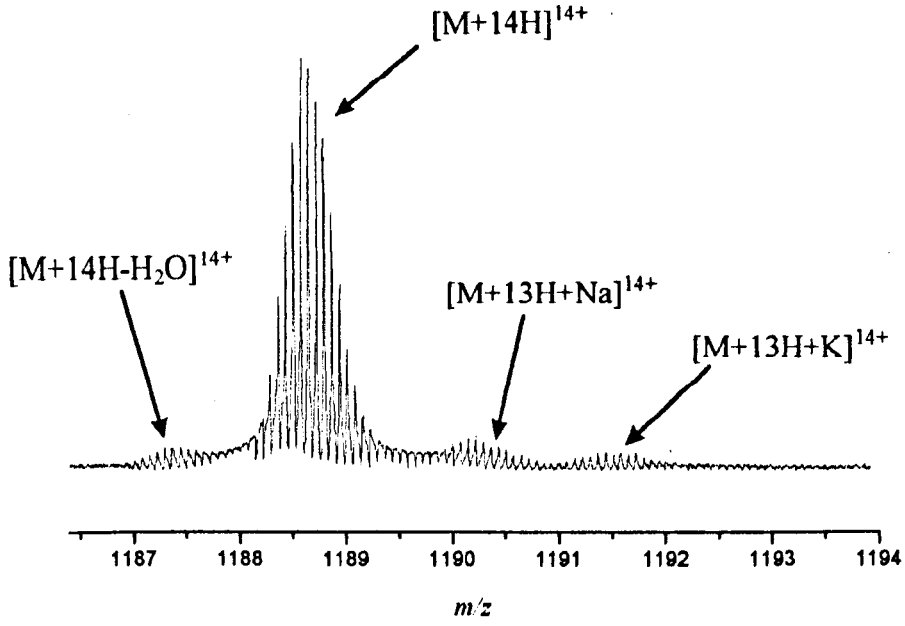

Figure 11: Close up of the 14^+ charge state of calmodulin in methanol/ water + 2% formic acid.

3.3.2 Capillary-Skimmer Collision-Induced Dissociation of Papain

A preliminary study was made using the FT-ICR, into the effect of solvent on the fragmentation pattern obtained by capillary-skimmer CID (see Figure 12). For papain in methanol/ water (1:1) + 3% formic acid, fragmentation seemed to consist of mainly y fragments from y_{82} to y_{92} (see tables 1a and 1b). The remaining peaks were assigned as either sequential water loss up to a maximum of three, or sequential water addition up to a maximum of two, for each of the *y* fragments. There were also a few peaks that were tentatively assigned to particular z and x fragments, however, there were no series of z and x fragments. The remaining peaks that were not identified could have been due to a variety of internal fragments. The great abundance of information available from this type of CID allowed the sequence of the protein from the C-terminus to be matched with some accuracy and thus provided a method for checking the protein for modifications.

By contrast the capillary-skimmer CID mass spectra (see Figure 13) obtained from analyte solutions utilising ammonium acetate as the solvent produced far less information on the protein (see table 2). Both sets of experiments were conducted at a capillary voltage and a skimmer voltage of approximately 160 V and 3 V respectively with an ionisation delay (delay applied to the hexapole) of 4 secs. A comparison of the mass spectra (Figures 12 and 13) show a dramatic difference in the amount of fragmentation peaks present. This lack of fragmentation could be attributed to the retention of higher order structure of the protein in solution when ammonium acetate and other buffers were used as analyte solvents. The resulting compact structure, which resulted in lower charge states than those produced for an analyte solution made up in polar solvents, means that the energy imparted to the parent molecule ion during the CID event was considerably less. The fact that the compact structure was retained in solution can be considered to

contribute to the fact that less structural information was obtained from the buffered analyte solution compared with the polar solvent system.

The fragments that are produced mainly come from the break up of the proteins C- and N-termini i.e. the very ends of the amino acid sequence. These termini are involved in fewer intra-molecular bonding events and are thus easier to break from the bulk of the protein than those portions of the amino acid chain that are embedded deep in the centre of the protein.

The nomenclature used in the following tables for the mass spectrometric fragmentation of peptides and proteins is described pictorially below:

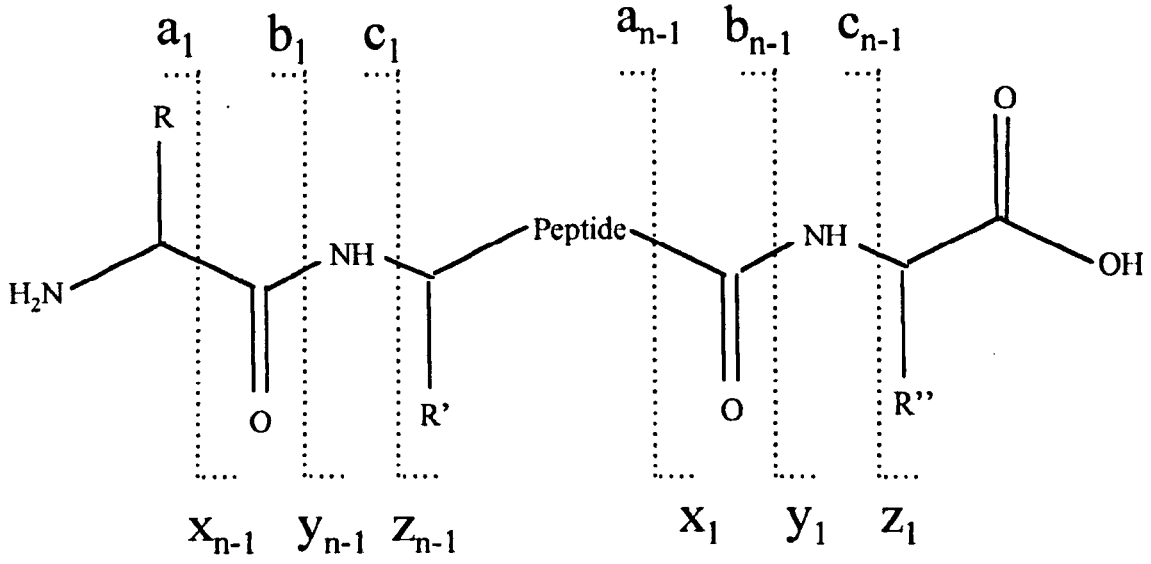

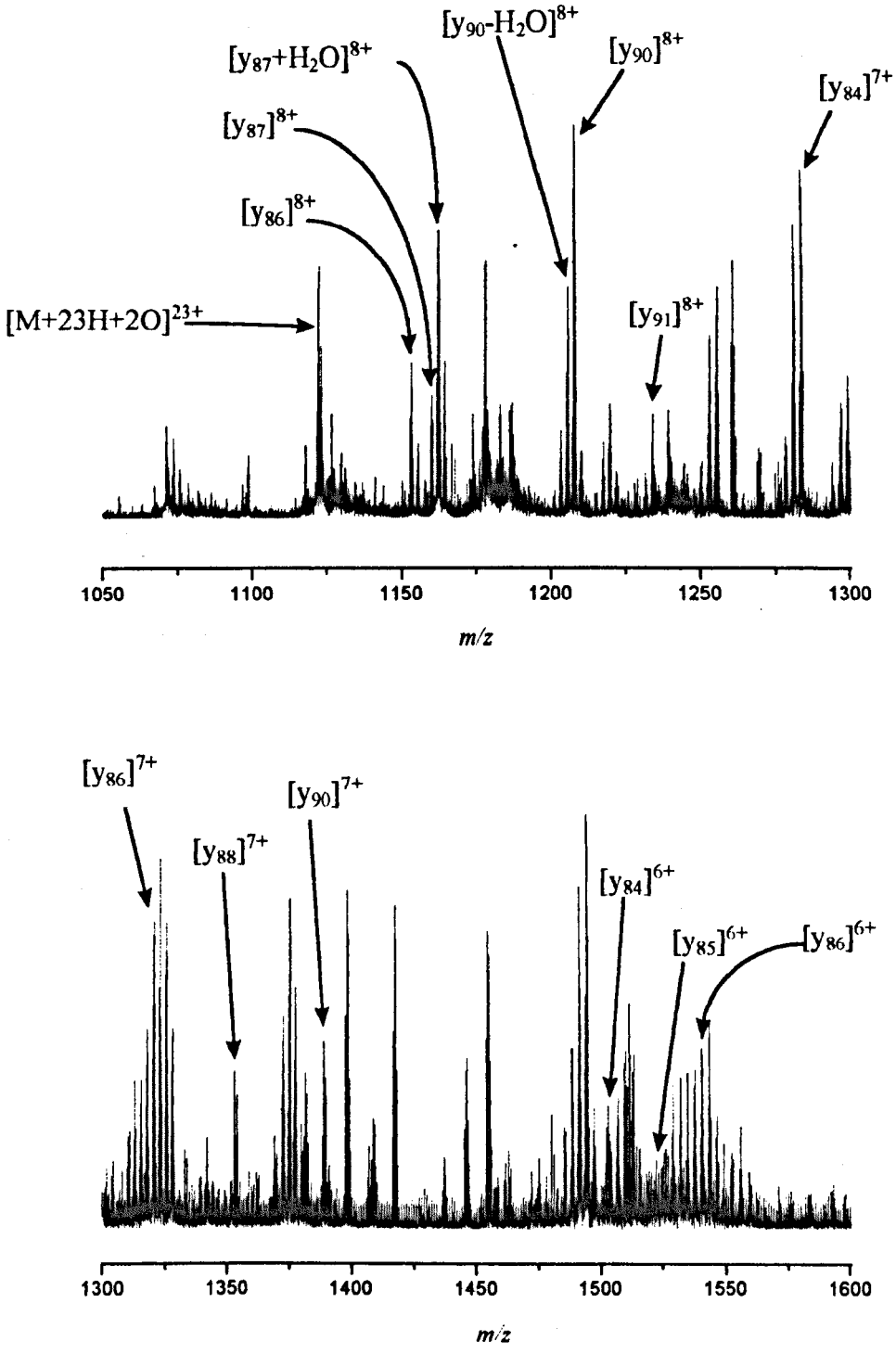

Figure 12: Capillary-skimmer CID of papain in methanol/ water + 3% formic acid.

Mass	Charge	Assignment	% Error	Mass	Charge	Assignment	% Error
4874.188	5	unassigned		8740.429	7	y82-2h2o	-0.02
7736.921	5	unassigned		8760.5	7	y82-h2o	-0.01
7756.01	5	unassigned		8777.52	7	y82	-0.004
7772.98	5	y72-2h2o/z72-h2o	-0.02	8842.598	7	y83-2h2o	-0.02
7790.99	5	y72-h2o/z72	-0.01	8885.55	7	unassigned	unassigned
8886.657	5	unassigned		8904.57	7	x83	unassigned
8903.67	5	x83	0.02	8920.58	7	y84-3h2o	-0.004
8921.66	5	y84-3h2o	-0.02	8939.64	7	y84-2h2o	-0.02
8939.69	5	y84-2h2o	-0.02	8956.65	7	y84-h2o	-0.01
8957.63	5	y84-h2o	-0.02	8974.67	7	y84	-0.01
8574.43	6	z80/y80-h2o		9048.63	7	y85-3h2o	-0.00
8743.54	6	y82-2h2o	-0.02	9067.69	7	y85-2h2o	-0.02
8780.51	6	y82-2h2o		9084.71	7	y85-h2o	-0.004
8806.53	6	x82		9120.71	7	unassigned	
8824.59	6	y83-3h2o	-0.02	9137.72	7	unassigned	
8842.8	6	y83-2h2o	-0.02	9163.69	7	y86-3h2o	-0.01
8860.58	6	z83/y83-h2o	-0.02	9181.71	7	y86-2h2o	-0.01
8895.61	6	unassigned		9199.71	7	y86-h2o	-0.01
8903.61	6	x83		9216.72	7	y86	-0.003
8921.63	6	y84-3h2o	-0.02	9236.72	7	y86+h2o	-0.02
8939.65	6	y84-2h2o	-0.02	9252.73	7	y86+2h2o	-0.003
8956.67	6	y84-h2o	-0.01	9270.74	7	y87-h2o	-0.01
8974.67	6	y84	-0.005	9287.78	7	y87	-0.00
8997.62	6	y84+na	-0.005	9306.75	7	y87+h2o	-0.01
9013.7	6	unassigned		9344.77	7	unassigned	
9032.68	6	unassigned		9365.83	7	y88-2h2o	-0.01
9049.66	6	y85-3h2o	-0.02	9383.88	7	y88-h2o	-0.01
9067.69	6	y85-2h2o	-0.02	9400.88	7	y88	-0.002
9085.68	6	y85-h2o	-0.02	9416.89	7	y88+h2o	0.02
9102.72	6	y85	-0.004	9435.91	7	y88+2h2o	0.01
9164.7	6	y86-3h2o	-0.03	9451.92	7	unassigned	
9182.72	6	y86-2h2o	-0.03	9597.95	7	unassigned	
9200.73	6	y86-h2o	-0.03	9615.98	7	y90-2h2o	-0.01
9217.71	6	y86	-0.01	9632.99	7	y90-h2o	-0.001
9235.74	6	y86+h2o	-0.01	9652	7	y90	-0.01
9252.75	6	y86+2h2o	-0.003	9673.95	7	y90+na	-0.01
9270.78	6	y87-h2o	-0.01	9692.96	7	unassigned	
				9708.93	7	z91-2h2o	-0.02
				9729.04	7	z91-h2o	-0.0004

Table 1a: Fragments obtained by capillary-skimmer CID of papain in methanol/ water + 3% formic acid.

Mass	Charge	Assignment	% Error
8690.473	8	y81	0.004
8775.507	8	y82	0.03
9191.754	8	unassigned	
9198.73	8	y86-h2o	-0.003
9218.7	8	y86	-0.02
9234.66	8	y86+h2o	-0.002
9250.75	8	y86+2h2o	0.02
9287.8	8	y87	-0.003
9305.821	8	y87+h2o	-0.003
9598.93	8	unassigned	
9615.957	8	y90-2h2o	-0.01
9633.98	8	y90-h2o	-0.01
9650.998	8	y90	-0.0001
9670.99	8	y90+na	0.02
9712	8	z91-2h2o	0.17
9729.04	8	z91-h2o	-0.19
9747.069	8	y91-h2o	-0.01
9764.067	8	y91	-0.00002
9779.02	8	y91+h2o	0.03
9786.08	8	y91+na	-0.009
9796.02	8	y91+2h2o	
9842.13	8	y92-2h2o	-0.61
9860.15	8	y92-h2o	-0.01
9304.797	9	y87+h2o	-0.38
9487.9	9	y89	-0.002
9555.094	9	unassigned	
9649.956	9	y90	0.01
9763.035	9	y91	0.01
9860.106	9	y92-h2o	-0.01
9875.137	9	y92	0.02
9899.115	9	unassigned	
9556.058	10	unassigned	
11217.08	10	unassigned	
13685.62	10	unassigned	

Table 1b: Fragments obtained by capillary-skimmer CID of papain in methanol/ water + 3% formic acid.

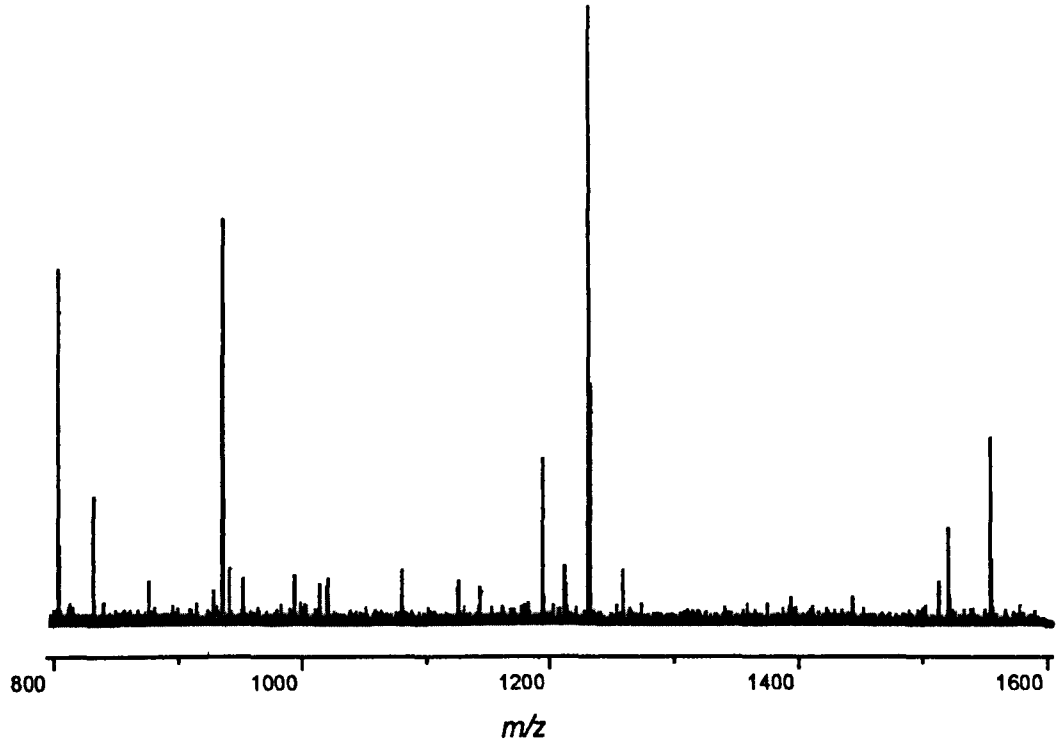

Figure 13: Capillary-Skimmer CID of papain in ammonium acetate (5mM, pH 5.8)

Mass	Charge	Assignment	%Error	Mass	Charge	Assignment	%Error	Mass	Charge	Assignment	%Error
801.50989	1	y6+2h2o	0.05	1257.662	2	c"9+h2o	-0.02	3038.764	3	unassigned	
875.50379	1	a7	0.05	1660.903	2	x15	-0.002	5022.003	5	x45-2h2o	0.01
940.4905	1	y8	-0.04	1855.047	2	c16-2h2o	-0.04	7541.551	9	x70-h2o	0.01
1079.63704	1	b'8+h2o	-0.03	1868.146	2	z'17	-0.002	10275.75	10	x96	0.008
1210.71204	1		unassigned	1901.108	2	y17+h2o	0.0008				
1230.61512	1	x10	0.1	1985.133	2	z'18	-0.1				
1552.8198	1	a'13+2h2o	unassigned	1997.212	2	y18	0.0001				
1601.90992	1	122-136	unassigned	2038.253	2	z'19	0.04				
1675.88505	1	c14-h2o	0.00008	2248.352	2	y21+2h2o	0.004				
1855.01654	1	c16-2h2o	-0.04	2284.24	2	y21+4h2o	0.01				
1868.1628	1	z'17	-0.1	2410.354	2	a22-h2o	0.05				
				3021.78	2	unassigned					
				3037.747	2	unassigned					

Table 2: Fragments obtained by Capillary-skimmer CID of papain in ammonium acetate (5mM, pH 5.8).

3.4 Conclusion

The conformations of the proteins in solution have been shown to influence ESI mass spectra. Analyte solutions that are specifically formulated to retain the natural conformations of the proteins in solution, show an electrospray mass spectrum consisting of peaks of lower charge compared to those analyte solutions where conditions necessitate an unfolded/ unnatural conformation (see Figures 6 and 9).

This change in charge distribution between buffered and MeOH/ H_2O analyte solutions is a result of the basic amino acids involved in charging , becoming more or less open to "attack" from the protons responsible for charging in electrospray ionisation. Both Figures 6 and 9 show that when proteins are present in a solvent system consisting in some part an organic solvent, then the resulting spectra typically show a much broader distribution of more highly charged peaks than those spectra produced from buffered solutions. The organic solvent and the acidic nature of the analyte solution has denatured (or opened) the protein in solution, and otherwise hidden basic amino acids now become available for protonation by electrospray ionisation.

This observation has been seen many times with a wide variety of different proteins as analytes. For analysis of biological interactions i.e. protein-peptide, protein-metal ion, protein-protein etc. by electrospray ionisation mass spectrometry it should be obvious that analyte solution conditions are extremely important when trying to confirm what are essentially solution phase interactions, using a gas phase experimental technique such as mass spectrometry. The fact that there is a change at all in the mass spectra is a good indicator that mass spectrometry linked with electrospray ionisation is a good technique for the quick, easy analysis of the interactions of large biological molecules. However, it

has still to be proven whether the conformation of the protein is conserved from the solution phase to the gas phase.

The capillary-skimmer dissociation experiments indicate that the fragmentation information obtained from CID is also dependent on the analyte solution conditions. This is due to the fact that the charge state distribution is altered significantly by the nature of the solvent used. That is buffered analyte solutions cause the charge state distribution observed in the ESI spectra to become narrower and centred at much lower charge states than seen for analyte solutions containing denaturing solvents. (See Figures 6 and 9)The energy imparted to the parent molecule ion under investigation would therefore be considerably less with the same source parameters and the corresponding fragmentation information would therefore decrease. The conformation of the protein in solution therefore influences information obtained from CID spectra.

References

[1] J. A. Loo, *Mass Spectrom. Rev. 16* (1997) 1.

[2] H.-K. Lim, Y. L. Hsieh, B. Ganem, J. Henion, *J. Mass Spectrom. 30* (1995) 708.

[3] C. Meunier, M. Jamin, E. D. Pauw, *Rapid Commun. Mass Spectrom. 12* (1998) 239.

[4] S. K. Chowdhury, V. Katta, B. T. Chait, *J. Am. Chem. Soc. 112* (1990) 9012.

[5] R. D. Smith, J. A. Loo, R. R. O. Loo, M. Busman, H. R. Udseth, *Mass Spectrom. Rev. 10* (1991) 359.

[6] D. M. Roberts, R. Crea, M. Malecha, G. Alvarado-Urbina, R. H. Chiarello, D. M. Waterson, *Biochemistry 24* (1985) 5090.

[7] T. A. Craig, D. M. Waterson, F. G. Prendergast, J. Haiech, D. M. Roberts, *J. Biol. Chem. 262* (1987) 3278.

[8] R. R. Hudgins, J. Woenckhaus, M. F. Jarrold, *Int. J. Mass Spectrom. Ion Proc. 165/166* (1997) 497.

[9] K. B. Shelimov, D. E. Clemmer, R. R. Hudgins, M. F. Jarrold, *J. Am. Chem. Soc. 119* (1997) 2240.

[10] S. J. Valentine, A. E. Counterman, D. E. Clemmer, *J. Am. Soc. Mass Spectrom. 8* (1997) 954.

[11] M. C. Killhoffer, D. M. Roberts, A. Adibi, D. M. Watterson, J. Haiech, *Biochemistry 28* (1989) 6086

4.0 Non-Covalent Interactions Of Biological Molecules

4.1 Introduction

Protein-ligand interactions can be initiated in the solution phase and directly analysed by the mass spectrometer. Other mass spectrometric techniques such as MALDI [1-3]are also useful for the analysis of biomolecules but the low resolution of such instruments (typically time-of-flight analyser) and the fact that the MALDI process produces predominantly singly charged ions means that larger biomolecule-ligand interactions cannot be investigated with much accuracy. The multiple charging of the electrospray technique means that even large molecules can be observed at high resolution by FT-ICR since the mass is effectively "folded" down to a region on the *m/z* scale that has the highest resolution and mass accuracy. Electrospray can therefore take advantage of the high resolution and mass accuracy inherent to FT-ICR mass spectrometry.

Typical ESI mass spectra of non-covalent complexes usually consist of peaks at high *m/z* and therefore low charge, compared to ESI mass spectra of the protein alone.[4] This must be due to the fact that there are less sites available for protonation when the ligand is bound than there are in the free protein, either because a conformational change has been induced by the ligand or that the ligand simply obscures those basic amino acids that would normally pick up a proton during the charging process. Similar results are observed when disulfide bridges (responsible for some of the tertiary structure of the protein) are broken by reduction of the protein. Before reduction there is a smaller charge envelope presumably due to the structure of the protein being more open after reduction or coulombic constraints that restrict charging of the more compact structure. As already mentioned in this section, solvent conditions play an important part in the conformation of the protein. With appropriate buffer as the solvent a narrow charge distribution is

observed, a consequence thought to be due to the retention of the higher order structure of the "natural" protein. The fact that the conformation changes with solvent can be used as a useful control experiment in investigations of specific non-covalent interactions. Specific interactions between the active site of the protein and the target should only be observed when the protein analyte solution is buffered to retain the proteins natural conformation. Interactions observed from organic solvent based analyte solutions can be thought of as non-specific, since the protein conformation in solution can be considered random. A proteins function is intrinsically tied up with its conformation. Thus an analyte solution that disrupts the conformation of a protein cannot produce results that would be representative of the proteins function *in vivo*.

Arguments still rage over the validity of results obtained by electrospray on such complexes. The fact that both solution phase chemistry and gas phase chemistry are involved leads to the question does a gas phase measurement give us information on a solution phase problem?[4]

Published data has characteristically been in direct correlation with results obtained by solution-phase methodology. Some argue, however, that results that do not show expected non-covalent interactions, or non-covalent interactions where none are expected, are not reported. The nature of this argument means that it is hard to prove; none the less experiments are consistently being published that provide direct correlation with results reported from solution-phase experiments. Investigations where the ligands are in much greater concentration than the protein i.e. competitive conditions, show relative abundances of complexes in the mass spectra consistent with their relative binding constants in solution [5, 6] and multimeric complexes that are known to be biologically active are also observed under "natured" conditions.

There are a variety of non-covalent interactions agreed to be involved in protein folding, including ionic interactions, Van der Waals forces, hydrophobic effects and hydrogen bonds. Changing from solution to the gas phase may cause some types to be strengthened while others are weakened. It is still undetermined whether this is the case but it is worth considering. [7]

Experiments by Lim *et al* [5]and Loo *et al* [6], however, have shown the ability of electrospray ionisation mass spectrometry to provide quantitative results for binding constants between antibiotics and peptides and proteins and peptides respectively. Lim *et al* constructed Scatchard plots for the interactions of vancomycin and ristocetin, at a variety of concentrations, with an assortment of cell wall peptide ligands. These plots provided binding constants that were in good agreement with those found in solution by other techniques. For example ristocetin + Ac_2KAA had a binding constant (K_a) in solution of 5.9×10^5 M compared with 6.25×10^5 M calculated from the Scatchard plots in the gas phase. Experiments carried out by Loo *et al* monitoring the binding of phosphopeptides to Src SH2 Domain protein showed a similar correlation.

These ESI experiments on such non-covalent complexes are necessarily carried out using appropriate source conditions and there is a careful balance between the energy needed to desolvate the ion and the energy that will dissociate the complex. Protein-peptide interactions are especially weak and much care is needed in order to be able to observe the complexes. Protein-oligonucleotide complexes on the whole are typically much stronger due to extensive electrostatic forces between the partners and are consequently more forgiving of harsh ESI conditions. [8]The energy imparted to the ions by electrospray ionisation can also be utilised to provide information on the strengths of the interactions. For example, if a variety of peptides are allowed to bind to a protein and

CID carried out, the relative strengths of the complexes can be ascertained. [9]Similar studies using blackbody infrared radiative dissociation with FT-ICR mass spectrometry on myoglobin-heme and α-hemoglobin-heme complexes showed a consistency with results from solution. [10]

4.2.1 Papain

There are 20 families of peptidases with cysteine at the active site , of which, papain is the best known. [11]They are found in a wide variety of organisms including baculavirus, eubacteria, yeast and probably all protozoa, plants and animals. The activity of papain and its family members is dependent on a catalytic dyad of Cys and His. [11]The order of these amino acids in the linear sequence varies from family to family within this class of peptidases with, for example, papain having a Cys/ His sequence and Hepatitus C virus endopeptidase 2 His/ Cys. Other residues are also important within the active site of papain including Gln 19 which helps form an "oxyanion hole" [12, 13](so called because the two hydrogens from the His and Cys stabilise the carbonyl oxygen of the target), Asn 175[14] which orientates the imidazolium ring of His 159[15] and Ser 205 which lies at the bottom of the pocket. [11]

These peptidases are lysozomal (vacuolar) or secreted proteins and papain itself is found extracellular in the latex of papaya. The activity of the peptidases within the papain family varies greatly from endopeptidases with broad specificity such as papain to those with narrow specificity such as glycyl endopeptidase. Others have little or no catalytic activity.

Papain is a non-specific cysteine protease that consists of 212 amino acids (RMM approximately 23,425). It consists of two hydrophobic cores each made up of five helical

segments and a region of approximately 30 amino acids that forms a distorted β pleated sheet (see Figure 3). The active site of papain exists within the cleft between these hydrophobic cores and contains the amino acids mentioned previously, Cys 25 and His 159 being on opposite lobes. Papain and its family members catalyse the hydrolysis of peptide, amide, ester, thiol ester and thiono ester bonds. [16]The mode of action of papain can be considered to be very similar to that of chymotrypsin, a serine protease. [17] It consists of the formation of a covalent acyl-enzyme intermediate (Figure 2) which occurs because of nucleophilic attack at the carbonyl carbon of the substrates scissile bond by the thiol group of the active site. The mechanism is supposed to be similar to chymotrypsin because of the resemblance of their active sites. In both, an Asn amino acid is in close proximity to the histidine. The oxygen of the asparagine (Asn) side chain is hydrogen bonded to a nitrogen in the histidines ring forming a Cys-His-Asn triad that is comparable to the Ser-His-Asp of chymotrypsin. The Asn is proposed to orientate the imidazole ring of the histidine for the different stages of the mechanism.

As can seen from the schematic of the mechanism (Figure 1) it is incompletely understood. Many other intermediates/ transition states are believed to be present along the pathway, these are denoted by (tetrahedral intermediates) TTI_1 and TTI_2 with their attendant transition states.[16] Figure 2 shows the covalent acyl-enzyme intermediate in more detail.

The substrate carbonyl group sits in the "oxyanion hole" (at the bottom of which lies Gln 19) and is therefore brought into the vacinity of the thiolate anion of Cys 25 (Stage A, Figure 1). This carbonyl undergoes nucleophilic attack forming the first tetrahedral intermediate (TTI_1), the His 159 then rotates allowing the proton to be donated to the amide hydrogen of the substrate. This causes TTI_1 to break down, expelling a free amine

and forming the acyl enzyme intermediate (Stage B, Figure 1). The His 159 then removes a hydrogen from the water molecule that assails the acyl enzyme intermediate, causing the breakdown of TTI_2 which regenerates the enzyme (Stages C and D, Figure 1).

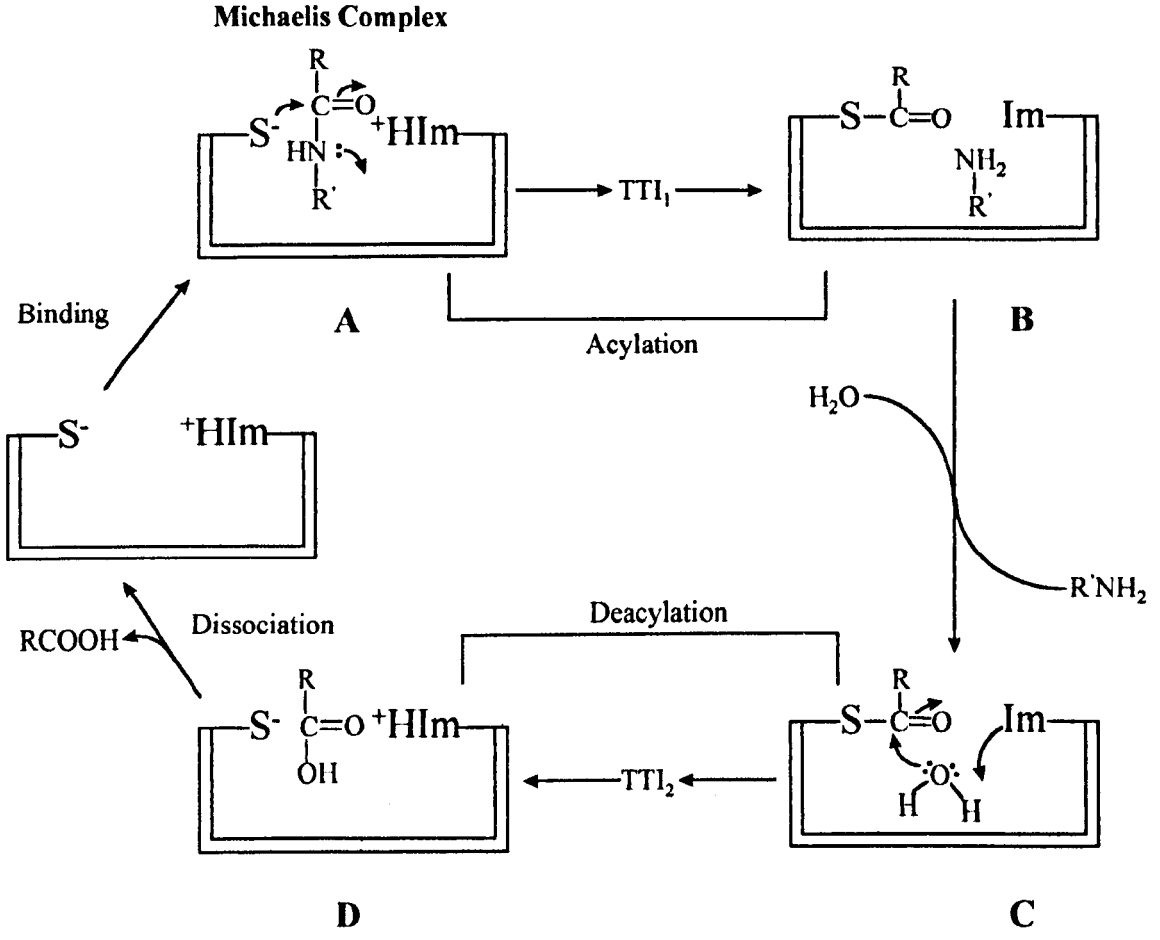

Figure 1 : Schematic diagram of the mode of action of papain.

Papain is inhibited by a variety of molecules including reducing agents, heavy metal ions, alkylating reagents and some peptides. For example, the tetra-peptide GGYR used in this study is known to be an inhibitor of papain. This is due to the specificity of papain for cleaving peptide bonds in sequences where an aromatic amino acid is bound to a basic amino acid which in turn is bound to any other amino acid. Its specificity for the peptide bond after the basic residue means that a peptide that ends in an aromatic-basic

moiety is an effective inhibitor of the enzyme. [18]The other peptide used in this study N_{α},N_{ε}-diacetyl-Lysine-d-Alanine-d-Alanine is known to be an inhibitor of serine proteases. [19]

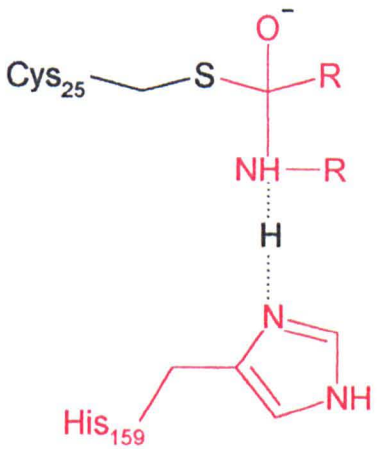

Figure 2 **:** Covalent acyl enzyme intermediate.

Inhibition of papain has been studied before by mass spectrometry. Using a pneumatically assisted electrospray source coupled with a triple quadrupole mass spectrometer, [20]the interaction of papain with a peptidyl O-acyl hydroxomate was investigated with the observation of oxidised papain, and at higher concentrations of inhibitor a significant peak corresponding to a papain-inhibitor complex.

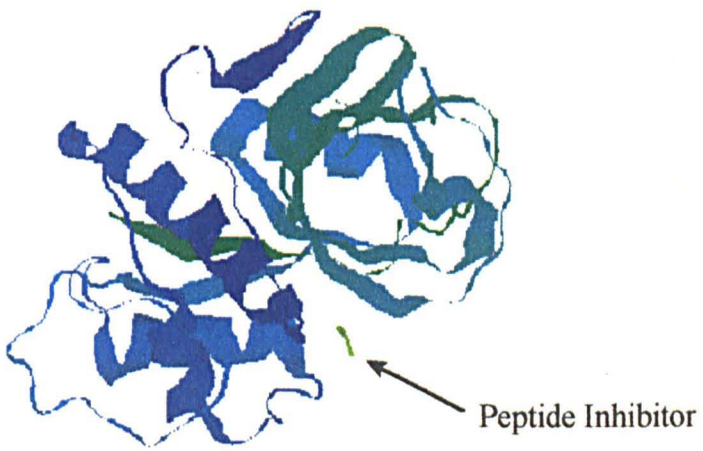

Figure 3: Papain plus peptide inhibitor. Note the two hydrophobic cores and the cleft containing the active site.

4.2.2 Experimental

Experiments were conducted using the 9.4 Tesla Fourier transform ion cyclotron resonance (FT-ICR) mass spectrometer (see chapter 2). CO_2 was used as a drying gas at a temperature of approximately 50°C in the source. The analyte was directly infused into the source at a flow rate of 1µl min^{-1} making use of a syringe pump. Source parameters were carefully controlled during the experiments to minimise unwanted dissociation of the analyte and its complexes. Thus the capillary-skimmer voltage bias and heating-gas temperature were kept low to prevent capillary-skimmer CID and thermal decomposition respectively.

The best quality spectra were found to be obtained from a sample consisting of a papain suspension in sodium acetate + 1% thymol purified using the Pharmacia Biotech PD 10 Sephadex gel chromatography columns.

ESI FT-ICR mass spectrometry experiments were carried out in ultra-pure water (Elga system) and plastic laboratory equipment to minimise unwanted salt contamination. Before introduction to the instrument papain was purified by desalting as per section 3.2.2.4.

The peptides used in this study were the tetra-peptides Gly-Gly-Tyr-Arg (GGYR) and Gly-Gly-Gly-Gly (GGGG) and the tri-peptide N_{α},N_{ε}-diacetyl-Lys-d-Ala-d-Ala. All were obtained as lyophilised powders from Sigma (Poole, UK) and used as purchased.

4.2.3 Results

Initial investigations into the non-covalent interactions of papain and its peptide inhibitors involved ascertaining the solvent and source conditions that would allow the observation of non-covalent interactions. Non-covalent interactions were eventually observed under specific conditions, which included a solvent pH of around 4.6 in ammonium acetate and a source temperature around 50°C. The interactions of papain and the peptides were investigated by circular dichroism. (see Figures 4 and 5)Initial experiments into the purification of papain, that is, to remove the unwanted salt contamination also made use of two MALDI time-of-flight mass spectrometers, the Kratos MALDI IV bench top time-of-flight instrument and the Micromass TOFSpec.

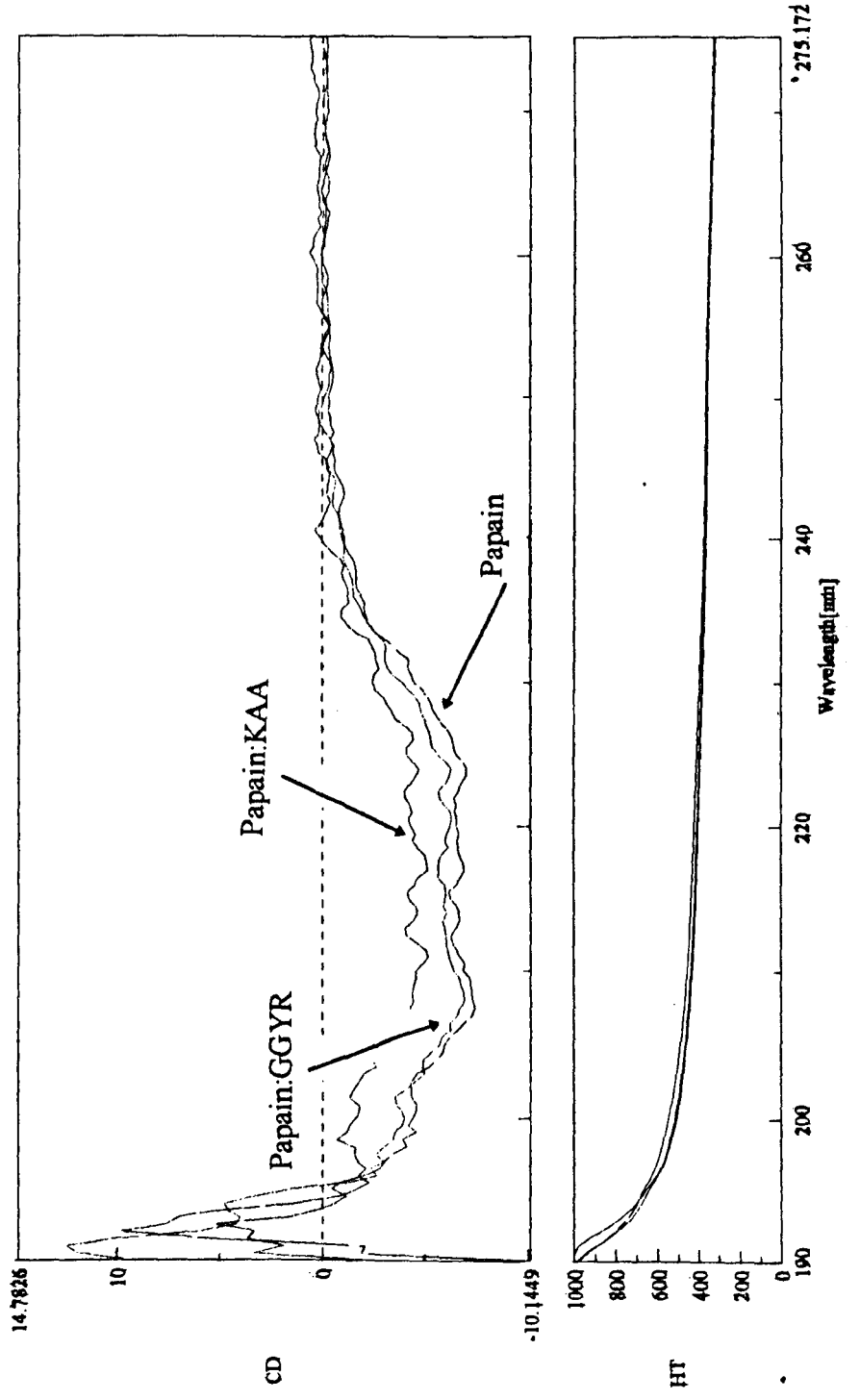

Figure 4: CD spectra of papain plus the peptides GGYR and KAA in water. Papain:Peptide ratio 1:5, papain concentration approximately 75 μM, pathlength 1cm.

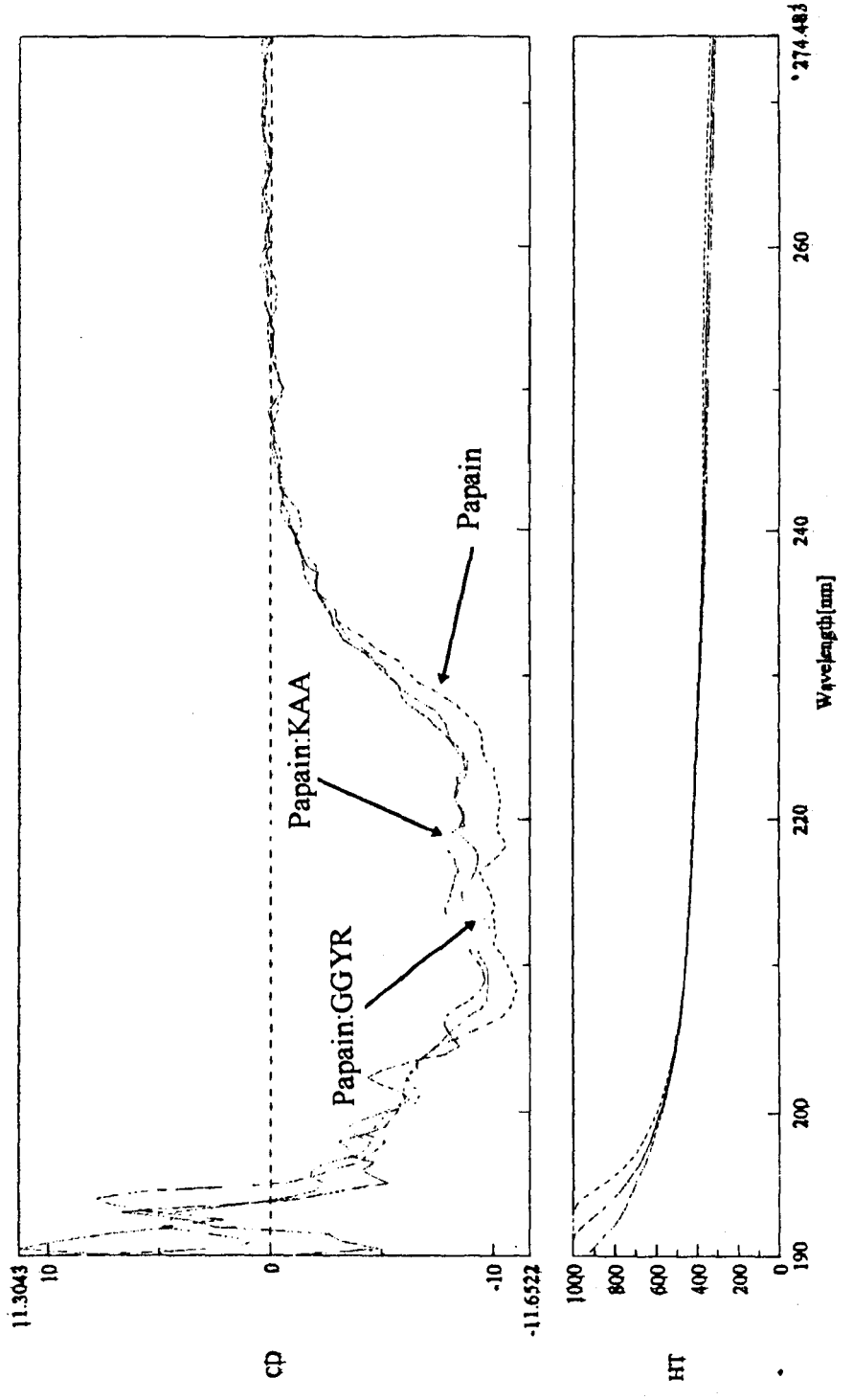

Figure 5: CD spectra of papain plus the peptides GGYR and KAA in ammonium acetate (5mM, pH 4.6). Papain:Peptide ratio 1:5, papain concentration approximately 75 μM, pathlength 1cm.

Figures 4 and 5 show the CD spectra, the addition of peptides, in this case KAA and GGYR, alter the conformation of the protein. This can be observed from the spectra by noting the change in the spectra on addition of the peptides. It can be deduced that the tri-peptide causes the greatest perturbation of the protein structure in both water and ammonium acetate, due to the greater shift in the recorded CD spectra.

Circular dichroism (CD) is becoming widely used as a tool for the study of biological molecules.[4] The technique allows changes in the conformation of the biomolecule to be monitored, this can be achieved when the biomolecule is alone in the analyte solution or can be used to monitor the effect of small molecules on the conformation of the biomolecule of interest. Due to the complexity of the circular dichroism spectra, interpretation is usually of a qualitative nature. Thus the examples presented here show the overall effect of small peptides binding to papain but make no other attempts to interpret the spectra. The ease and rapidity with which CD experiments can be carried out, the fact that experiments are carried out in the solution phase and the low concentrations of analyte required are all advantages of CD for the acquisition of complementary data for these mass spectrometric experiments.

The technique makes use of right and left-polarised light, with the different absorption of left and right handed chiral analyte molecules determining the CD spectra. Biological molecules, consisting of predominantly L-amino acids and secondary structures such as the α-helix are chiral. Thus the interaction of left- and right-handed photons with the biomolecule will be different forming the basis of circular dichroism. [21]

Spectropolarimeters (circular dichrometers) require a source of monochromatic left- and right-handed light and a detector capable of detecting the difference in the absorbance of left- and right-handed light by the analyte molecule. This is usually achieved using a

polarisation phase-modulation technique. A light source of constant intensity such as a photo-elastic modifier with a typical frequency of 50 kHz is utilised and when the light passes through the sample of interest the absorption of the left- and right-handed light is different. The intensity of the light fluctuates in phase with the photo-elastic modifier and this can be monitored by detecting the number of unabsorbed photons striking a photo-multiplier. The current produced, which is detected by a lock-in amplifier, has a magnitude related to the number of incident photons, information on the CD of the analyte molecule can be determined from the AC component, which, with the aid of the lock-in amplifier can be phase determined. Meanwhile, the DC component of the current gives the total absorption of light by the sample.

CD of proteins is usually aimed at investigating the backbone region (the amide transitions) from 190 to 240 nm. This gives distinctive CD spectra for the α-helix and β-pleated sheets present in such molecules, with the overall spectra being a summation of the different components present in the analyte molecule. For example, the CD spectrum of the α-helix consists of a negative peak with separate maxima at 222 nm and 208 nm. This motif is the largest present in CD spectra of proteins and is readily apparent with just a cursory examination of a CD spectrum.

Preliminary mass spectrometry experiments used a high ratio of peptide to papain (of the order 25:1). This produced numerous observable non-covalent complexes, with the peptides binding to both the oxidised and the phosphorylated-oxidised form of papain (see Figures 6 and 7). It is assumed that only a single peptide actually binds to the active site of papain, while the remaining peptide complexes are formed from non-specific non-covalent interactions. Thus of the observed papain: GGYR complexes, the most abundant was the single GGYR bound to papain. The maximum number of tetra-peptides bound

was six(see Figure 6). The most abundant complex was that in which six tri-peptides were bound, with a maximum at twelve (see Figure 7).

The observations would seem to indicate that GGYR has a greater specificity for the active site (since the maximum is at one tetra-peptide bound to papain); one tetra-peptide binds into the active site predominantly. KAA on the other hand binds to the active site as indicated by later experiments, but non-specific non-covalent interactions dominate the spectra at high peptide concentrations as indicated by the bell shaped distribution of complexes in Figure 7.

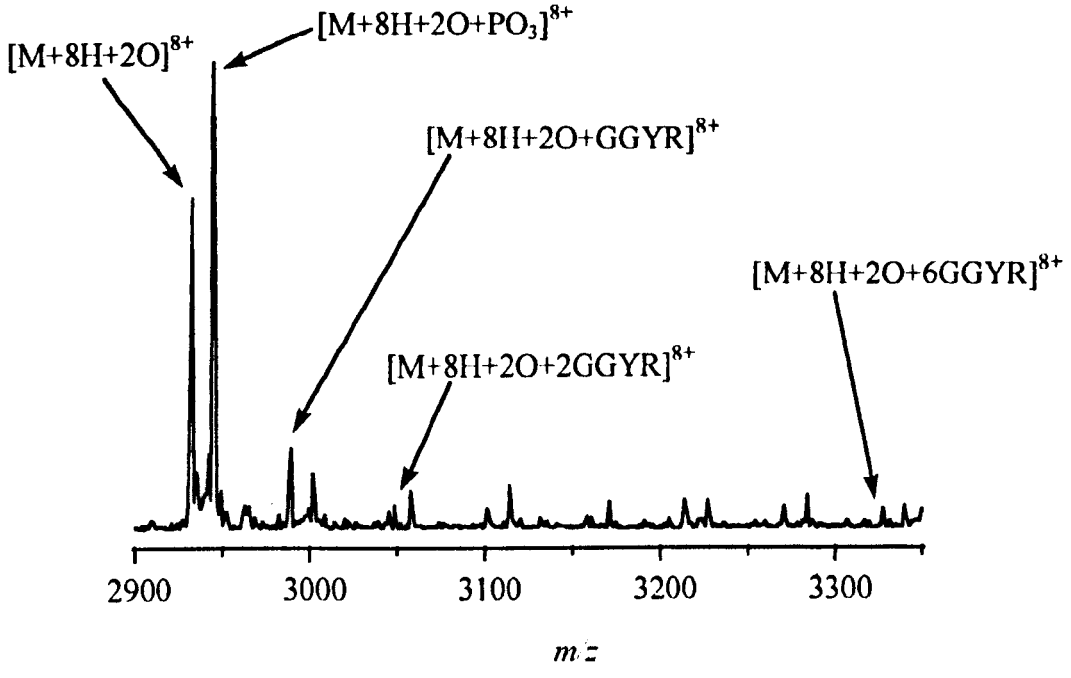

Figure 6: Papain:GGYR (1:25) in ammonium acetate (5mM, pH)

At lower ratios of peptide: papain the distribution of non-covalent complexes distribution for both peptides looked very similar, with both GGYR and KAA binding predominantly a single peptide (see Figures 9a and 10a). In these cases there was presumably not enough of each of the peptides to form significant non-specific interactions. Thus the interactions observed, are interpreted as relating to a single peptide

binding to the active site. Note that in both Figures 9a and 10a the complex corresponding to peptide bound to the phosphorylated-oxidised form of papain was absent. This is attributable to a purer sample of the peptides or papain, with the removal of the phosphate buffer contamination from the analyte and as a result its corresponding peak from the spectra.

Since both peptides bound to the protein, the obvious questions were which showed the strongest interaction and whether either peptide was binding to the active site. These questions seemed to be most easily answered by a capillary-skimmer CID experiment. The results are shown in Figures 9 and 10. In both cases the peptides remained bound up to a capillary voltage of 120V meaning that both must be bound quite strongly to the oxidised form of papain since this voltage is very high and would normally cause all weak bonds to be broken. This is consistent with both peptides being bound to the active site.

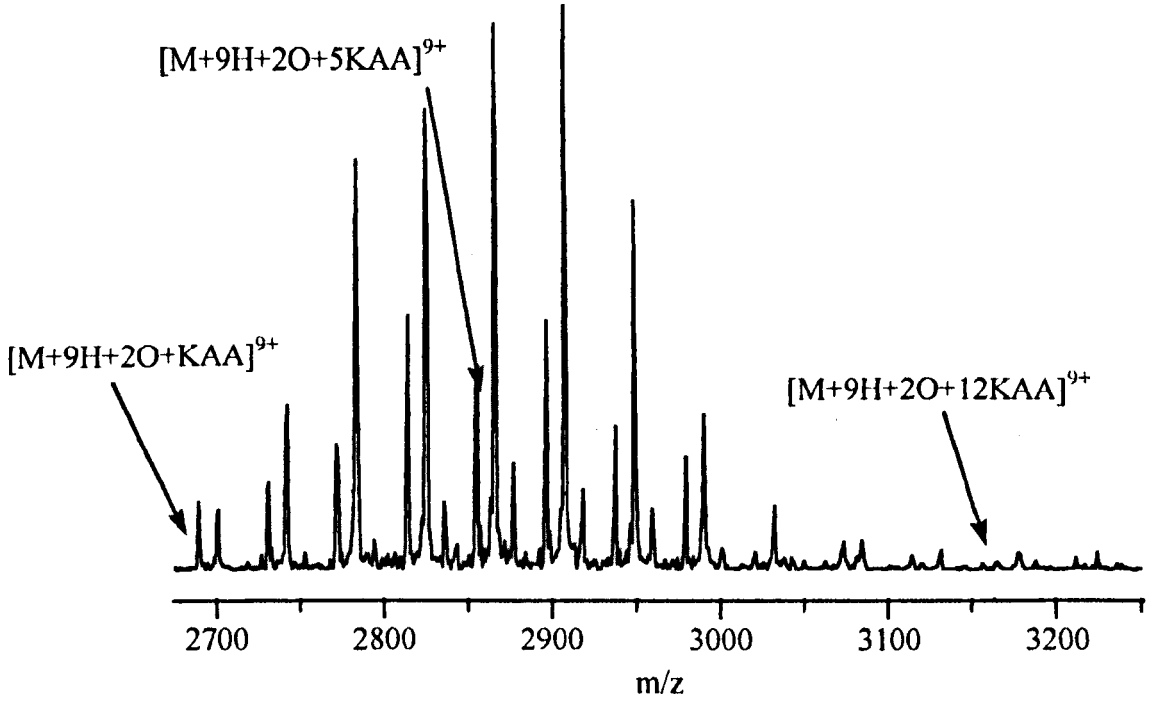

Figure 7: Papain: KAA (1:25)in ammonium acetate (5mM, pH 4.6)

The tri-peptide KAA remained bound to papain up to a capillary voltage of 160V (see Figure 10d) , compared to 140V for GGYR; Figure 9d. Thus it would seem that in the gas phase the tri-peptide was bound more strongly into the active site of papain. This conclusion was supported by a complementary experiment where both GGYR and KAA (at a concentration ratio of papain: GGYR: KAA (1:8:8)) were mixed with the protein. Figure 11 shows that the peak corresponding to one KAA bound to papain was predominant again suggesting that KAA was bound preferentially to papain.

Similar experiments to those described above were carried out using GGGG, a peptide that was not expected to bind to the active site. No non-covalent complexes were observed in the spectra (see Figure 8)

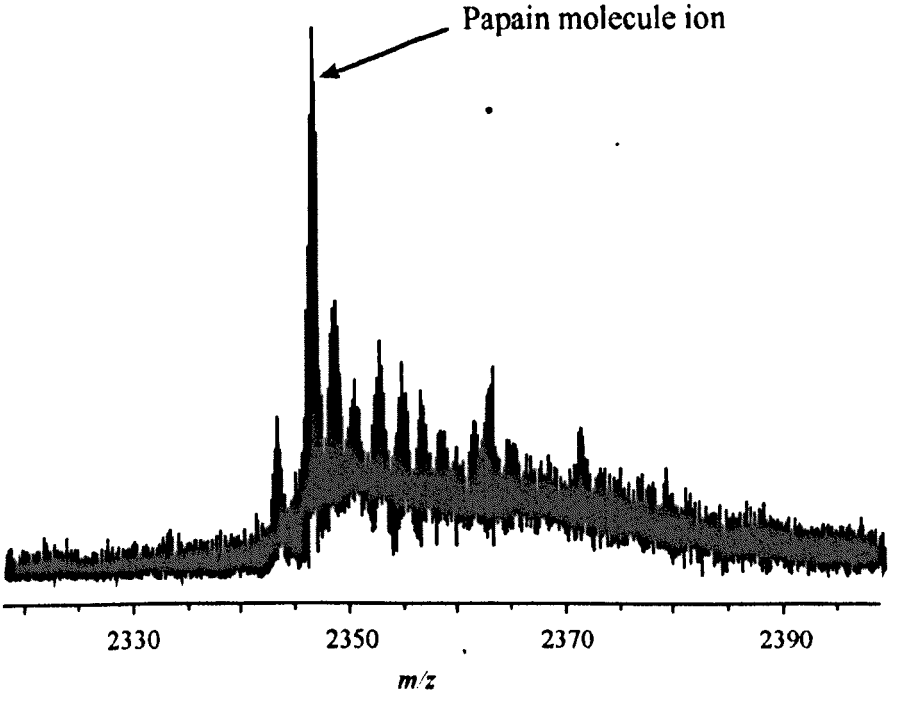

Figure 8: Electrospray mass spectra of papain: GGGG (1:10) in ammonium acetate (5mM, pH 4.6). Note the absence of any papain: GGGG complexes.

The lower regions of the *m/z* scales for both GGYR and KAA contained peaks due to various multimers of the peptides. Figure 12 illustrates this with the easily observed trimer of GGYR. Even lower on the *m/z* scale dimers and multiply charged pentamers and hexamers could also be seen (not shown). It is therefore possible that there may not be 6 individual non-covalent interactions from the oxidised papain to the tetra- and tri-peptides; there may in fact be a single non-covalent interaction between oxidised papain and say a hexamer of the peptide in question. Thus each individual peak representing a non-covalent interaction may involve the oxidised form of papain and the multimer of the relevant peptide. This is especially true for the experiments carried out under high concentrations of peptide.

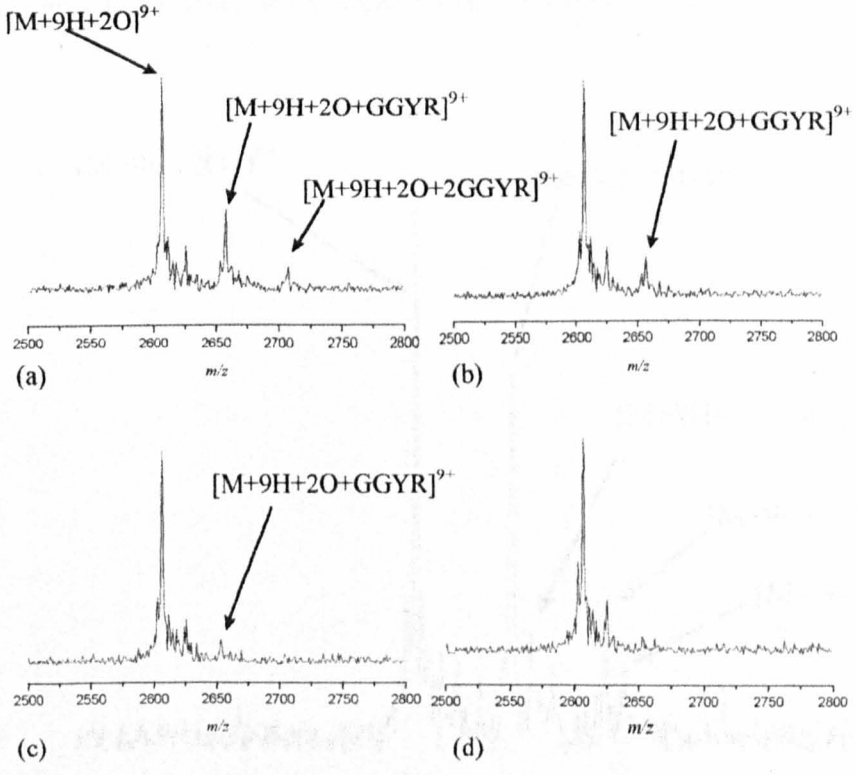

Figure 9: Capillary-skimmer CID of papain:GGYR (1:8) in ammonium acetate (5mM, pH 4.6) (a) capillary voltage 85V (b) 100V (c) 120V and (d) 140V

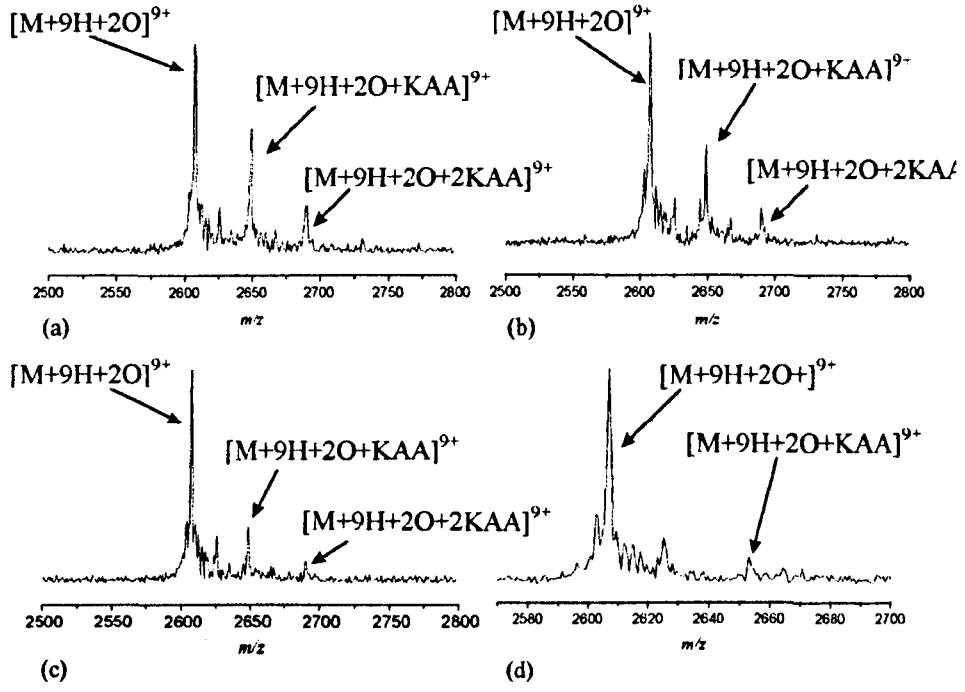

Figure 10: Capillary-skimmer CID of papain: KAA (1:8) in ammonium acetate (5mM, pH 4.6) (a) capillary voltage 85 V (b) 100V (c) 140 V and (d) 160 V.

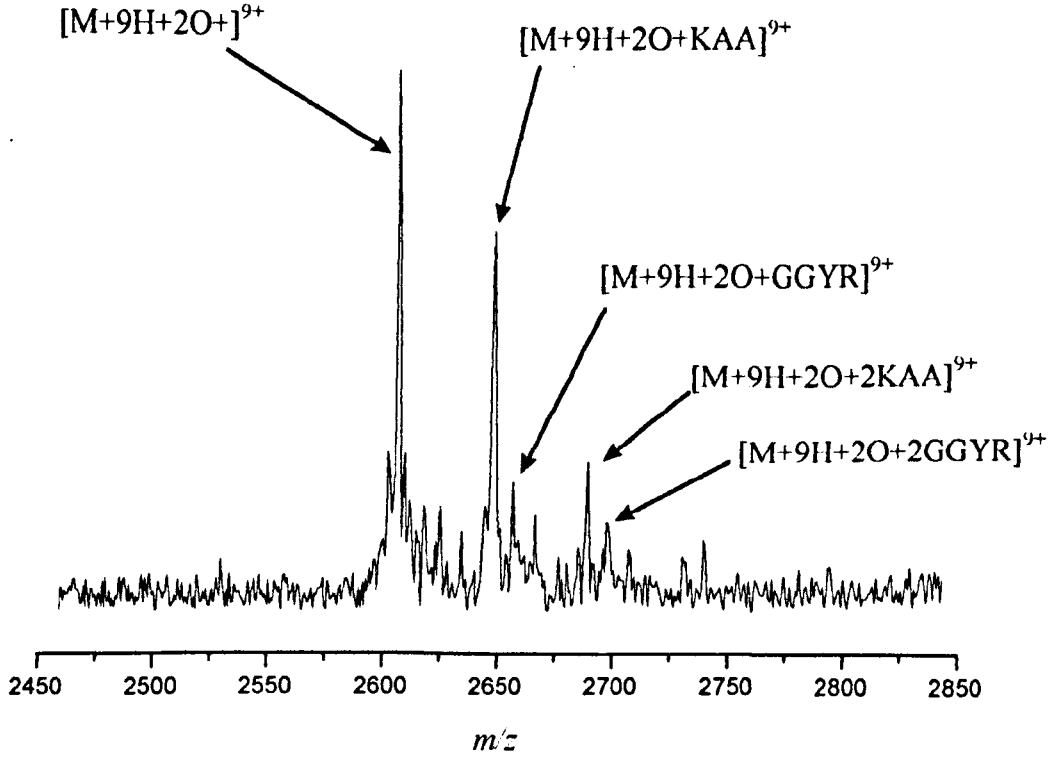

Figure 11: Papain: GGYR: KAA (1:8:8) in ammonium acetate (5mM, pH 4.6). Capillary voltage 85V. KAA bound preferentially.

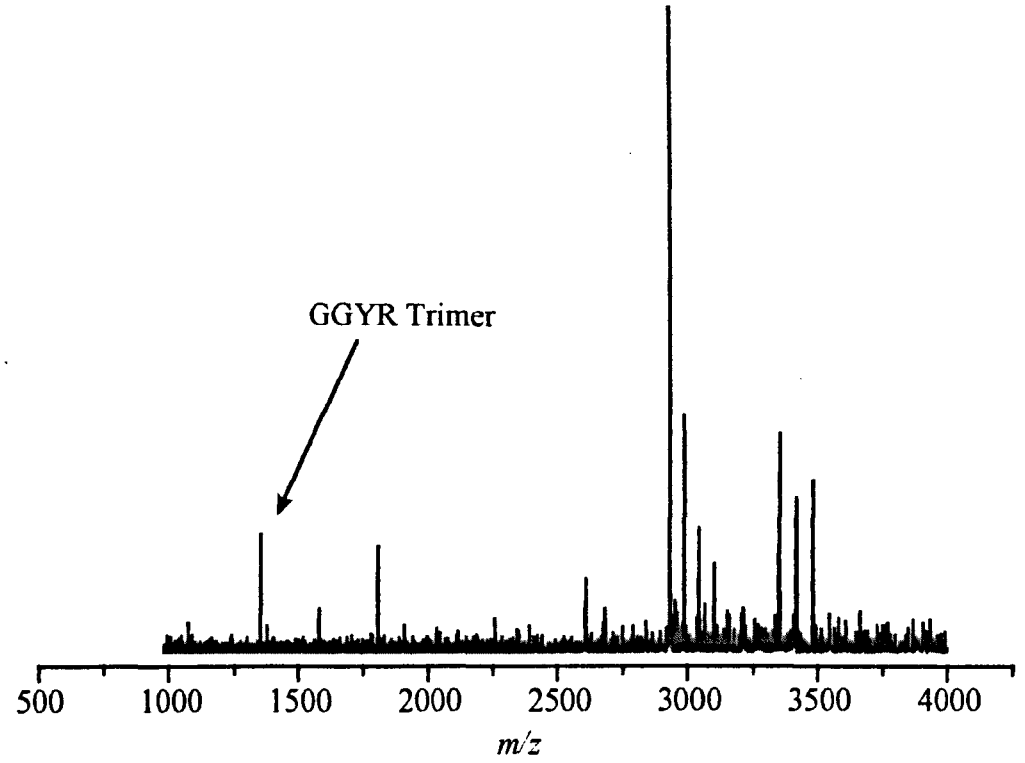

Figure 12: Papain: GGYR (1:25), capillary voltage 96V. Note the trimer of the tetra-peptide GGYR.

4.3 Calmodulin

Calmodulin (CaM) is a relatively small acidic protein of approximately 148 amino acid residues and RMM~16,626. [22, 23]It is found in all eukaryotic cells[24] and is a mediator in many cellular processes including muscle contraction, cellular metabolism, cellular motility, division and growth of the cell, ion transport and membrane permeability.

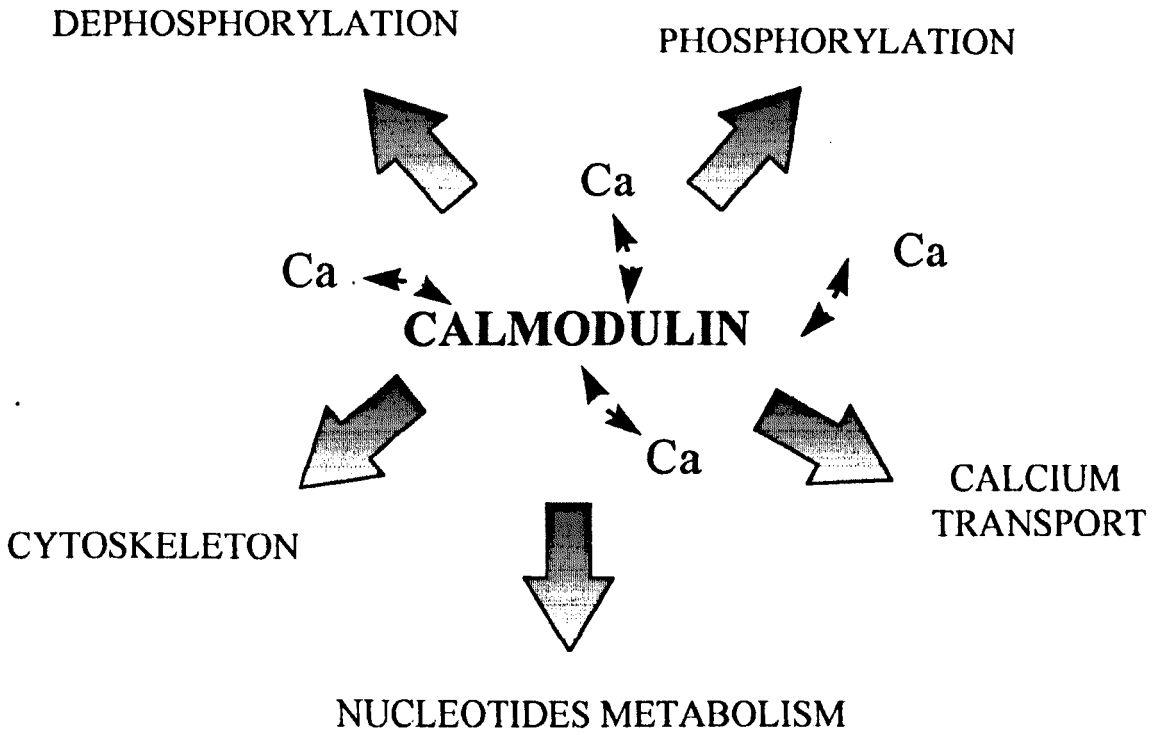

Figure 13: Calmodulin and its enzyme targets.

CaM has a dumbbell-type shape in solution , that is, at the C- and N-terminus there are globular domains which contain two so-called EF hands (see Figure 14). [25-29]These EF hands consist of a helix-loop-helix motif with the C-terminus sites (III and IV) thought to have a higher affinity for Ca^{2+} than the N-terminus (I and II). This is inferred from the most satisfactory model for Ca^{2+} ion binding to CaM. [30, 31]This states that Ca^{2+} ions bind sequentially to the sites on the C-terminus first and then into the sites on the N-terminus i.e. sites III→IV→I→II (see Figure 14). [30-36]This information was deduced

from data acquired on the macroscopic dissociation constants of each of the binding domains (K_1=2x10^{-5}M, K_2=9x10^{-5}M, K_3=2.9x10^{-4}M and K_4=1x10^{-5}M). [30, 31]

It has been observed that CaM can bind up to four Ca^{2+} ions to four primary sites at a pH of between six and eight. [35, 36]A further four to six Ca^{2+} ions can bind to so called auxiliary sites. [36]The dissociation constants for these sites are in the milli-molar range for Ca^{2+}.[37, 38]It has also been shown that Cam binds other cations such as Sr^{2+}, Zn^{2+}, Mn^{2+}, Mg^{2+}, Cu^{2+}, Hg^{2+}, La^{3+}, Tb^{3+}, Pb^{2+} and Cd^{2+}. Thus Ca^{2+} and Sr^{2+} would both bind to the primary sites; Zn^{2+}, Mn^{2+}, Cu^{2+}, Hg^{2+} to the auxiliary sites only and La^{3+}, Tb^{3+}, Pb^{2+} and Cd^{2+} could bind to both. [38]

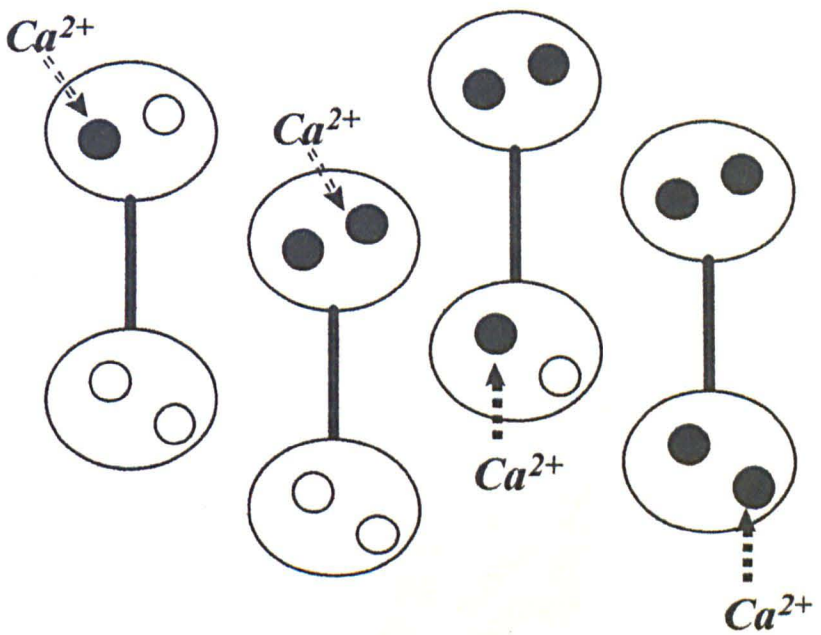

Ala-Asp-Gln-Leu-Thr-Asp-Glu-Gln-Ile-Ala-Glu-Phe-Lys-Glu-Ala-Phe-Ser-Leu- **Asp-Lys-Asp-Gly-Asp-Gly-Thr-Ile-Thr-Thr-Lys-** -Leu-Gly-Thr-Val-Met-Arg-Ser-Leu-Gly Gln-Asn-Pro-Thr-Glu-Ala-Glu-Leu-Gln-Asp-Met-Ile-Asn-Glu- **-Asp-Ala-Asp-Gly-Asn-Gly-Thr-Ile-Asp-Phe-Pro-Glu**-Phe-Leu-Asn-Leu-Met-Ala-Arg-Lys-Met-Lys-Asp-Thr-Asp-Ser-Glu-Glu-Glu-Leu-Lys-Glu-Ala-Phe-Arg-Val- **Asp-Lys-Asp-Gly-Asn-Gly-Phe-Ser-Ala-Ala-Glu-Leu**-Arg-His-Val-Met-Thr-Asn-Leu-Gly-Glu-Lys-Leu-Thr-Asp-Glu-Val-Asp-Glu-Met-Ile-Arg-Glu-Ala-**Asp-Val-Asp-Gly-Asp-Gly-Gln-Val-Asn-Tyr-Glu**-Phe-Val-Gln-Val-Met-Met-Ala-Lys

Figure 14: (a) sequential calcium binding to calmodulin and (b) the amino acid sequence of calmodulin with "EF" hands shown in red.

Existing literature indicates that calcium binding to calmodulin induces conformational changes that expose hydrophobic residues in each globular lobe. These exposed residues make up important binding sites for most of the target proteins. [39]Calmodulin is then thought to interact with, and regulate selectively, a wide variety of proteins. (These target proteins have little sequence homology in the region where calmodulin is known to bind, although they do have a propensity for forming basic amphiphilic α-helices. [40])This allows the calcium-bound (holo) form of calmodulin to be involved in the regulation of a wide range of metabolic processes. [22, 23]The interactions of calmodulin with target proteins have been shown to be arbitrated by both hydrophobic and electrostatic forces occurring between the N-terminal of calmodulin and the C-terminal of the target protein, and *vice versa.* [29, 41]

Figure 15: Molecular model of apo-calmodulin.

The Ca^{2+} mediated conformational change in CaM is believed to involve the loosening of the structure of the C-terminus domain (and the N-terminus domain to a more limited extent). This "opening/loosening" of the C- and N- terminus domains uncover solvent exposed hydrophobic surfaces that engulf aromatic and aliphatic side chains of amino acid

residues on the target. [42]These hydrophobic surfaces are approximately 10 x 12.5 Angstroms, one per globular domain, which are surrounded by a polar rim that contains numerous negatively charged residues. [43]The negatively charged residues are currently thought to aid in "binding" CaM to the target protein of interest by interacting with the positively charged residues present on the target. According to existing theories Ca^{2+} ion binding could be responsible for opening up the hydrophobic cavities and allowing CaM-target interactions to take place.

The hydrophobicity of CaM is due in part (slightly less than 50%) to the presence of nine methionine residues in the amino acid sequence, four in each of the hydrophobic cavities and one in the "linker" region. The polarisability and flexibility of methionine residues has been postulated as being essential for calmodulin function.

Assuming the sequential model for calcium binding [39, 44-46]it can be proposed that there exists at any one time a series of calmodulin conformations, analogous to zero, one, two, three and four calciums bound. The conformational change induced by just one calcium binding to calmodulin may be thought of as enough to favour target peptide/ protein binding. Alternatively, it may be that calmodulin would bind to its target protein/ peptide, followed by the sequential addition of the Ca^{2+} ions resulting in activation of the target. The presence of calmodulin: target complexes (without any calcium ions present) gives some support to this latter theory. [47]Regardless of the mechanism a series of complexes corresponding to various amounts of Ca^{2+} ions bound to the free calmodulin and the target protein/ peptide: calmodulin complex should be observed by mass spectrometry.

Rabbit skeletal-muscle myosin light-chain kinase (MLCK) is well known to be calmodulin directed and the peptide used in these studies (RS20) is a synthetic construct

based on the binding domain of MLCK. The calmodulin binding domain of MLCK was the first to be identified, and peptides derived from this particular amino acid sequence are known inhibitors of calmodulin activation (pico- to low nano-molar binding constants[48-50]. These peptides are important for the study of calmodulin-target interactions by analytical techniques including mass spectrometry. The low masses of the peptides allow the complexes' molecular masses to be kept low and within the useful range of mass spectrometric measurements.

Circular dichroism has shown that MLCK peptide analogues affect an α-helical conformation upon binding with calmodulin. Investigation of calmodulin/ MLCK-peptide complexes by proton NMR studies, small angle X-ray and small angle neutron scattering experiments indicate a more compact conformation of calmodulin after peptide binding.

The use of ESI mass spectrometry to study the conformational changes, peptide interactions and ion-binding properties of calmodulin has been reported. [33, 34, 51-54]More recently electrospray ionisation high resolution Fourier transform ion cyclotron resonance (FTICR) mass spectrometry has also been reported. [55]

4.3.1 Computer Modeling of the Mg Binding Sites of Calmodulin

Computer modelling of the magnesium binding sites of calmodulin was accomplished in collaboration with Mr Nick Barton under the supervision of Dr Leo Caves from the York Structural Biology Laboratory at the University of York. It was hoped that computer modeling would help to identify the auxiliary magnesium binding sites present in calmodulin when the four primary sites were utilised for Ca^{2+} binding and give a better insight into the interactions of calmodulin with metal ions other than calcium. It was also hoped that the computer modelling would finally lead to an understanding of exactly how

many auxiliary metal binding sites exist on the calmodulin molecule. To this end the protein data bank (pdb) file for CaM + 4 Ca^{2+} ions was used as the primary data set, allowing the exact position of the amino acids to be known. To facilitate the calculation, the conformation of calmodulin when binding Ca^{2+} ions was taken to remain constant on binding the extra magnesium ions to the auxiliary sites. The changes that could result from Mg^{2+} binding to calmodulin were thought to be impossible to evaluate or predict. It should therefore be remembered that the following information is only valid if this assumption is correct.

The first step of the modeling process was to identify the residues that were most likely to be involved in Mg^{2+} binding. Initially this was accomplished by identifying the acidic residues that had β carbon atoms within a given distance of a β carbon on another acidic residue. This gave a rough indication of where to start looking for potential Mg^{2+} binding sites. However, this was far from conclusive, the position of these residues relative to one another in space had to be evaluated to provide information on likely pairs that could co-ordinate to the Mg ion without altering the initial conformation of calmodulin.

This step narrowed the potential binding sites down to 9 pairs of amino acids, these were (6,7) (11,14) (47,50) (78,82) (80,83) (84,87) (119,120) (118,122) and (123,127) where the numbers indicate the residue number of the amino acid in the pdb sequence. In addition, a further site was found that contained only a single acid side chain but contained the necessary geometry i.e. (29,49,45). This latter site seemed almost pre-organised for the Mg^{2+} ion. These areas of interest could then be manually manipulated to allow the side chains to take the appropriate orientations to allow them to bind to Mg^{2+} without significantly altering the underlying conformation of calmodulin. The side chains produced by this method were considered to look very odd, but minimisation calculations could be used to evaluate each side chain. The following diagram represents the solvent

accessible surface for calmodulin in the absence of magnesium atoms. The atoms were added afterwards with a Van der Waals representation to represent their space filling. The electro-static potential shows how the atoms are situated in areas of negative charge as expected.

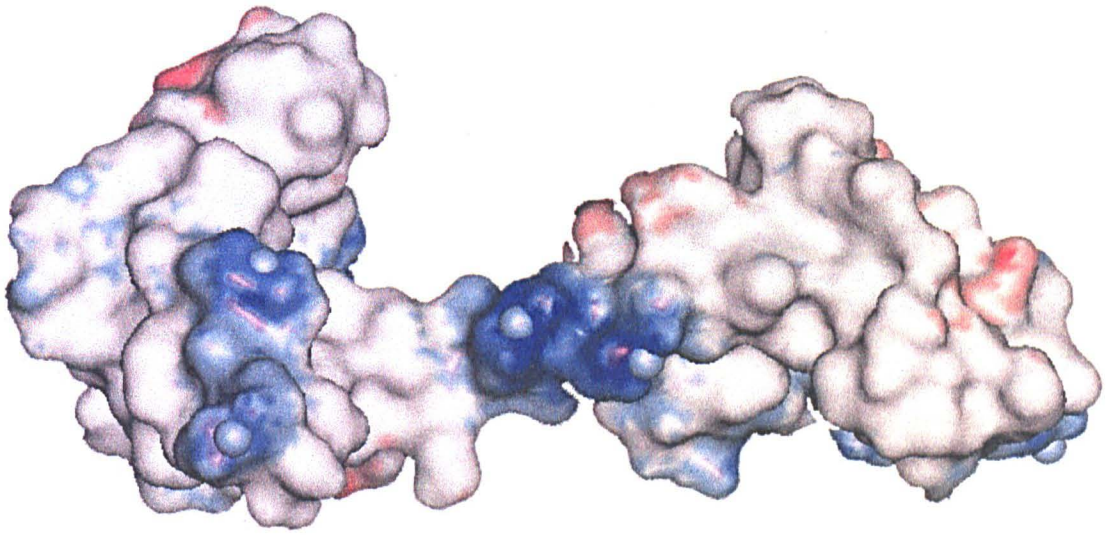

The next step in the modeling, as already mentioned, consisted of energy minimisation calculations. These were performed one at a time with the whole protein fixed and only the two (or three) residues and the magnesium allowed to alter their positions. The positions of the magnesium binding sites can be seen in the following diagrams of the electrostatic surface of calmodulin.

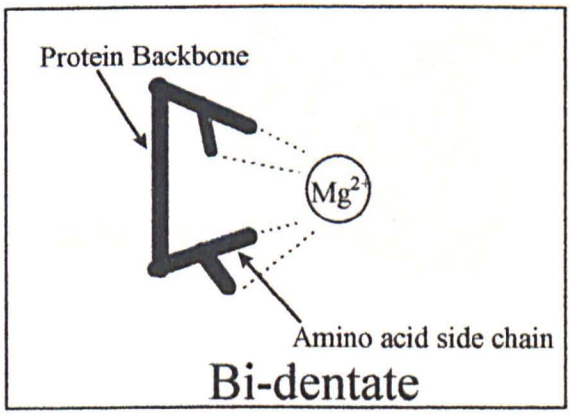

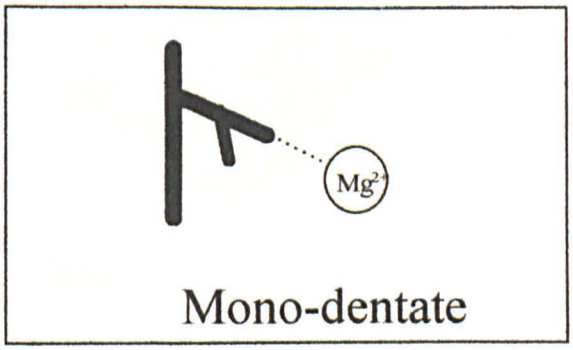

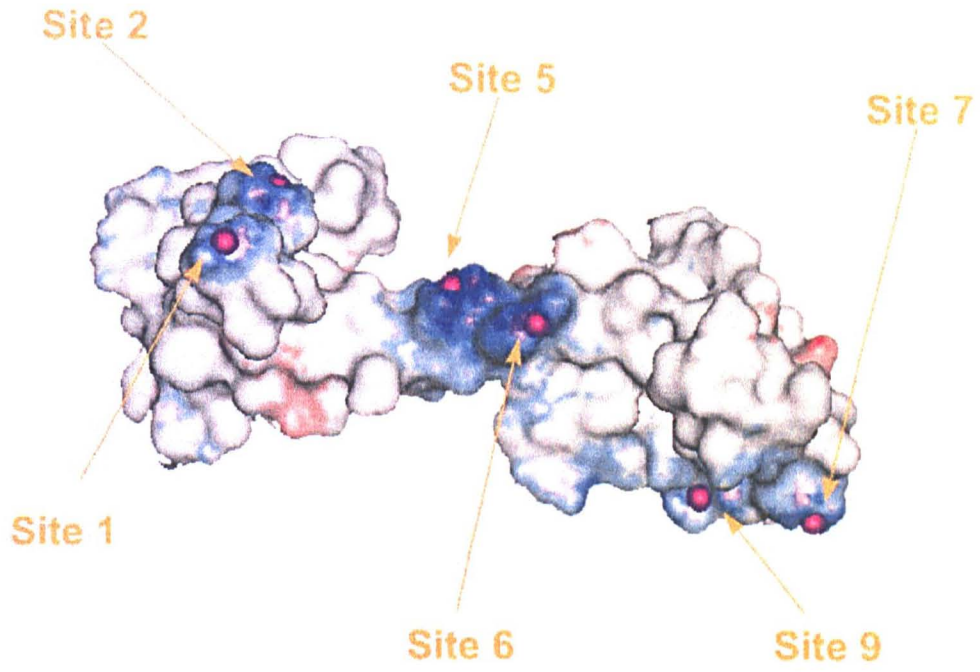
Site 2
Site 5
Site 7
Site 1
Site 6
Site 9

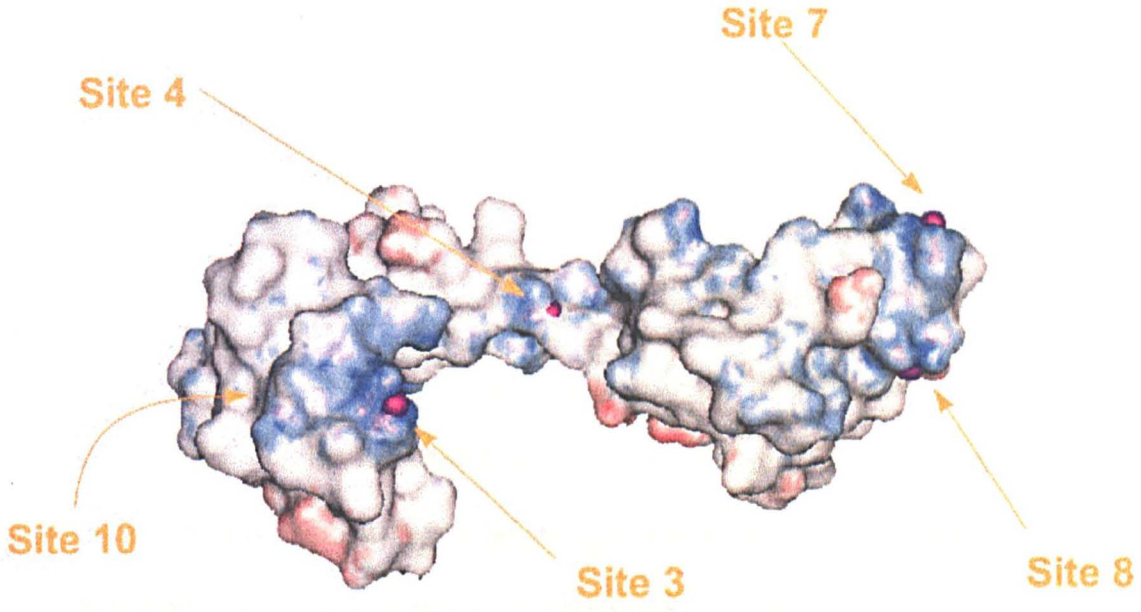
Site 7
Site 4
Site 10
Site 3
Site 8

The following table provides the relevant information on the magnesium binding sites.

Site	Residues	O-Mg Distance (Angstroms)
1	Glu 6	2.097, 2.071 (bi-dentate)
	Glu 7	2.101, 2.135 (bi-dentate)
2	Glu 11	2.073, 2.172 (bi-dentate)
	Glu14	2.164, 2.092 (bi-dentate)
3	Glu 47	2.059, 2.101 (bi-dentate)
	Asp 50	2.022, 3.940 (mono-dentate)
4	Glu 78	2.141, 2.101 (mono-dentate)
	Asp 82	3.153, 5.337 (mono-dentate)
5	Asp 80	2.178, 2.115 (bi-dentate)
	Glu 83	2.143, 2.104 (bi-dentate)
6	Glu 84	2.015, 3.843 (mono-dentate)
	Glu 87	2.058, 2.067 (bi-dentate)
7	Glu 119	2.092, 2.114 (bi-dentate)
	Glu 120	2.065, 2.061 (bi-dentate)
8	Asp 118	2.149, 2.121 (bi-dentate)
	Asp 122	2.107, 2.129 (bi-dentate)
9	Glu 123	1.597, 3.595 (mono-dentate)
	Glu 127	1.900, 3.615 (mono-dentate)
10	Thr 29	2.177
	Glu 45	2.070, 2.585 (bi-dentate)
	Gln 49	2.284

This simple model has shown that the binding of up to 10 magnesium ions is highly feasible using the simple binding motif of two acid residues. There exists one main problem, it is generally thought that a magnesium ion is too small to allow bi-dentate binding from a protein. Indeed it should be noted that even the larger calcium ion when bound to calmodulin is never co-ordinated by more than one bi-dentate acid. A possibility is that the solvent waters are involved in the co-ordination of magnesium ions to

calmodulin. These, theoretically, could bind at any angle and from any position, which would also result in a difficulty in modeling these interactions. It should be noted, however, that some of the pockets predicted by this model are so deep that the magnesium ions are totally enclosed by the rest of the protein. Site 10, for example, is invisible through the surface. Thus, the sites containing only two residues should be more than adequate for magnesium binding.

Further investigations, whereby the protein backbone is allowed to change conformation, and the solvent waters are taken into account are needed before any complete conclusions can be made from the computer modeling. However, the results so far provide a useful aid to thinking about calmodulin-metal ion interactions.

4.3.2 Experimental

4.3.2.2 Calmodulin Synthesis and Purification

DNA encoded calmodulin supplied by Dr. Daniel Lafitte had been produced by previously described procedures and purified by column chromatography in the laboratories of Jaques Haiech (Laboratoire de Chimie Bacterienne, University of Marseille). [56, 57]The purity of the protein, which was found to be greater than 99%, was then checked by SDS polyacrylamide gel and high-pressure capillary electrophoresis. ESI FT-ICR mass spectrometry experiments were carried out in ultra-pure water (Elga system) and plastic laboratory equipment to minimise unwanted salt contamination such as sodium and magnesium ions. Before introduction to the instrument calmodulin was further purified by desalting the sample using a Pharmacia Biotech Sephadex (Uppsala, Sweden) PD 10 column (see section 3.2.1). The concentration of these aliquots was determined by UV absorption on a Jasco V-550 spectrophotometer. The molar extinction coefficient

used for these experiments was ε_{280nm}=1560 $M^{-1}cm^{-1}$ and the concentration of the fractions was found to be between 20 and 25 μM.

The synthetic peptide analogue used for this study (RS20; sequence RRKWQKTGHAVRAIGRLSSS) is derived from the phosphorylation site of myosin light chain kinase (a protein known to be regulated by calmodulin) This peptide has been shown to inhibit calmodulin-stimulated light chain kinase activity and must therefore be interacting with calmodulin in preference to myosin light chain kinase (MLCK).

4.3.3 Results

Figure 16 shows the spectrum of calmodulin in ammonium acetate (5mM, pH 5.8) in the absence of organic solvents. As can be seen clearly from the spectra at least two charge distributions can be seen. This suggests that there are at least two conformations of calmodulin present even when electrosprayed from solvent that is supposed to maintain the natural conformation of the protein. The higher charge state distribution centered around the 12^+ is similar to that observed when calmodulin is electrosprayed in organic solvents ,and as has previously been postulated (see section 3.3.1), this is due to the protein being in a more open conformation. [58-61]The lower charge state distribution centred around 8^+ is believed to be representative of calmodulin in its natural or active conformation. In this case the experimentally determined monoisotopic mass of calmodulin was 16,616.84±0.02 Da compared with the theoretical mass calculated from the sequence of 16,616.821 Da. Also to be noted in this spectrum is the presence of peaks attributed to non-covalent calmodulin dimers. [55]

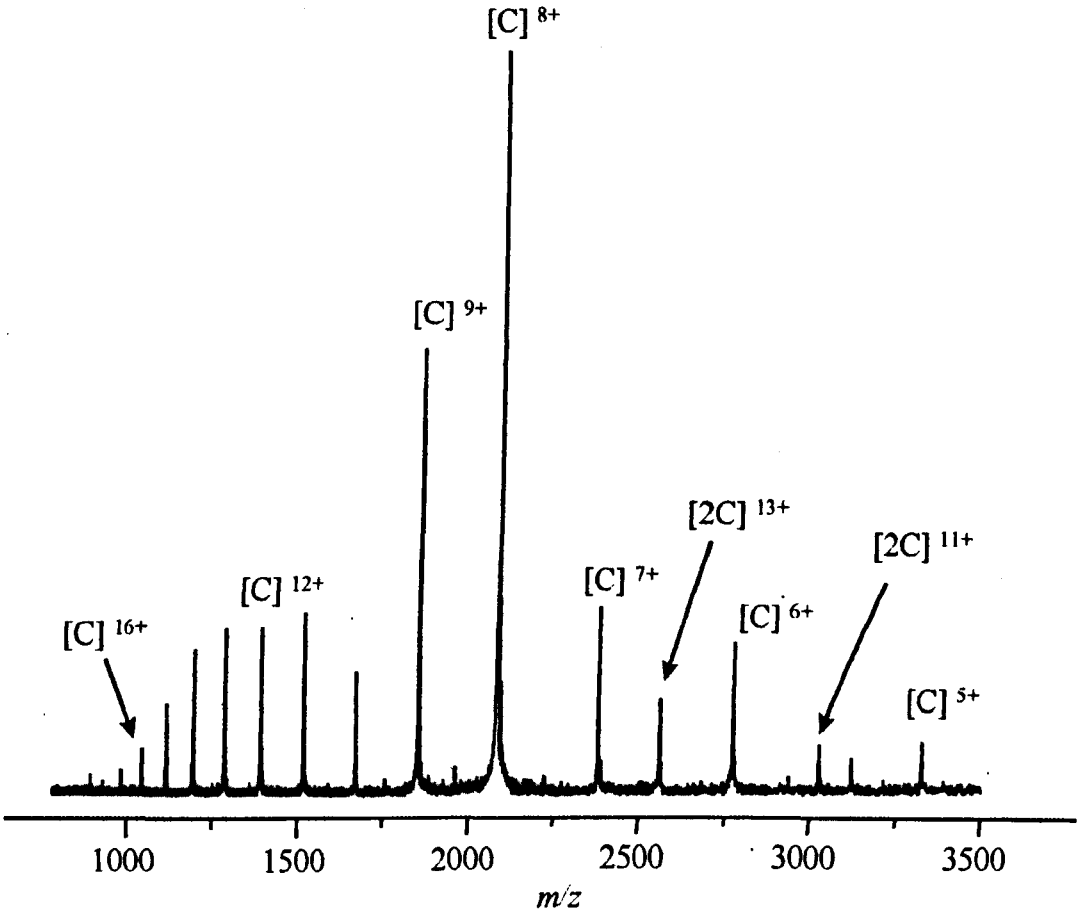

Figure 16: Calmodulin in the absence of Ca^{2+} ions in ammonium acetate (5mM, pH 5.8), where C represents the calmodulin molecule. The bimodal distribution is due to the presence of both the natural conformation and the denatured form of papain being present in the analyte solution.

4.3.3.1 Interaction Of Calmodulin-RS20

Previous investigations of calmodulin and calmodulin binding peptides have shown a propensity for calmodulin-peptide interactions to occur only in the present of Ca^{2+} ions [51], although there are cases where Ca^{2+} ions have been found not to be necessary for binding to occur. [47]An extensive literature search at the time of completion of this work revealed no evidence for RS20 interacting with apo-calmodulin. It is proposed from the spectra in Figure 18 that apo-calmodulin binds a single RS20.

The inset shows a species $[C+P]^{9+}$ (where C represents calmodulin and P the RS20 peptide) that has an average mass of 18,922.14 Da. Since calmodulin and RS20 have an average mass of 16,627.37 Da and 2,294.65 Da respectively, a complex should have an average mass of 18,922.02 Da which is in very good agreement with the experimental number.

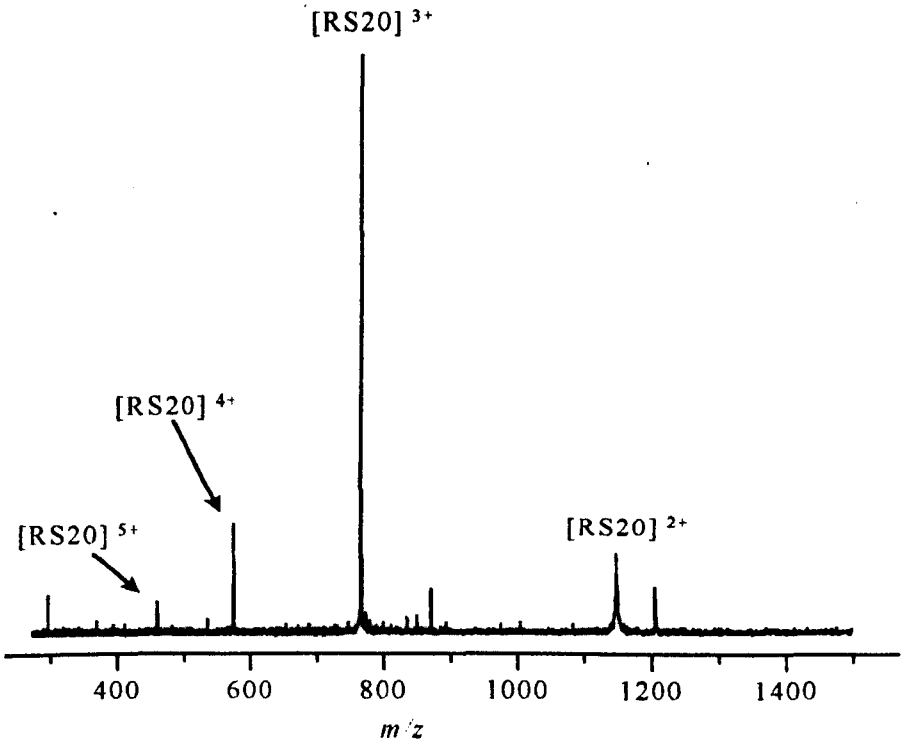

Figure 17: Electrospray mass spectrum of RS20 in ammonium acetate (5mM, pH 5.8).

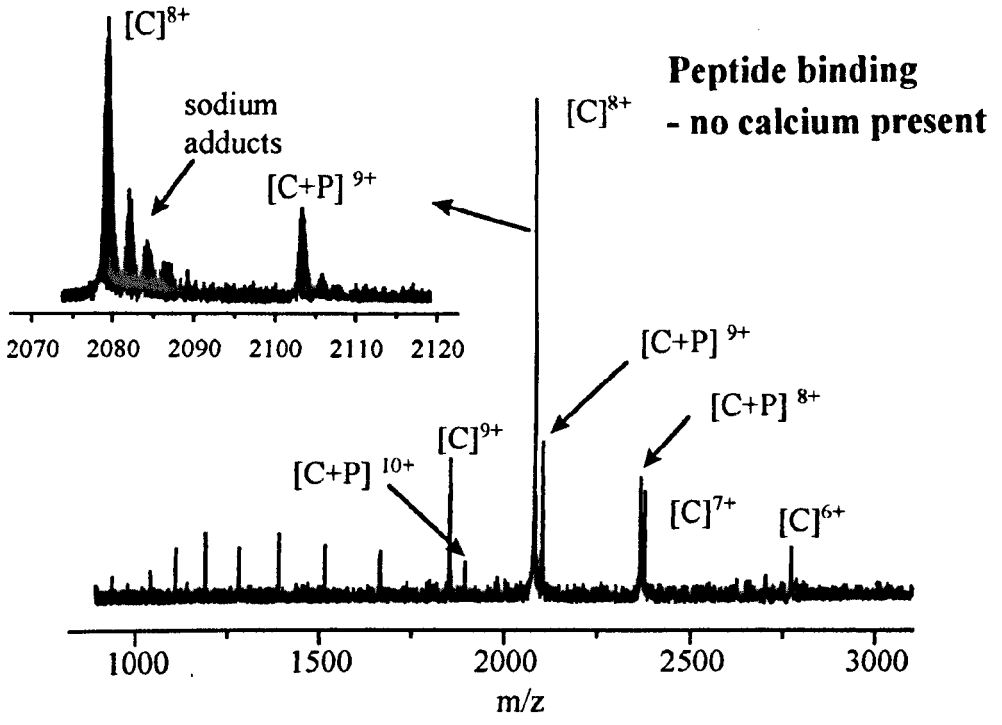

Figure 18: ESI mass spectrum of apo-calmodulin and RS20 (1:1.5) in ammonium acetate (5 mM, pH 5.8).

In previous experiments carried out by other groups on the characterisation of calmodulin-peptide interactions by mass spectrometry, this type of interaction may have been prevented because use was made of EDTA or EGTA to remove unwanted Ca^{2+} ions from the analyte solution. It was observed in this work that both EDTA and EGTA bind to calmodulin (see Figure 19, also section 5.3.2).

Close inspection of Figure 18 suggests that the binding of RS20 to apo-calmodulin has caused the charge state of the complex to increase by one. That is to say, RS20 binding to the 8^+ charge state of apo-calmodulin has caused the charge state to increase by one to 9^+. Either the peptide is bringing a single positive-charge site with it when it binds to calmodulin or the peptide causes apo-calmodulin to form a more open conformation.

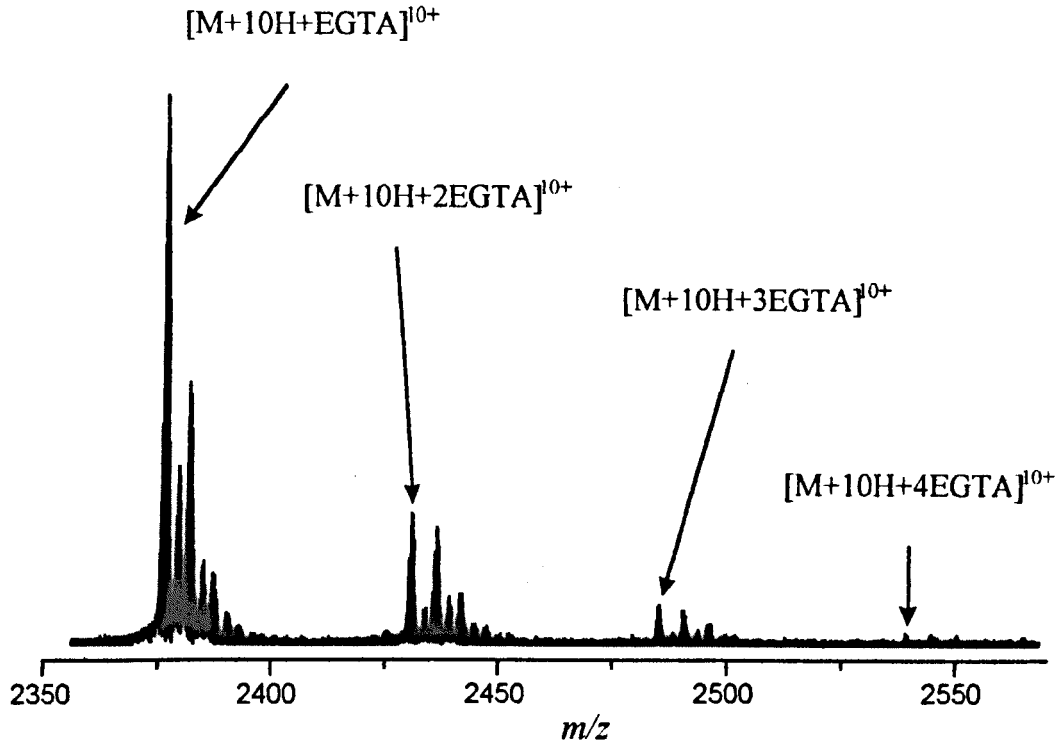

Figure 19: Calmodulin with EGTA added to remove excess Ca^{2+} ions in ammonium acetate (5mM, pH 5.8). Note the Cam+EGTA complexes.

Both scenarios would result in an overall increase in charge in the mass spectrum but it is not obvious how to distinguish them.

On increasing the proportion of RS20:calmodulin the lower charge states were observed to decrease and eventually disappear (see Figure 20). This indicates a loss of the more tightly folded or natural conformation of calmodulin due to a disruption by RS20. It can also be seen that the numbers of peptides binding to calmodulin increased after the ratio exceeds 1:6. From a ratio of 1:1.5 to 1:6 (calmodulin:RS20) only a stoichiometry of 1:1 (calmodulin:RS20) was observed. However, the higher concentrations of RS20 result in two RS20's binding at a calmodulin: RS20 ratio of 1:13 and up to four RS20's bound at a ratio of 1:17. At a ratio of 1:17, peptide dimers are observed at low *m/z* formed by peptide aggregation. This raises the question as to whether $[C+4P]^{14+}$, for example, is a result of four RS20 monomers or two RS20 dimers binding to calmodulin, since the mass increase observed for both scenarios would be identical.

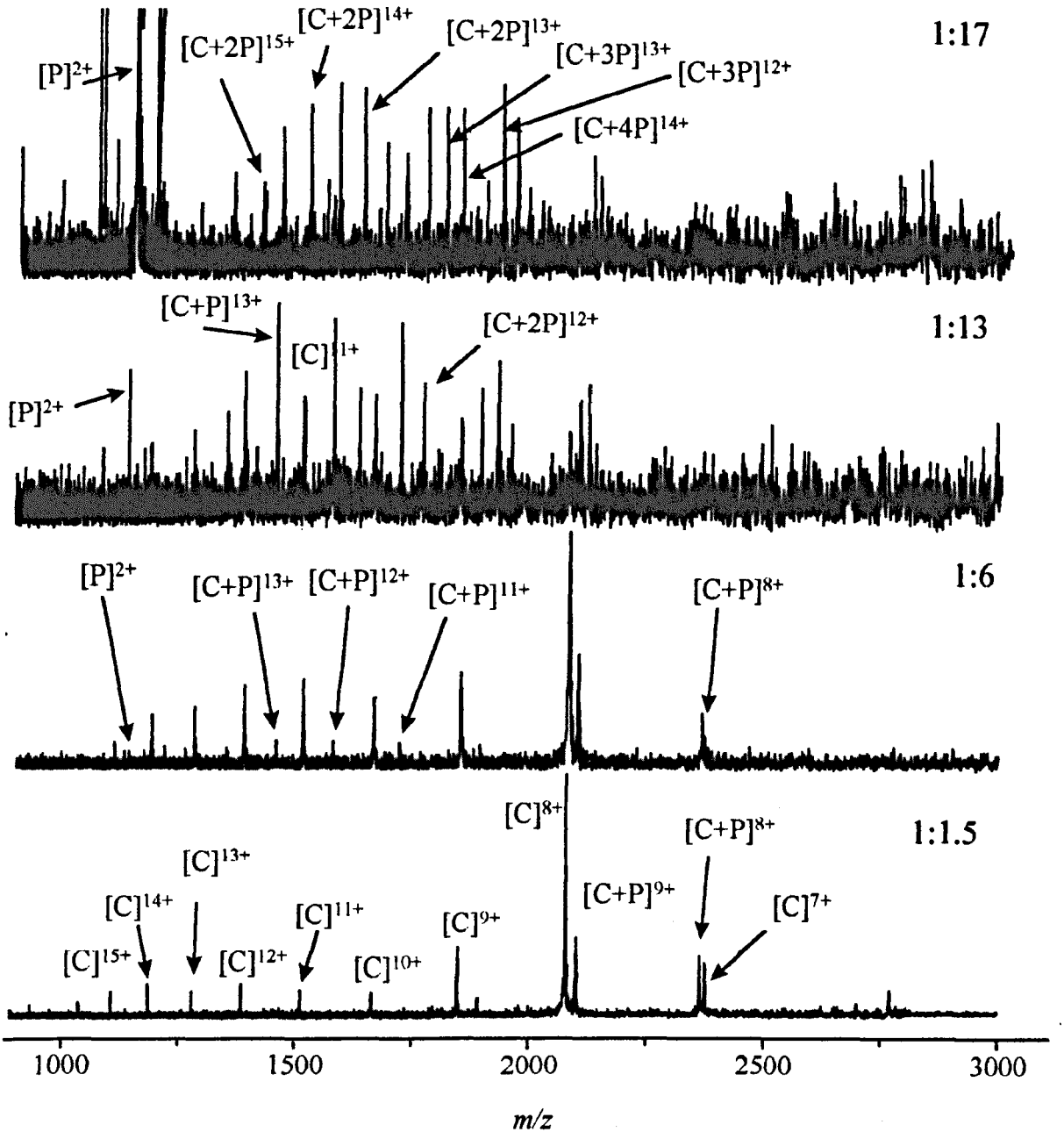

Figure 20: Calmodulin: RS20 at various ratios in ammonium acetate (5mM, pH 5.8).

4.3.3.2 Effect of Calcium on Calmodulin: RS20 Non-covalent Interactions

A comparison of the spectra shown in figures 18, 21 and 22 shows the effects of increasing calcium concentration on the binding of RS20 to calmodulin. Comparing figures 18 and 21 i.e. changing from a ratio of calmodulin: Ca^{2+} of 1:0 to one of 1:1.5, there is an obvious change in the intensity distribution of the peaks. In the absence of Ca^{2+} ions (Figure 18) the most intense peak for un-complexed calmodulin corresponded to the 8^+ charge state, compared with the similarity in intensity of the 8^+ and 7^+ charge states in Figure 21. The charge state distribution has effectively altered and, as previously stated, a shift in the charge distribution of an electrospray spectrum of a protein is indicative of an underlying conformational change of the protein in the sprayed solution. The addition of even this small amount of Ca^{2+} ions to apo-calmodulin can therefore be said to have initiated a conformational change. This can be observed in Figure 21 not only in the change of intensities of the peaks corresponding to calmodulin alone, but also in the apparent greater affinity of RS20 for holo-calmodulin compared to apo-calmodulin. Considering the insets of figures 21 and 22, there are increases in the intensities and thus the abundances of the complex ions on increasing Ca^{2+} ion concentration while retaining the same calmodulin:RS20 ratio. Comparing Figure 18 and Figure 22 it is clearly seen that there are many more non-covalent complexes between calmodulin and RS20 in the presence of a large number of Ca^{2+} ions.

It should be noted, however, as evident from figures 18 and 20 that Ca^{2+} ions were not required for calmodulin: peptide interactions to take place. In both figures peaks corresponding to $[C+P]^{9+}$ through to $[C+P]^{6+}$ complexes are present. This is in direct contradiction to mass spectrometric investigations in the negative ion mode of calmodulin by Gross *et al* and Veenstra *et al* [53]that showed a calcium dependence of calmodulin

when binding to target peptides and proteins. It is believed that this is the first mass spectrometric evidence for calmodulin: peptide interactions in the absence of calcium ions.

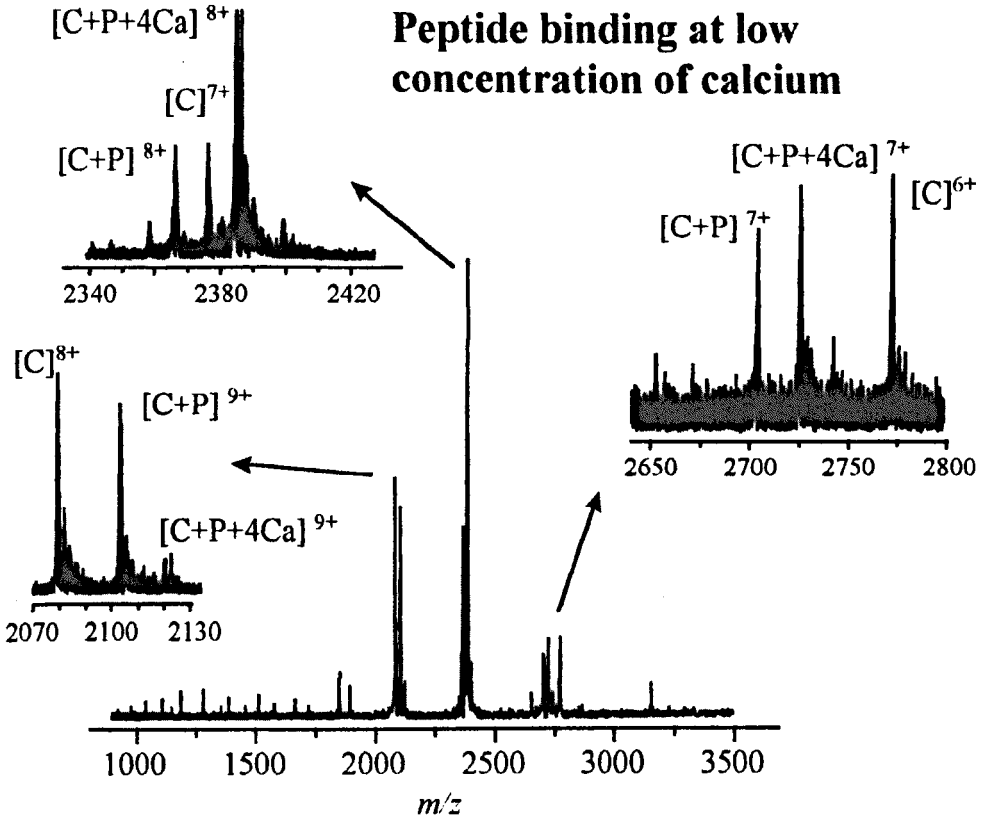

Figure 21: ESI mass spectrum of apo-calmodulin and RS20 (1:1.5) plus 0.01 mM $CaCl_2$ in ammonium acetate (5mM, pH 5.8). Where C represents the protein calmodulin and Ca = Ca^{2+}. [CaM:RS20:Ca] is 1:1.5:0.4.

Finally it should be noted that in figures 21 and 22 a marked preference exists for calmodulin: RS20: Ca^{2+} complexes with a ratio of 1:1:4. This is especially evident in the insets of Figure 22. A complete loss of the higher charge states at 0.1 mM $CaCl_2$ was observed meaning that the Ca^{2+} ions have induced a complete conformational change of all the calmodulin present in the analyte solution i.e. the calmodulin conformation is now completely in its "natural" state.

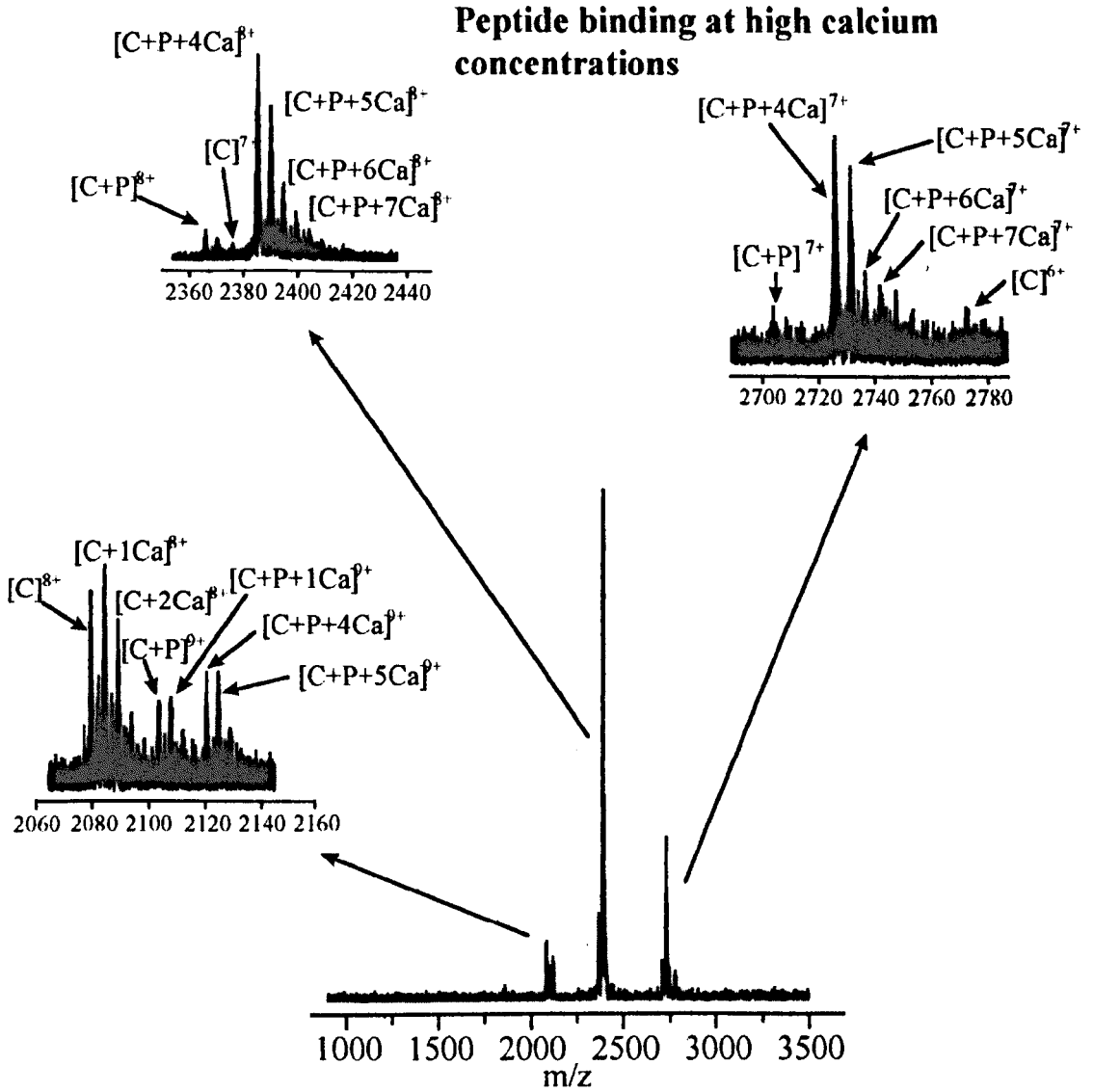

Figure 22: ESI mass spectrum of apo-calmodulin and RS20 (1:1.5) plus 0.1 mM $CaCl_2$ in ammonium acetate (5mM, pH 5.8). [CaM:RS20:Ca] is 1:1.5:4.

4.3.3.3 Effect of Magnesium on Calmodulin: RS20 Non-covalent Interactions

Experiments involving Mg^{2+} ions in a 1:6:1.5 mixture of calmodulin: magnesium: RS20 were also carried out.. Magnesium was shown to bind to calmodulin (see Figure 23), with up to four bound to the protein. However, unlike calmodulin with $CaCl_2$ there was no preference for the stoichiometry 1:1:4

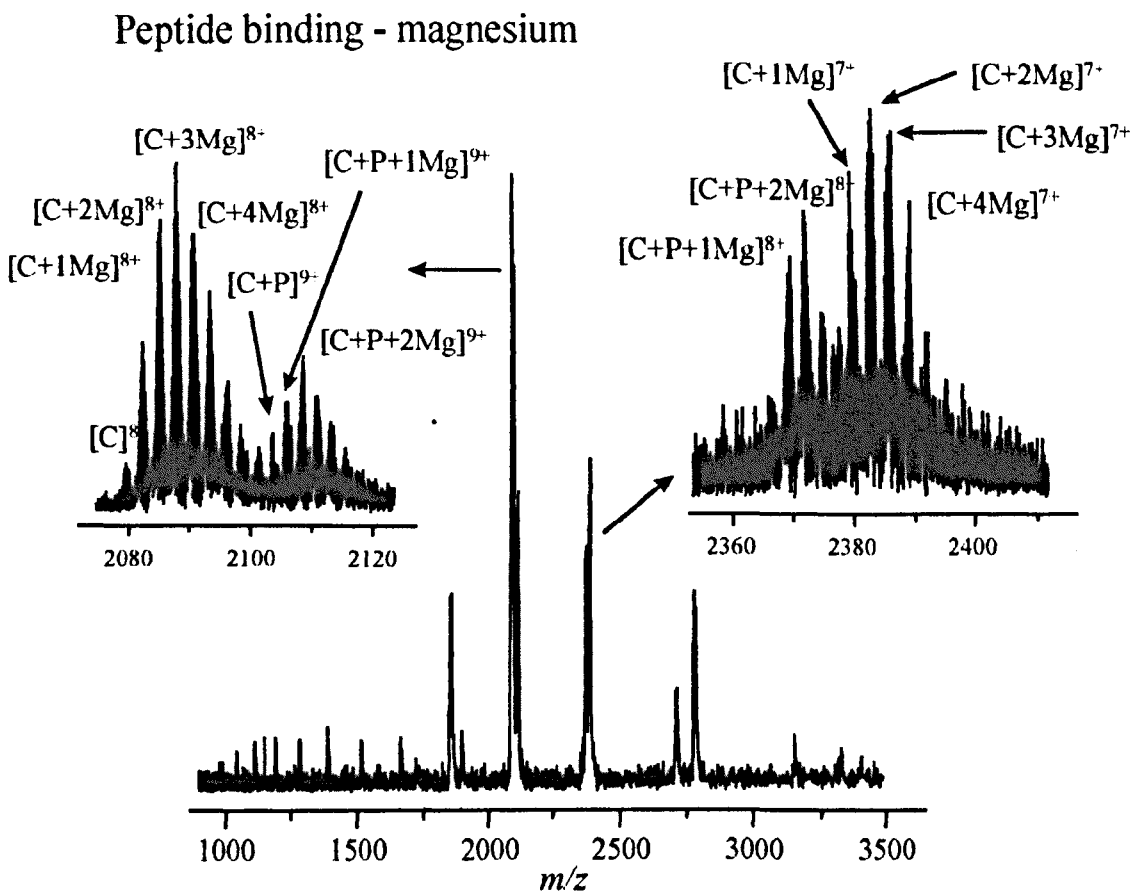

Figure 23: ESI mass spectrum of apo-calmodulin and RS20 (1:1.5) plus 0.3 mM $MgCl_2$ in ammonium acetate (5mM, pH 5.8). [CaM:RS20:Mg] is 1:1.5:12.

(calmodulin: RS20: Ca^{2+}). Stoichiometries of 1:1:1 and 1:1:2 (calmodulin: RS20: Mg^{2+}) were observed (see insets of Figure 23). Non-covalent complexes between apo-calmodulin and RS20 also existed in the $MgCl_2$ doped analyte solutions.

It suggests that there was no shift in the charge states, as there was for the $CaCl_2$ loaded sample. This suggests that although Mg^{2+} ions do bind to calmodulin, they do not induce a conformational change in the protein.

4.4 Conclusion

Papain has been proven to bind both the tetra-peptide GGYR and the tri-peptide KAA, with the tri-peptide binding more strongly to the active site in comparison with GGYR. A complimentary study using circular dichroism has confirmed this observation; the conformational change induced on the protein by KAA is greater than that induced by GGYR. The strength of the bond between the peptides has also been investigated using capillary skimmer collision induced dissociation techniques whereby it was noted that KAA was still bound at a voltage of 160 V compared with only 140 V for GGYR. The small size of the KAA compared with GGYR probably accounts for the stronger bond between peptide and protein, since it will fit deeper into the active site and thus be more completely surrounded by the coordinating amino acids of papain. Attempting non-covalent interactions of papain with tetra-glycine (GGGG) (Figure 8) produced no observable protein-peptide complexes, suggesting that peptides are specific for the active site. Some non-specific binding of peptides to proteins should be, and indeed are, seen at higher ratios of papain: peptide, but lower ratios should provide information on the specificity of peptides for proteins. This is confirmed by varying the ratios of protein: peptide from 1:25 to 1:8 for both KAA and GGYR. In both cases at higher ratios more than one peptide is observed to bind to papain, due to non-specific non-covalent interactions about the protein surface. It is interesting to note that the protein: peptide distributions differ between GGYR and KAA bound to papain. The spectra show a bell shaped distribution of papain: KAA complexes (Figure 7) centred at 1:6 (papain: KAA) compared to a distribution for GGYR that has a maximum at a ratio of 1:1 (Figure 6). This can be considered to indicate that either (1) KAA and GGYR bind non-specifically to papain in the form of multimers at these higher concentrations of peptide i.e. hexamers of

KAA bind to papain, either at the active site or somewhere on the surface of the protein or (2) that numerous individual peptides bind to different positions on the protein surface and also possibly at the active site. It is more consistent that multimers are binding to the protein, since results obtained with the peptides alone and spectra with papain and peptide (with an extended lower mass range) show the presence of free multimeric forms of the peptides (see Figure 12) at these higher concentrations.

The results obtained for calmodulin, RS20 and Ca^{2+} or Mg^{2+} metal ions show the first mass spectrometric evidence of apo-calmodulin binding a peptide. As already mentioned experiments carried out in the negative mode by Gross *et al* and Veenstra *et al* [53] indicated that calmodulin peptide complexes were only observed in the presence of Ca^{2+} ions. This may have been due to their use of EGTA or EDTA to remove all the Ca^{2+} ions from solution. It has been noted in the process of these studies (section 5.3.2) that EGTA and EDTA bind to calmodulin (see Figure 19), this may have prevented the observation of the apo-calmodulin: peptide complex in these studies. The fact that the apo-calmodulin: RS20 complex is observed does not mean, however, that the peptide has been activated. It may be that for activation to occur, the four Ca^{2+} ions, as proposed in the sequential binding model, would have to present. In this particular case calmodulin may be in some intermediate stage of peptide activation i.e. the protein may be weakly bound to the target peptide by only a single domain; the protein may then be "waiting" Ca^{2+} to bind and cause the full activation. Such a mechanism could involve calmodulin binding to the target protein and then being activated by an intra-cellular rise in Ca^{2+} ion concentration. This would be a faster alternative to the currently established mechanism where four Ca^{2+} ions must bind sequentially to calmodulin to activate it, and then calmodulin must diffuse

to the site of target interaction. However, it has been successfully proven that for calmodulin to bind to the target peptide no Ca^{2+} ions are required.

The conformation of calmodulin has been shown to be changed by the addition of Ca^{2+} ions to the analyte solution as seen by the change in the charge state distribution. This is from high charge states (the open conformation) to low charge states (the natural or native conformation); a gradual change as the Ca^{2+} ion concentration is gradually increased. Simultaneously with the loss of the more open conformation, auxiliary sites present in calmodulin are filled as indicated by the presence of species such as $[C+P+6Ca]^{7+}$ and $[C+P+5Ca]^{7+}$. It should also be noted that the conformation "tightens" even more at the highest levels of Ca^{2+} ion addition as evidenced by the shift in the relative intensities of the peaks in the lower charge states (9^+ to 7^+) see figures 18 and 21.

There is a definite preference for calmodulin:RS20:Ca^{2+} complexes in the ratio 1:1:4 and an absence of protein: peptide complexes with 1,2 and3 Ca^{2+} ions bound. This is the case even at the lowest concentrations of Ca^{2+} doping of the analyte solution. Thus the co-operativity of the Ca^{2+} ion-binding sites are illustrated by these experiments and the affinity of calmodulin for calcium ions is obviously greatly increased in the presence of RS20.

Mg^{2+} ions do not promote a conformational change in calmodulin as seen for Ca^{2+} ions. This is indicated by the retention of the higher charge states in the electrospray spectra obtained. The complexes of calmodulin: RS20: Ca^{2+} with RS20 are typically in the ratios 1:1:1 and 1:1:2. This is un-like calmodulin in the presence of calcium, as the most abundant species in the Mg^{2+} doped analyte solutions seems to be controlled purely by the salt concentration.

The utility of mass spectrometry for the analysis of non-covalent interactions has been demonstrated conclusively in this chapter. The wealth of information available from a relatively simple set of experiments has proven that electrospray ionisation coupled with the high resolution and sensitivity of FT-ICR mass spectrometry is a valuable technique for the analysis of biological molecules and their interactions.

References

[1] X. Tang, J. H. Callahan, P. Zhou, A. Vertes, *Anal. Chem. 67* (1995) 4542.

[2] A. S. Woods, J. C. Buchsbaum, T. A. Worral, J. M. Berg, R. J. Cotter, *Anal. Chem. 67* (1995) 4462.

[3] I. Gruie-Sovulj, H.-C. Ludemann, F. Hillenkamp, I. Weygand-Durasevic, Z. Kucan, J. Peter-Katalinic, *J. Biol. Chem. 272* (1997) 32084.

[4] J. A. Loo, *Mass Spectrom. Rev. 16* (1997) 1.

[5] H.-K. Lim, Y. L. Hsieh, B. Ganem, J. Henion, *J. Mass Spectrom. 30* (1995) 708.

[6] J. A. Loo, P. Hu, P. McConnell, W. T. Meuller, T. K. Sawyer, V. Thanabal, *J. Am. Soc. Mass Spectrom. 8* (1997) 234.

[7] R. Feng, *43 rd ASMS Conference on mass spectrmetry and allied topics* (Atlanta, GA), Unusually strong binding of a non-covalent gas phase spermine complex and its dramatic temperature dependence, pp. 1264 (1995).

[8] X. H. Cheng, A. C. Harms, P. N. Goudreau, T. C. Terwilliger, R. D. Smith, *Proc. Natl. Acad. Sci. USA. 93* (1996) 7022.

[9] J. A. E. Kraunsoe, R. T. Aplin, B. Green, G. Lowe, *FEBS Letters 396* (1996) 108.

[10] P. D. Schnier, D. S. Gross, W. D. Price, Y. Zhao, E. R. Williams, *44th ASMS Conference on Mass Spectrometry and Allied Topics* (Portland, OR), BIRD: binding energies of non-covalent biomolecule complexes in the gas phase, pp. 473 (1996).

[11] N. D. Rawlings, A. J. Barrett, in A. J. Barrett (Ed.): *Methods in Enzymology, Proteolytic enzymes : Serine and Cysteine Peptidases, Vol. 244*, Academic Press, Inc. 1994, p. 461.

[12] R. Menard, J. Carriere, P. Laflamme, C. Plouffe, H. E. Khouri, T. Vernet, D. C. Tessier, D. Y. Thomas, A. C. Storer, *Biochemistry 30* (1991) 8924.

[13] R. Menard, C. Plouffe, P. Laflamme, T. Vernet, D. C. Tessier, D. Y. Thomas, A. C. Storer, *Biochemistry 34* (1995) 464.

[14] T. Vernet, D. C. Tessier, J. Chatallier, C. Plouffe, T. S. Lee, D. Y. Thomas, A. C. Storer, R. Menard, *J. Biol. Chem. 270* (1995) 16645.

[15] D. Bromme, P. R. Bonneau, E. Purisima, P. Lachance, S. Hajnik, D. Y. Thomas, A. C. Storer, *Biochemistry 35* (1996) 3970.

[16] A. C. Storer, R. Menard, in A. J. Barrett (Ed.): *Methods in Enzymology, Proteolytic Enzymes : Serine and Cysteine Peptidases, Vol. 244*, Academic Press, Inc. 1994, p. 487.

[17] L. Stryer, *Biochemistry*, Freeman 1988.

[18] M. O. Funk, Y. Nakagawa, J. Skochdopole, E. T. Kaiser, *Int. J. Peptide Protein Res. 13* (1979) 296.

[19] B. Granier, M. Jamin, M. Adam, M. Galleni, B. Lakaye, W. Zorzi, J. Grandchamps, J. M. Wilkin, C. Fraipont, B. Joris, C. Duez, M. Nguyen-Disteche, J. Coyette, M. Leyh-Bouille, J. Dusart, L. Christiaens, J. M. Frere, J. M. Ghuysen, in A. J. Barrett (Ed.): *Methods in Enzymology, Proteolytic Enzymes : Serine and Cysteine Peptidases, Vol. 244*, Academic Press, Inc. 1994.

[20] R. Menard, R. Feng, A. C. Storer, V. J. Robinson, R. A. Smith, A. Krantz, *FEBS Letters 295* (1991) 27.

[21] A. Rodger, B. Norden, *Circular Dichroism and Linear Dichroism*, Oxford University Press 1997.

[22] J. A. Cox, *Biochem. J. 249* (1988) 621.

[23] H. J. Vogel, *Biochem. Cell. Biol. 72* (1994) 37.

[24] R. H. Kretsinger, *CRC. Critrev. Biochem. 8* (1980) 118.

[25] Y. S. Babu, C. E. Bugg, W. J. Cook, *J. Mol. Biol. 204* (1988) 191.

[26] R. Chattopdahyaya, W. E. Meador, A. R. Means, F. A. Quiocho, *J. Mol. Biol. 1117-1192* (1992) .

[27] A. Persechini, R. H. Kretsinger, *J. Biol. Chem. 263* (1988) 12175.

[28] J. J. Falke, S. K. Drake, A. L. Hazard, O. B. Peerson, *Q. Rev. Biophys. 27* (1994) 219.

[29] M. Ikura, M. Clore, A. M. Gronenborn, G. Zhu, C. B. Klee, A. Bax, *Science 256* (1992) 632.

[30] J. Haiech, C. B. Klee, J. Demailee, *Biochemistry 20* (1981) 3890.

[31] I. M. Klotz, *Q. Rev. Biophys 18* (1985) 227.

[32] I. Protasevich, B. Ranjibar, V. Lobachov, A. Makarov, R. Gilli, C. Briand, D. Lafitte, J. Haiech, *Biochemistry 36* (1997) 2017.

[33] R. Gilli, D. Lafitte, C. Lopez, M. Kilhoffer, A. Makarov, C. Briand, J. Haiech, *Biochemistry 37* (1998) 5450.

[34] D. Lafitte, J. P. Capony, M. Comte, J. A. Cox, *Biochemistry 34* (1995) 13825.

[35] M.-C. Kilhoffer, D. M. Roberts, A. O. Adibi, D. M. Watterson, J. Haiech, *J. Biol. Chem. 32* (1988) 17023.

[36] M. Milos, J. J. Schaer, M. Comte, J. A. Cox, *J. Inorg. Biochem. 36* (1986) 11.

[37] J. S. Mills, J. D. Johnson, *J. Biol. Chem. 260* (1985) 15100.

[38] M. Milos, M. Comte, J. J. Schaer, J. A. Cox, *J. Inorg. Chem. 26* (1989) 11.

[39] M. C. Kilhofer, M. Kubina, F. Travers, J. Haiech, *Biochemistry 31* (1992) 8098.

[40] A. R. Means, M. F. A. V. Berkum, I. Bagchi, K. P. Lu, C. D. Rasmussen, *Pharmacol. Ther. 50* (1991) 255.

[41] A. Barth, S. R. Martin, P. M. Bayley, *J. Biol. Chem. 273* (1998) 2174.

[42] M. Ikura, *Nature 256* (1992) 632.

[43] M. Afshar, *J. Mol. Biol. 244* (1994) 554.

[44] S. Pedigo, M. A. Shea, *Biochemistry 34* (1995) 1179.

[45] S. Pedigo, M. A. Shea, *Biochemistry 34* (1995) 10676.

[46] M. A. Shea, A. S. Verhoeven, S. Pedigo, *Biochemistry 35* (1996) 2943.

[47] M. Zhang, T. Tanaka, M. Ikura, *Nat. Struct. Biol. 2* (1995) 758.

[48] D. K. Blumenthal, K. Takio, A. M. Edelman, H. Charbonneau, K. Titani, K. A. Walsh, E. G. Krebs, *Proc. Natl. Acad. Sci. USA. 82* (1985) 3187.

[49] R. E. Klevit, D. K. Blumenthal, E. G. Krebs, J. T. Stull, *Biochemistry 24* (1985) 8152.

[50] D. B. Heidorn, P. A. Seeger, S. E. Rokop, D. K. Blumenthal, A. R. Means, H. Crespi, J. Trewhalla, *Biochemistry 28* (1989) .

[51] O. V. Nemirovskiy, R. Ramanathan, M. L. Gross, *J. Am. Soc. Mass Spectrom. 8* (1997) 809.

[52] T. D. Veenstra, K. L. Johnson, A. J. Tomlinson, S. Naylor, R. Kumar, *Eur. Mass Spectrom. 3* (1997) 453.

[53] T. D. Veenstra, A. J. Tomlinson, L. Benson, R. Kumar, S. Naylor, *J. Am. Soc. Mass. Spectrom. 9* (1998) 580.

[54] P. Hu, Q. Z. Ye, J. A. Loo, *Anal. Chem. 66* (1994) 4190.

[55] D. Lafitte, A. J. R. Heck, T. J. Hill, K. Jumel, S. E. Harding, P. J. Derrick, *Eur. J. Biochem.* (1998) .

[56] D. M. Roberts, R. Crea, M. Malecha, G. Alvarado-Urbina, R. H. Chiarello, D. M. Waterson, *Biochemistry 24* (1985) 5090.

[57] T. A. Craig, D. M. Waterson, F. G. Prendergast, J. Haiech, D. M. Roberts, *J. Biol. Chem. 262* (1987) 3278.

[58] S. K. Chowdhury, V. Katta, B. T. Chait, *J. Am. Chem. Soc. 112* (1990) 9012.

[59] R. Feng, Y. Konishi, *J. Am. Soc. Mass Spectrom. 4* (1993) 638.

[60] M. Hamdan, O. Curcuruto, *Rapid Commun. Mass Spectrom. 8* (1994) 144.

[61] J. A. Loo, R. R. Ogorzalek-Loo, H. R. Udseth, C. G. Edmonds, R. D. Smith, *Rapid Commun. Mass Spectrom. 5* (1991) 101.

5.0 Conformational Study Of Calmodulin

5.1 Introduction

Solution and gas-phase H/D exchange have been investigated using ESI FT-ICR mass spectrometry to measure changes in the mass of calmodulin with a view to probing the conformation of this protein. The resolution obtainable from FT-ICR makes it possible to assign unequivocally peaks present in the mass spectra to specific adducts. Most commonly in this part of the study, these were calcium adducts.

Conformational changes as a result of calcium ion addition to the analyte solution will also be discussed and evaluated.

5.1.2 Hydrogen-Deuterium Exchange

The replacement of hydrogens by deuteriums in peptides, proteins and other biological and non-biological samples has been the basis of a standard probe of molecular conformation for a number of years in the field of mass spectrometry. Significant advances in the amount of information obtainable from this technique in solution have occurred, which have allowed mass spectrometry to be used to probe the conformations of molecules in more and more detail. [1]For example, deuterium levels at specific peptide amide linkages have been determined [2, 3] and by making use of proteolytic fragmentation the exchange levels in specific parts of the protein can be ascertained. [4, 5]

Solution hydrogen/deuterium (H/D) exchange has usually utilised deuterium oxide (D_2O) as the solvent of choice. The procedure is to incubate the sample in this solution for set periods of time and the number of hydrogen for deuteriums exchanged monitored by mass spectrometry. From these changes it is possible to build up a profile that reflects in some way the protein conformation in solution. The binding of substrates, for example,

metal ions or peptides, to a protein will change the conformation of the protein, and will thus affect how many hydrogens are accessible to the deuterated solvent. Thus if the structure of the protein were to become more open, an increase in the number of exchanges would be expected, while a contraction of the structure would be expected to in a reduction. Thus, for example, a protein on binding an inhibitor at the active site might become more compact as the protein backbone wrapped around the inhibitor; the consequence should be a noticeable reduction in the number of hydrogens exchanged for deuterons.

For proteins and peptides, H/D exchange is observed to take place mainly at the peptide bonds and at the N terminus. [1]The other hydrogens present in the molecule i.e. on the functional side-chains of the amino acid back-exchange too rapidly for routine detection by mass spectrometry. This is due to the fact that H/D exchange must be quenched after the desired period by a reduction in temperature to around 0°C and the lowering of the sample's pH to around 2. [1]The sample is then introduced to the mass spectrometer, but this delay means that most of the rapidly exchangeable deuteriums from the side chains will back exchange before analysis.

Gas phase H/D exchange, on the other hand, does not suffer in the same way from this problem of back exchange, since the analyte ions in the gas phase react with a deuterated gas such as ND_3 or D_2O. The hydrogens therefore "remain exchanged" for deuterium since there is no time-delay between "quenching" and detection. Such gas phase reactions are ideally suited to Fourier transform ion cyclotron resonance mass spectrometry, since the deuterated gas can be admitted to the cell where detection occurs. Variable delays are also easily implemented due to the temporal rather than spatial nature of detection in FT-ICR mass spectrometry. Thus delays, during which H/D exchange occurs, of several hours

for small molecules and peptides, and proteins have been reported in the gas phase, allowing information on gas phase conformations to be obtained. [6-9]

Further developments of solution-phase H/D exchange include the use of pepsin, a non-specific enzyme that breaks up the target protein under the acidic conditions used to quench the reaction. [1]This allows segments of the analyte protein to be monitored and the amount of exchange in different areas of the protein to be ascertained. If the amino acid sequence of the analyte is known, the fragments can be assigned to specific parts of the sequence, with the number of hydrogens exchanged for deuteriums giving information on the structure of those parts of the protein in solution. Thus, for example, a segment that does not exchange many deuteriums for hydrogens may be buried in the bulk of the protein, while a segment that exchanges many hydrogens may be near the surface of the protein and thus nearer the solvent. From this sort of data, some general idea of the protein folding in solution can be built up.

In the gas phase the rate and extent of H/D exchange is determined by both the analyte's structure and the properties of the exchange reagents. H/D exchange rates of protonated sample increase with the basicity of the gas-phase reagent gas, such that $D_2O<CD_3OD<CD_3CO_2D<ND_3$. [6]Thus for larger-mass samples a reagent gas such as ND_3 should be used in order to encourage complete exchange.

Numerous mechanisms have been proposed for the exchange of protons for deuterons in solution in H/D exchange experiments. These include the onium ion mechanism, the relay mechanism, tautomer mechanism, the salt bridge mechanism and the flip-flop mechanism. [6]The first three of these mechanisms involve the N-Terminus hydrogens, while the last two deal with exchange at the C-terminus. These particular mechanisms are based on results from an investigation of glycine oligomers and as such may not be

representative of mechanisms appropriate for larger protein H/D exchange. The results are, however, complimented by experiments carried out by other groups on other small peptides. [10, 11]For reagent gases with high proton affinity, such as ND_3, the onium ion mechanism has been proposed in which the ND_3, for example, exchanges a hydrogen for a deuterium on the N-terminus. This exchange is accompanied by the solvation of the reagent base by the peptide. This mechanism is shown below, and it is argued is favoured by the low endothermicity of the proton transfer for such a reaction.

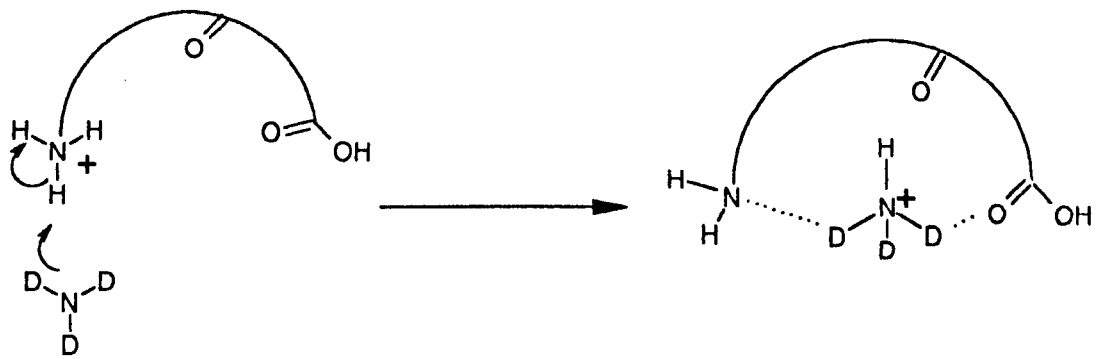

Onium Ion Mechanism

A relay mechanism (shown below) is proposed for those reagent bases such as D_2O with low proton affinity. These reagents cannot overcome the endothermicity of the proton transfer from the peptide, thus a mechanism where a proton is transferred from the N-terminus to a carboxyl oxygen in the amide bond, which is a less basic site, is postulated.

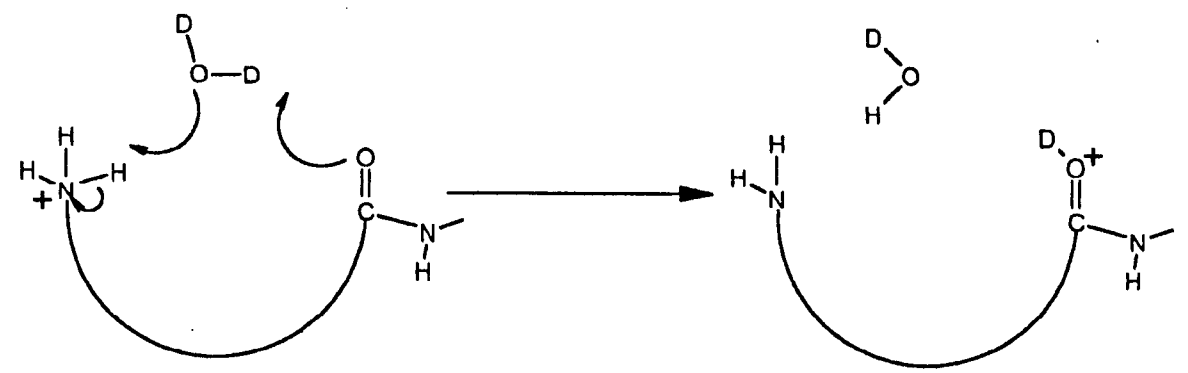

Relay Mechanism

The final mechanism that is proposed for the exchange of protons for deuterons involving the N-terminus is the tautomer mechanism. Semi-empirical molecular orbital calculations show that the exchange of amide protons is unfavourable compared to exchange of protons at the N-terminus. The tautomer mechanism is a possible explanation of the observation of amide hydrogen exchange for deuterium. In this mechanism, a proton is transferred from the N-terminus to the carbonyl oxygen in an amide bond. At the same time the hydrogen present in the same amide bond is transferred to the reagent gas.

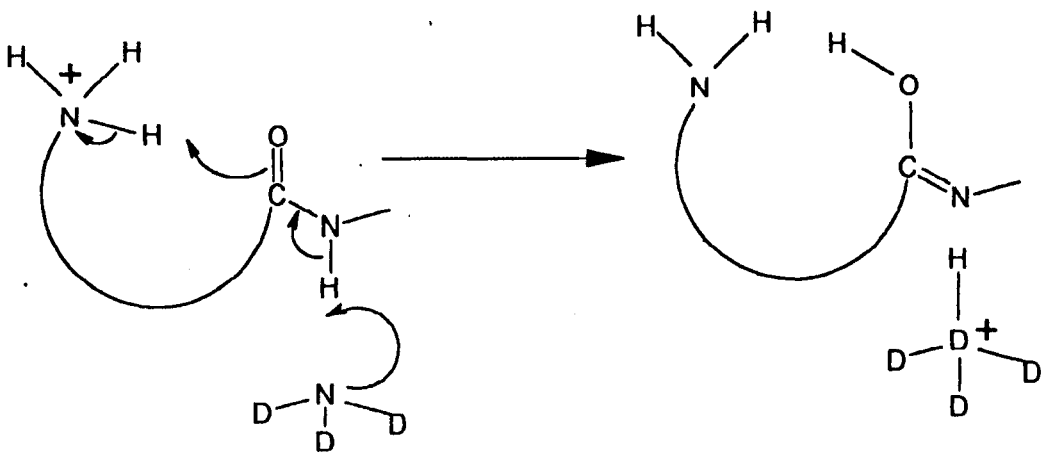

Tautomer Mechanism

The possible exchange mechanisms for hydrogens at the C-terminus of glycine oligomers are represented graphically below. The first mechanism, known as the salt-bridge mechanism is proposed for the more basic reagent gases such as ND_3, while the so called flip-flop mechanism has been proposed for the less basic reagents.

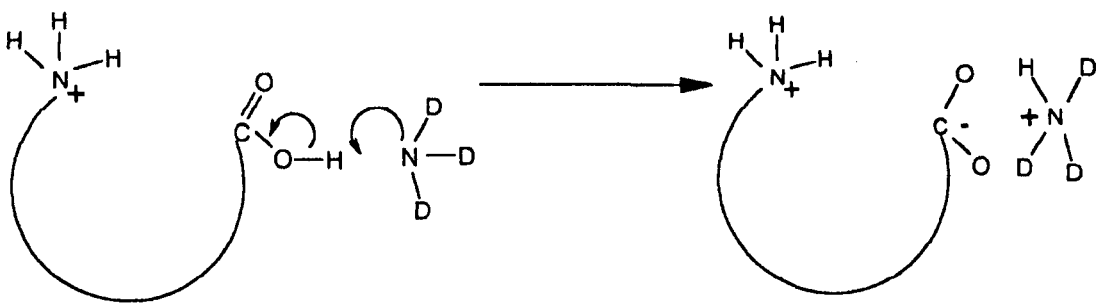

Salt Bridge Mechanism

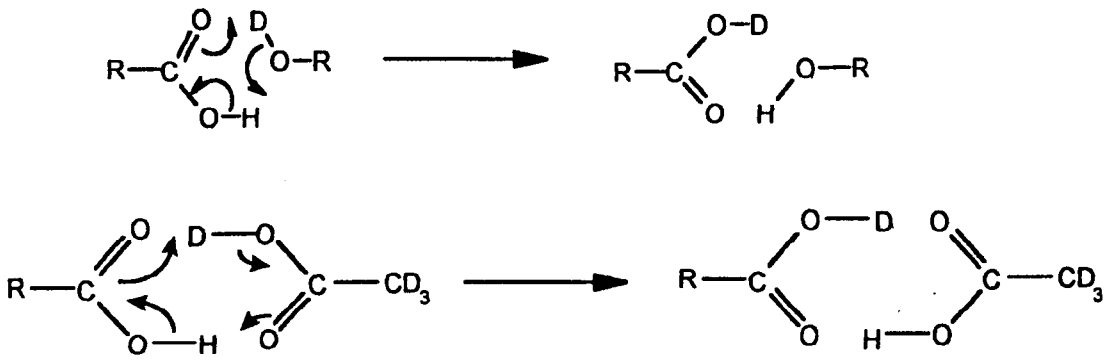

Flip-Flop Mechanism

McLafferty *et al* have shown in the gas phase that for different charge states in cytcohrome C, myoglobin and ubiquitin spectra there exist different rates of exchange.[7]These range from 2 x 10^{-13} to 4 x 10^{-12} cm^3 $molecule^{-1}$ s^{-1}, with the highest charge state showing the fastest exchange.[7] It has been postulated that the coulomb repulsion among charge sites results in a lower proton affinity for the species [12]; protein samples can therefore interact with weak basic reagents such as D_2O for which interaction might otherwise be expected to be energetically unfavourable. It has also been proposed that each multiply charged protein may contain more than one conformation in the gas phase compared to one active conformation in solution. This proposal rests on gas phase H/D exchange.[7-9] Thus for cytochrome C gas phase ions, i.e. without water present, it has been suggested that there exist up to seven individual conformations compared to one folded conformation in solution. These different gas phase conformations, can be considered to be "intermediates", distinguishable by gas phase hydrogen/ deuterium exchange. The total exchange alters for each conformation: the conformations in the gas phase inter-convert over a period of many hours compared to a few seconds in solution, allowing the "intermediate" conformations to be observed in the gas phase by mass spectrometry. Thus it follows that these "intermediate" conformations exist for much longer in the gas phase due to non-covalent intramolecular stabilisation. In solution, water

screens this stabilisation and the conformation is therefore more "fluid" consisting mainly of the one active form. [7]Experiments employing an infra-red laser to "heat" the ions in the gas phase have shown that one conformation can be transformed into another. [8]

5.2 Experimental

5.2.1 Gas Phase Hydrogen/ Deuterium Exchange

These experiments were carried out using the 9.4 Tesla Bruker BioAPEX II Fourier transform ion cyclotron resonance (FT-ICR) mass spectrometer with an electrospray ionisation source (Analytica, Branford, USA), as described in a previous section (see chapter 2).

The experiments were conducted in the "infinity" cell of the FT-ICR mass spectrometer and were thus in the gas phase. The pressure in the cell was monitored by Pirani ion guages and was adjusted using a leak valve at the liquid-sample inlet, through which the deuterated gas of choice passed. This inlet consists of a threaded adapter, positioned close to the analyser cell, to which a glass vial containing the liquid analyte of interest would be attached. The sample would then be frozen using liquid N_2, the remaining atmosphere pumped away using the Edwards Rotary pumps and finally the sample introduced to the instrument using a thumb screw leak valve. In these experiments deuterated ammonia (ND_3) was used and thus a stainless steel transfer line was required. The transfer line was attached to the instrument via the same threaded adapter as the glass vial in the previous description. The background pressure of ND_3 in the cell was maintained, by judicious use of the leak valve, at a pressure of approximately 2×10^{-8} Torr. Deuterated ammonia was chosen due to its high basicity as this allowed rapid exchange of protons for deuterons in the analyte of interest. For large molecules with a great number of potential exchangeable

sites such as proteins, this characteristic is obviously advantageous. Signal quality was found to be hard to maintain, due presumably to collisions of the ions with neutrals in the cell (see section 1.4). The rapidity of the exchange with ND_3, increased the detail obtained from the experiments within a sufficiently short period of time. Thus for calmodulin, experiments with delays up to 60 seconds gave specific information on the system of interest and spectra with relatively good signal-quality were achievable. Figure 4 shows a typical shift in molecule ion peaks brought about by H/ D exchange with ND_3.

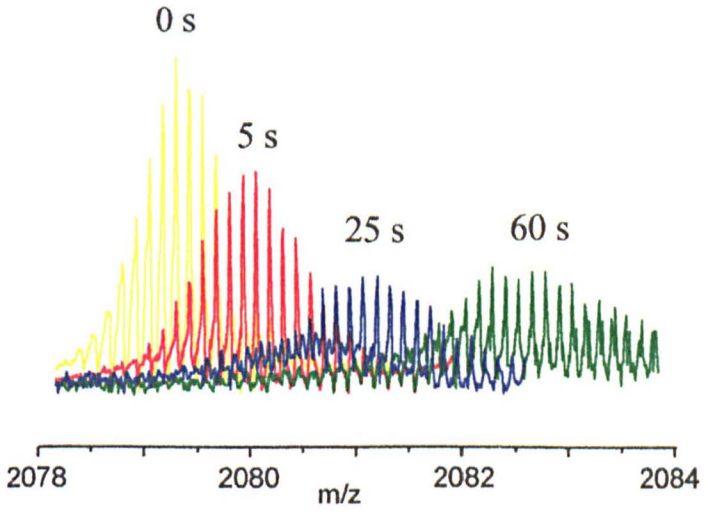

Figure 4: Gaseous Hydrogen/Deuterium Exchange of $[M+8H]^{8+}$ apo-Calmodulin

Calmodulin was purified by gel chromatography to remove unwanted salts and was dissolved in ammonium acetate (5mM, pH 5.8). The gel chromatography column used was manufactured by Pharmacia Biotech (Uppsala, Sweden) and was a gravity-fed Sephadex PD 10 column. The procedure for desalting this sample has been discussed previously in section 3.2.1. The final purified analyte solution was either analysed directly from the column, and as such was salt free, or a measured aliquot of $CaCl_2$ (typically 0.1 mM) was added to allow the Ca^{2+} binding sites to be filled. In both cases, the calmodulin was believed on the basis of the mass spectra to be in its active or natural conformation,

due to the fact that the buffered aqueous solution should retain calmodulin's tertiary structure. Thus, it was hoped that H/D exchange would illustrate any conformational changes that occurred on binding Ca^{2+} ions.

Calmodulin was introduced into the analyser cell of the mass spectrometer via the electrospray ionisation source. The typical flow rate was 1μl min^{-1} with CO_2 (heated to about 50°C in the source) as drying gas. The ions were passed through the ion optics into the "infinity" cell, where the ions were trapped for various times from 0 to 60 seconds. Successive spectra were acquired and added together, thus building up a detailed spectrum. Throughout the course of the experiments new ND_3 was introduced to the cell every 30-45 minutes to prevent the reagent gas itself from exchanging hydrogens for deuterons since the analyser cell and the transfer line could not be completely evacuated. Exchange with water, for example, from the atmosphere causes a degradation of the reagent gas and thus a reduction in the efficiency of exchange.

5.2.2 Solution Phase Hydrogen/ Deuterium Exchange of Calmodulin

Solution experiments were undertaken for comparison and evaluation alongside the gas phase results.

The nature of the solution phase experiment means that extremely short delay times, as obtained in the FT-ICR mass spectrometry gas phase experiments were very difficult to obtain. The experiments therefore focused on longer periods of reaction.

The protein was purified, as previously described for the gas phase experiments as and the protein was incubated at 37°C in a D_2O environment. A small aliquot was removed from the bulk at a variety of times and the exchange halted by adding a small aliquot of acid and freezing. The samples were then analysed using ESI FT-ICR mass spectrometry. Precautions were taken to prevent back exchange at all points after the reaction was

quenched, including the use of dry CO_2 as the drying gas in the electrospray source. The entire source was normally at atmospheric pressure and therefore H_2O molecules were abundant. The heated CO_2 drove much of the water out of the source and prevented back exchange . The rest of the instrument was differentially pumped to very low pressures and as such there were very few molecules if any available for back exchange.

Solution-phase H/D exchange experiments were carried out on a sample of calmodulin that was in the presence of small amounts of metal ion impurities such as Na^+ and Ca^{2+}, and also on a sample where the metal ions were removed using ethylene glycol-bis(β-aminoethyl ether)-N,N,N',N'-tetra acetic acid (abbreviated to EGTA).

5.3 Results

5.3.1 Gas Phase Hydrogen/ Deuterium Exchange Of Calmodulin, Comparison Of Charge States

The maximum number of protons exchanged decreased with increasing charge as seen in Figures 5 and 6. Figures 5 and 6 represent results taken from two different experiments. There was a significant difference between the numbers of protons exchanged for deuterons. After 30 seconds, for example, the 8^+charge state (Figure 5) showed an exchange of approximately 31 compared to an exchange of approximately 45 (Figure 6). This was due to the different pressures of ND_3 at which the experiments were conducted. The results in Figure 5 were conducted with less ND_3 present. Both experiments showed the same pattern: a reduction in the number of protons exchanged with increasing charge.

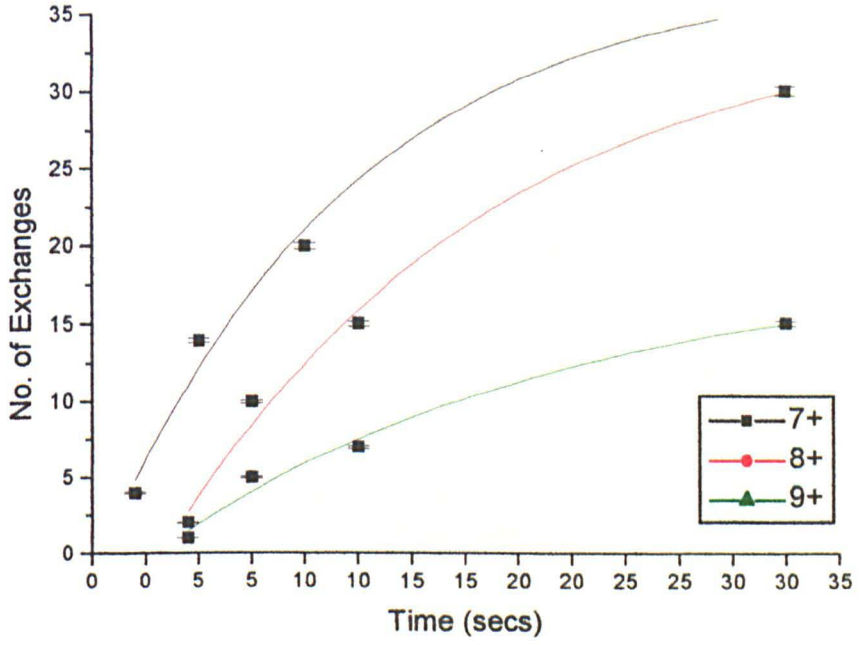

Figure 5: Gas phase H/D exchange of calmodulin in ammonium acetate (5 mM, pH 5.8), pressure in the cell approximately 8.5 x 10^{-8} Torr. Error bars represent a calculated 1% difference between different experimental runs.

Similar trends were discovered for cytochrome C ions by McLafferty *et al.*[7-9] These findings, however, are in apparent contradiction to ion mobility measurements.[13-16] Ion mobility measurements (the mobility of an ion is a measure of how rapidly it moves through a buffer gas under the influence of an electric field) showed that an increase in charge resulted in an increase in the cross section of the protein possibly due to electrostatic repulsions between the charge sites. The change in cross-section as the charge on the ion changes has also been observed in experiments using triple quadrupole mass spectrometers [17-19] and collisions with a surface.[20] In both cases it was noted that the cross-section of the protein was different for individual charge states.

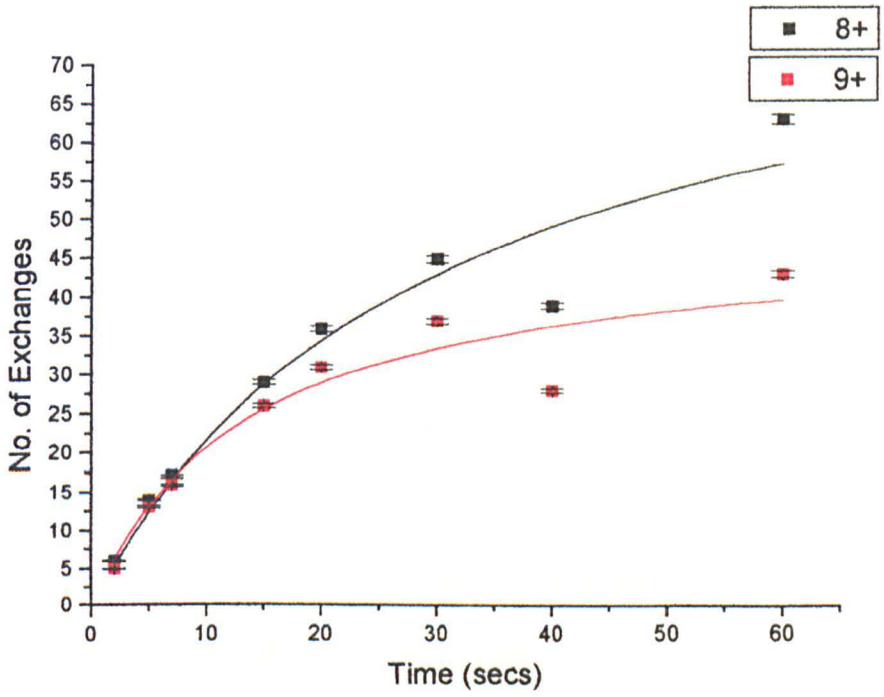

Figure 6: Gas phase H/D exchange of calmodulin in ammonium acetate (5mM, pH 5.8) pressure in the cell approximately 8.0 x 10^{-8} Torr. Error bars represent a calculated 1% difference between different experimental runs.

Clemmer *et al* [15]have made an effort to assign the native conformation of cytochrome C ions to a particular cross-section and charge state. By assuming hard-sphere interactions

and comparing experimentally measured collision cross-sections with collision cross-sections calculated for plausible geometries, it was concluded that the cytochrome C's native conformation collision cross-section was approximately 1090 x 10^{-10} m^2 for the 7^+ charge state. This corresponded to a drift time of 1100 μs in the ion mobility experiment. These experiments revealed that no peak existed at the relevant drift time; on the basis of similar calculations for a completely linear (and thus entirely denatured) protein again no peak was seen corresponding to the necessary drift time. The conformation of cytochrome C ions in the gas phase appeared be somewhere in between these two extremes.

Calculations on a protein conformation that retains its secondary structure but loses its tertiary structure (i.e. the secondary structural features such as the α-helix and β-pleated sheets are retained but the geometry of the amino acid chain connecting these features is random) predicted an average (taken for several such conformations) drift time of approximately 2100 μs for the 7^+ charge state. This prediction compared well with the main feature of the collision cross-section measurements, namely a sharp peak at approximately 2000 μs. This sharp peak was present within all the charge states selected from 7^+ to 20^+. The only difference among charge states was a gradual increase in the cross section with increasing charge. This increase in cross-section was attributed to partial unfolding of the α-helices or an attempt to minimise coulombic repulsions among the increasing number of charge sites. This will be discussed in more detail towards the end of this section.

It should be remembered that although the native conformation was apparently unobservable by ion mobility experiments, the possibility of it existing in the gas phase is not excluded. The nature of the ion mobility experiment required that the ions be injected into the drift region against a counter-current flow of the buffer gas. To achieve this the

ions were injected, with a high kinetic energy, from the external electrospray source. The collisions with the buffer gas experienced by such high-energy ions would cause some of the kinetic energy to be converted into internal energy, which could result in conformational changes in the gas phase protein. Thus the apparatus used in these experiments, provides only partial information on the gas phase ions that are actually produced by the electrospray source.

More recent experiments with a higher-resolution ion mobility instrument (compared to that just discussed) have allowed more conformations to be identified. [16]There still exists, however, many more conformations than just the natural (or natured) and completely de-natured states. This was evidenced by the broadness of the peaks seen in the ion mobility measurements. Compared to Clemmer *et als* experiments[15], the higher resolution measurements produced more detailed features. The design of the apparatus with the electrospray source directly coupled to the drift region allowed the ions to be introduced much more gently (by weak electric fields) into the system. The results obtained were thus more representative of the gas-phase ions produced directly by the electrospray source. This was evident from the results obtained for cytochrome C, in un-acidified aqueous electrospray conditions (much like those used for the calmodulin H/D exchange experiments in this chapter). The 6^+ to 9^+charge states showed peaks corresponding to the drift time attributed to the natural conformation. There also existed several other protein conformations in the gas phase, represented by broad features in the ion mobility measurements. These broad features could either be a result of partially folded cytochrome C in solution or coulombic repulsion among the charge sites in the gas phase forming a wide spread of conformations and cross-sections[15]. Coulomb repulsion would be more relevant to a protein in vacuo compared to a protein in solution and would,

therefore, provide a significant contribution to the variety of conformations in the gas phase.

These ion mobility experiments depict ions increasing in collision cross-section with increasing charge. They do not, however, present a clear explanation for the decrease in the number of H/D exchanges as charge state increases. If the cross section of the calmodulin ions in the gas phase increases in the same way as for cytochrome C, an increase in the number of H/D exchanges should occur as more potential sites for exchange are exposed to the deuterated environment.

Valentine *et al* [21] have tried to answer this question by combining ion-mobility measurements with gas-phase H/D exchange in a high-resolution ion mobility apparatus combined with an electrospray source. Again cytochrome C was studied and it was observed that the number of exchangeable hydrogens was independent of charge state despite the fact that the cross-section measurements again showed an increase with increasing charge. For example the compact conformers observed for the charge states between 8^+ and 10^+ showed a constant (approximately 46) number of exchanges despite the fact that the cross-section increased. This was approximately 20 less exchanges than found for the more diffuse structures.

The cross section for the diffuse conformer, selected experimentally by increasing the injection voltage, systematically increased by approximately 3% with each consecutive increase in charge, such that the 18^+ charge state was approximately 30% greater than the 10^+ charge state. However, the number of exchangeable hydrogens remained constant throughout the range of charge states. The increase in cross-section can be interpreted in a variety of ways. If only coulomb repulsion among the charge sites is considered, this would cause segments of the protein to be pushed apart causing the overall cross-section to

increase. It is also feasible that long-range interactions between the protein and the buffer gas, in this case helium, could cause the collision cross-section to increase even if the protein's physical cross-section remained constant. This type of interaction, however, according to modeling, can only account for an increase in cross-section of a few percent even for the highest charges. The overall increase must therefore be due to changes in geometry. The question therefore remains, if the cross section increases, why does the level of H/D exchange not also increase proportionally?

The increase in charge would not only result in a greater cross section, it would also increase the number of exchangeable hydrogens present in the molecule, since the charging process in electrospray ionisation brings extra protons to the neutral molecule. Thus the greater the charge, the greater should be the number of deuterons exchanged for protons. This lack of an increase (or decrease) in exchangeable hydrogens in the ion mobility/ hydrogen deuterium exchange measurements, and the decrease in FT-ICR experiments, might be explained by charge solvation, causing no net increase in H/D exchange levels as the protons would be effectively screened from the deuterating agent by the solvation shell.

The increase in cross section of the proteins and the concurrent low exchange levels are, however, difficult to explain since a diffuse conformer that nevertheless manages to protect so many exchangeable hydrogens seems to be contradictory. A further explanation may be that intra-molecular bonding could curb the H/D exchange. Significant levels of hydrogen bonding can still exist in the gas phase even for diffuse conformations, and there is also the possibility of dipole-dipole and dipole-induced dipole interactions that would result from the high polarity of the functional groups of which the exchangeable hydrogens are a part. These interactions, in the same way as hydrogen bonds, might effectively screen the "vulnerable" hydrogens from the deuterated reagent in the gas phase.

5.3.1.1 Gas Phase Hydrogen/Deuterium Exchange of Calcium loaded Calmodulin

Figures 7 and 8 illustrate the case of Ca^{2+}-loaded calmodulin (while Figure 9 shows some typical mass spectra from which the necessary data was determined, note that at longer delay times in ND_3 the higher calcium adducts are no longer observable due to the reduction in signal to noise). It is easily seen that consecutive additions of Ca^{2+} ions result in a reduction in the total number of deuterons exchanged for protons in these experiments. As has previously been discussed, consecutive addition of Ca^{2+} is thought to have the effect of changing the conformation of calmodulin to allow it to activate its target proteins. The gas phase H/D exchange experiments coupled with the high resolution of FT-ICR mass spectrometry might allow the exchange profile of the individual conformers to be followed.

Figure 7 shows four separate H/D exchange profiles for calmodulin loaded with Ca^{2+} ions for the 8^+ charge state, while Figure 8 shows data corresponding not just to calcium ions bound to the four primary sites but also data for those calcium ions bound to the auxiliary sites. These profiles, however, differed by approximately a single Dalton throughout the entire range, which is indicative of specific exchangeable hydrogens being "protected" or removed by the Ca^{2+} ions. Two protons are expected to be removed to allow charge balance to be retained for each Ca^{2+} ion that binds to the protein (see chapter 4). The exchange profiles shown here, however, differ by the mass of a single proton only.

The Ca^{2+} ions which are supposed to induce a conformational change in the protein, apparently do not cause a significant or noticeable change in calmodulin's conformation in the gas phase. Any significant changes in the conformation of calmodulin should be apparent throughout the course of H/D exchange experiments, whether it be over the course of hours in the case of solution phase H/D experiments or over periods of a minute

in the gas phase. There should be enough "proton" indicators spread along the length of the biomolecule of varying levels of exchangeability to allow major conformational changes to be readily apparent.

The conformational changes in the protein may be very subtle, perhaps a global tightening of each of the cores or alternatively the folding results in a conformation that allows the exchangeable protons to still be available to the deuterating reagent i.e. the exchangeable protons remain on the surface of the protein where they are readily accessible by the ND_3. The other possibility is that the conformational change could involve regions of the protein that contain hydrogens characterised by a very low rate of exchange. Longer delay times might conceivably allow observation of such exchanges and thus the conformational changes of the protein. Longer delay times were not, however, readily accessible with the FT-ICR for a biomolecule of this size.

Increasing the delay times of this experiment would have meant making use of an experimental method such as quadrupolar axialisation. This particular experiment would involve the introduction of a "buffer" gas to allow the magnetron motion of the ion to be converted to cyclotron motion. Such collisions, although they allow re-measurement of the ion packet in the cell and allow greater signal strength and resolution for individual scans, are known to cause collisional heating of the ions. In a study where conformations are being investigated this obviously poses a problem, since the collisions in the gas phase cause the kinetic energy of the ion to be converted to internal energy of the biomolecule and potentially change the conformation of the protein.

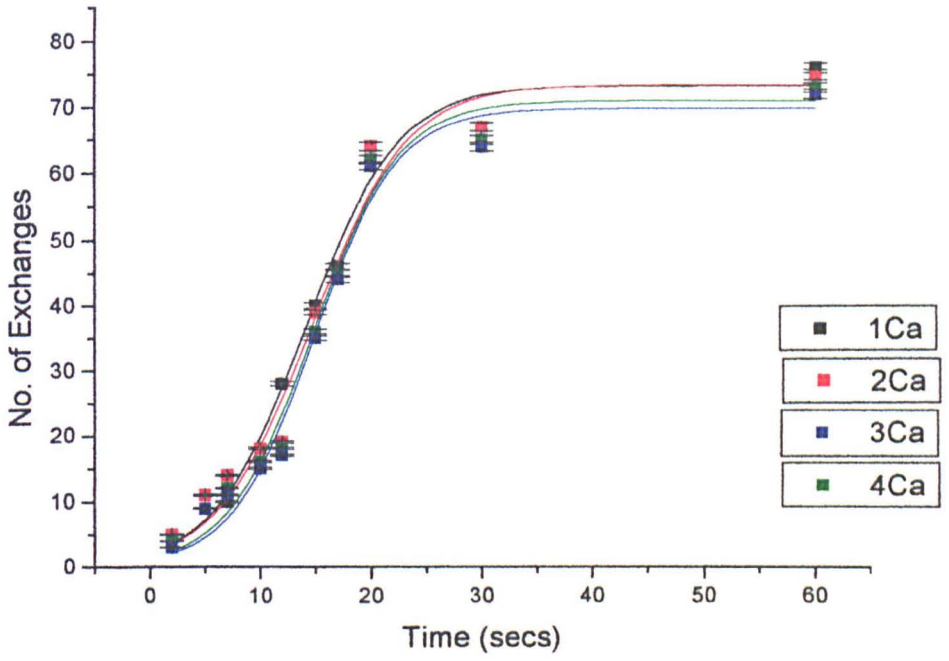

Figure 7: Gas phase H/D exchange of calmodulin loaded with 0.1 mM $CaCl_2$ in ammonium acetate (5mM, pH 4.6). 8^+ charge state.

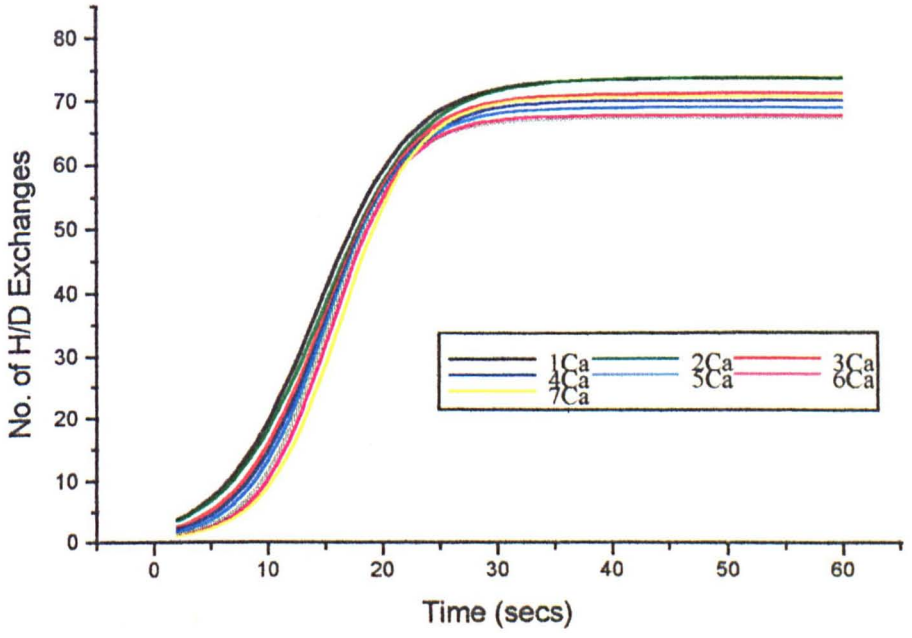

Figure 8: Gas phase H/D exchange of calmodulin loaded with 0.1 mM $CaCl_2$ in ammonium acetate (5mM, pH 4.6). Graph shows the H/D exchange profile for all the Cam+Ca complexes. 8^+ charge state.

Investigation of the other charge states, as achieved for apo-calmodulin was difficult with calcium binding. The peaks representing these other charge states were so small in comparison with the 8^+ charge state that it was difficult to assign accurately the masses for all the adduct peaks present in the spectra. These results, although potentially interesting, have been omitted from this chapter due to their poor quality. Further experiments with an exceptionally large number of scans, and thus a concurrent increase in experimental time, would be needed to elucidate reliably the necessary information from the spectra.

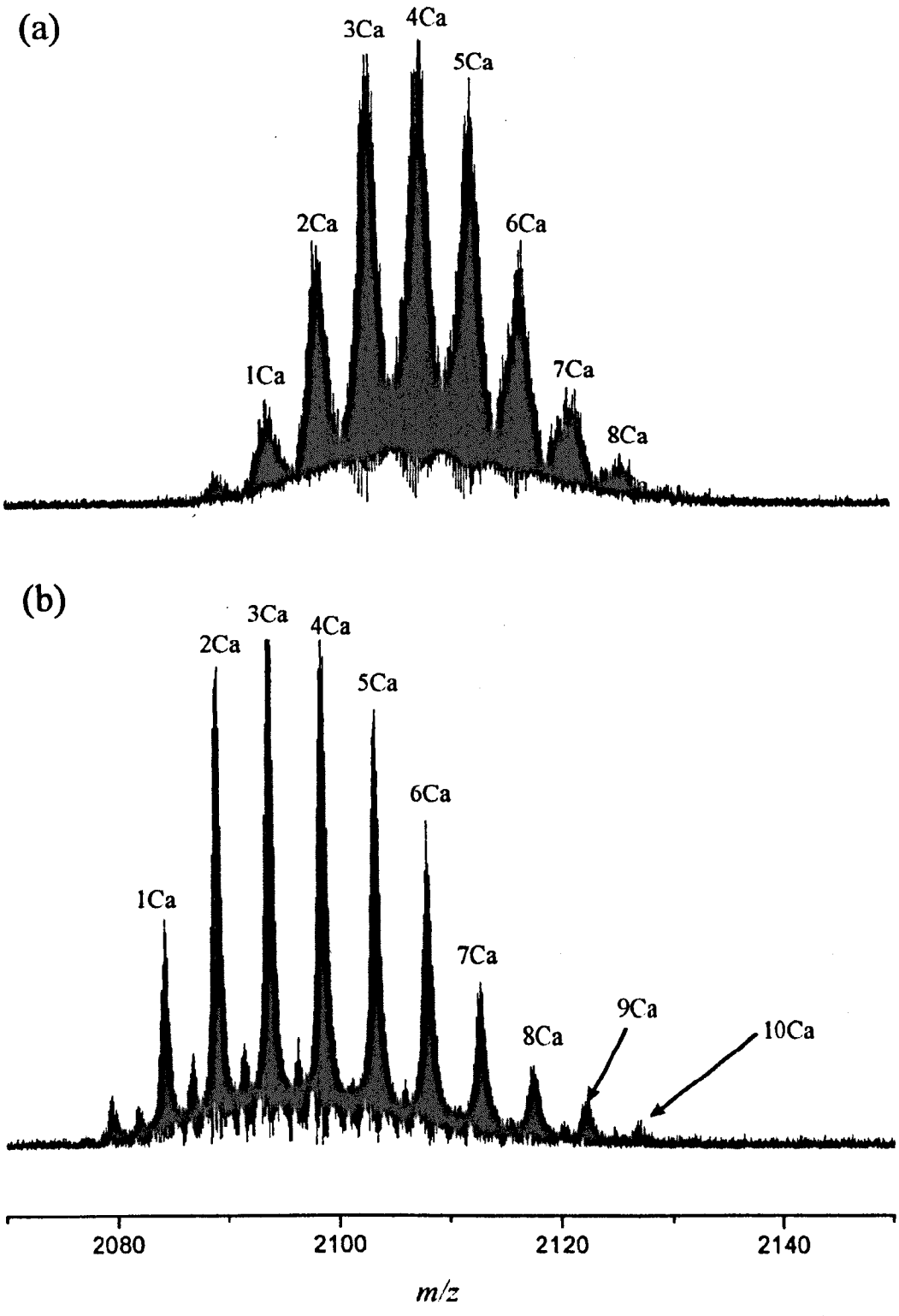

Figure 9: Gas phase (ND_3) hydrogen/ deuterium exchange of $CaCl_2$ loaded calmodulin (8+ charge state). (a) Delay = 0 secs (b) Delay = 60 secs

5.3.2 Solution Phase H/D Exchange of Calmodulin

As can be seen from Tables 1 and 2 (below), the exchange was virtually complete after the first hour. The total number of exchanges varied with the charge state. There was a general decrease by one in the number of hydrogens exchanged for deuterons as the charge state decreased for the calmodulin molecule ion. There was also a general decrease by one for each calcium ion bound to the calmodulin molecule ion, which can be explained either by the fact that a hydrogen is replaced by the metal ion or that an exchangeable hydrogen ion was obscured/ protected by the metal ion. The former proposal would seem to agree with the results presented in chapter 4 concerning the binding of Ca^{2+} ions to calmodulin. It should be expected that two hydrogens would be replaced by Ca^{2+} ions due to the double charge and the general size of the calcium ion. However, a possible explanation for the lack of this observation could be that one of the hydrogens that would be expected to bind to the Ca^{2+} ion was from an amino acid side chain. These hydrogens are known to undergo association/ disscociation reactions with deuterium that are extremely fast and can therefore back-exchange in the time it takes to measure by mass spectrometry the increase in mass of the protein. It could therefore be postulated that Ca^{2+} ions may replace the hydrogen present in part of the amide backbone plus a hydrogen from a more reactive amino acid side chain resulting in a net increase in mass of only one Dalton. This is, however, difficult to prove due to the inaccuracy in assigning masses to each of the adduct peaks present in each charge state. It is necessary to calculate an average mass from the isotopomer distribution. This was achieved in these experiments by fitting a Gaussian distribution to the data points and taking the peak of this distribution as being indicative of the mass of the particular adduct. The quality of the original data set obviously effects this and thus a variance of $\pm$ 1 Dalton can easily occur. It seems clear, however, that for each

adduct ion (be they calcium or sodium ions) bound to calmodulin there is a representative drop of one Dalton in the total H/D exchange until the fourth calcium is bound.

Closer inspection of the table for the 7^+ and 8^+ charge states (Table 1) show that there was a dramatic change in the number of exchanges occurring on binding of the fourth calcium . Up to that point there was a regular drop in the exchange level. For each metal ion bound to the calmodulin molecule ion there was roughly a drop of a single mass unit detected. After the fourth calcium bound to calmodulin, however, the exchange level dropped significantly from the expected reduction of four to seven. This may be indicative of a significant calcium-induced conformational change in calmodulin following the uptake of the fourth Ca^{2+} ion (in presumably the last free primary binding site available on calmodulin).

Similar work by Nemirovskiy *et al* [22] utilising a prototype VG ZAB-T four sector tandem mass spectrometer with a VG electrospray source also suggested that solution phase H/D exchange experiments coupled with electrospray mass spectrometry could be used to monitor protein-metal ion interactions. Nemirovskiy *et al* concluded that calmodulin undergoes a conformational change when titrated with calcium ions. This could be detected by the drop in the total level of H/D exchange as the concentration of calcium ions was increased as discussed here. As calcium concentration was increased in their experiments, the total exchange dropped by 24 protons, which was taken to be indicative of a tightening of the conformation on interaction with the calcium ions. This drop in exchange level ceased after the calcium ion titration reached a level sufficient to convert 80% of the protein present to a form with four calcium ions bound.

Experiments using EGTA to remove unwanted Ca^{2+} ions from the analyte solution for solution phase H/D exchange provided an interesting observation. EGTA binds to

calmodulin in the absence of Ca^{2+} ions and only four EGTA molecules were observed to bind to calmodulin in total. As previously discussed in section 4.4 this binding might prevent peptides binding to calmodulin, and might explain why other groups have not reported the observation of apo-calmodulin:peptide complexes. [23]A cursory examination of the H/D exchange observed showed that there was approximately an increase of four Daltons for each EGTA that bound to calmodulin. This was consistent with EGTA bringing exchangeable protons to the complex.

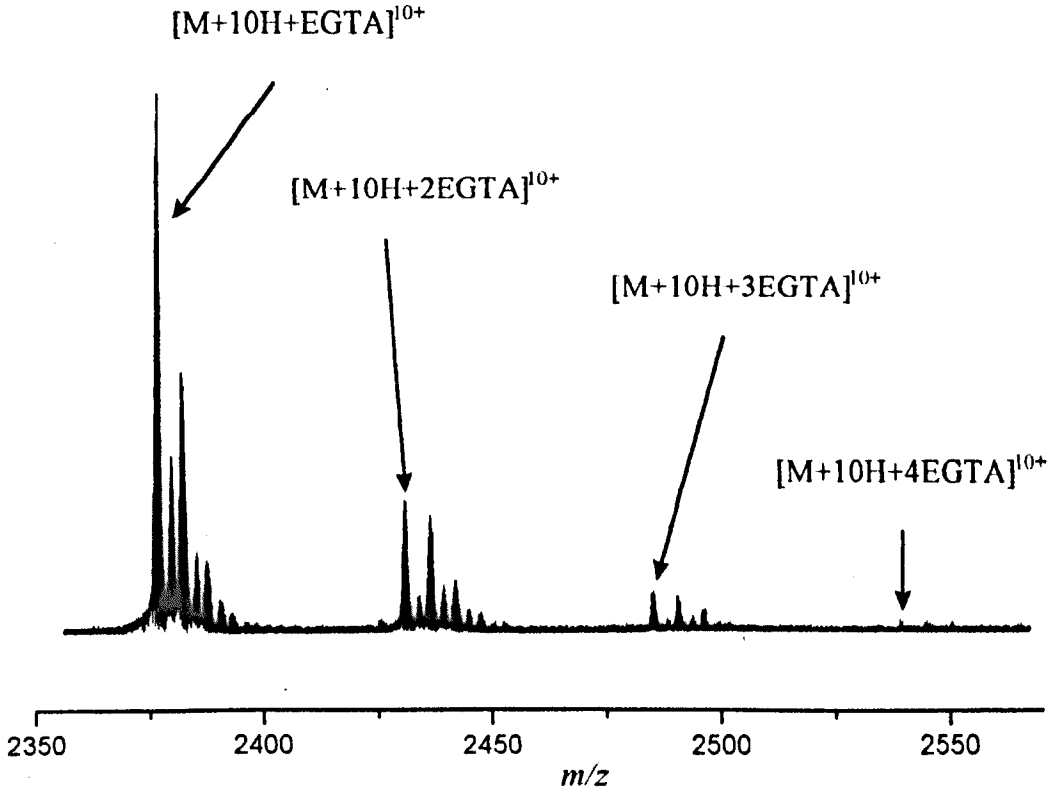

Figure 10:Calmodulin in ammonium acetate (5mM, pH 5.8) with EGTA present to remove the Ca^{2+} ions.

9+	CaM	Na	Ca	1Ca+ Na	2Ca	2Ca+ Na	3Ca
0 hrs	16626	16647	16664	16685	16702	16723	16740
1.5 hrs	16898	16919	16935	16956	16973	16992	17011
2.5 hrs	16899	16920	16937	16957		16994	17014
3.5 hrs	16899	16920	16937	16957		16994	
4.5 hrs	16900	16920	16937	16957	16975	16994	17013
Diff.	**274**	**273**	**273**	**272**	**273**	**271**	**273**

8+	CaM	Na	Ca	1Ca+ Na	2Ca	2Ca+ Na	3Ca	3Ca+ Na	4Ca	4Ca+ Na	5Ca	5Ca+ Na	6Ca
0 hrs	16626	16647	16664	16685	16702	16723	16740	16761	16778	16799	16816	16837	16854
1.5 hrs	16897	16918	16934	16955	16972	16992	17009	17029	17042	17064	17077		
2.5 hrs	16899	16919	16936	16956	16974	16993	17010	17029	17043	17064	17082	17102	
3.5 hrs	16899	16919	16936	16956	16975	16993	17011		17043	17065			
4.5 hrs	16899	16920	16936	16956	16974	16993	17011	17030	17044	17065	17082	17101	17122
Diff.	**273**	**273**	**272**	**271**	**272**	**270**	**271**	**269**	**266**	**266**	**266**	**264**	**268**

7+	CaM	Na	Ca	1Ca+ Na	2Ca	2Ca+ Na	3Ca	3Ca+ Na	4Ca	4Ca+ Na	5Ca	5Ca+ Na
0 hrs	16626	16647	16664	16685	16702	16723	16740	16761	16778	16799	16816	16837
1.5 hrs	16897	16917	16934	16954	16971	16992	17008		17041	17062	17080	17100
2.5 hrs	16898	16919	16935	16956	16973	16992	17008		17043	17063	17081	17102
3.5 hrs	16898	16919	16936	16956	16972				17042	17064	17083	
4.5 hrs	16898	16919	16935	16956	16972	16992	17012		17043	17064	17081	
Diff.	**272**	**272**	**271**	**271**	**270**	**269**	**272**		**265**	**265**	**265**	

Table 1: Solution phase H/D exchange of Ca^{2+} loaded calmodulin. Tables show the change in molecular weight of calmodulin over the reaction period of the experiments.

5.3.3 Calcium Induced Conformational Changes of Calmodulin

As has been previously mentioned, calmodulin on binding Ca^{2+} ions, is believed to exhibit a conformational change activating the protein to allow it to interact with its target molecules. Detailed examination of the spectra acquired by electrospray ionisation FT-ICR mass spectrometry with its inherent superior resolution allows us to probe the effect of Ca^{2+} and other divalent ions on the conformation of calmodulin. A study by Hu *et al* [24] making use of a Finigan MAT 900Q double-focusing mass spectrometer, yielded similar results to that presented here. However, the limited resolution of this type of instrument meant that interpreting the results easily and accurately was complicated. Due to the high resolution of the FT-ICR technique, the number and type of metal ions bound to calmodulin were easily determined.

It is apparent from Figure 11 that by varying the concentration of $CaCl_2$ in the analyte solution, it was possible to investigate the different conformations that were formed by Ca^{2+} ions non-covalently binding to calmodulin. At 0.1 mM $CaCl_2$, with a calmodulin concentration around 25 μM there are approximately four Ca^{2+} ions for every calmodulin. Examination of Figure 11a suggests conformational differences between calmodulin at 14^+ and 7^+. The distributions of adduct peaks at each charge state were significantly different from each other. At 7^+, there was a definite splitting of the Cam: Ca^{2+} adduct distribution, with the peak corresponding to $[Cam+3Ca]^{7+}$ being small. This observation is consistent with the sequential mechanism for calcium binding proposed by Haiech *et al* [25]and Klotz *et al*[26]. In this mechanism as has already been explained, binding of the first two Ca^{2+} ions to calmodulin causes a dramatic conformational change that allows the third and then the fourth Ca^{2+} ion to bind in quick succession. At the higher concentration of Ca^{2+} ions (Figure 11b), the adduct peak splitting was less pronounced, since there was an excess

of Ca^{2+} ions present in the analyte solution driving the conformational change of calmodulin to completion.

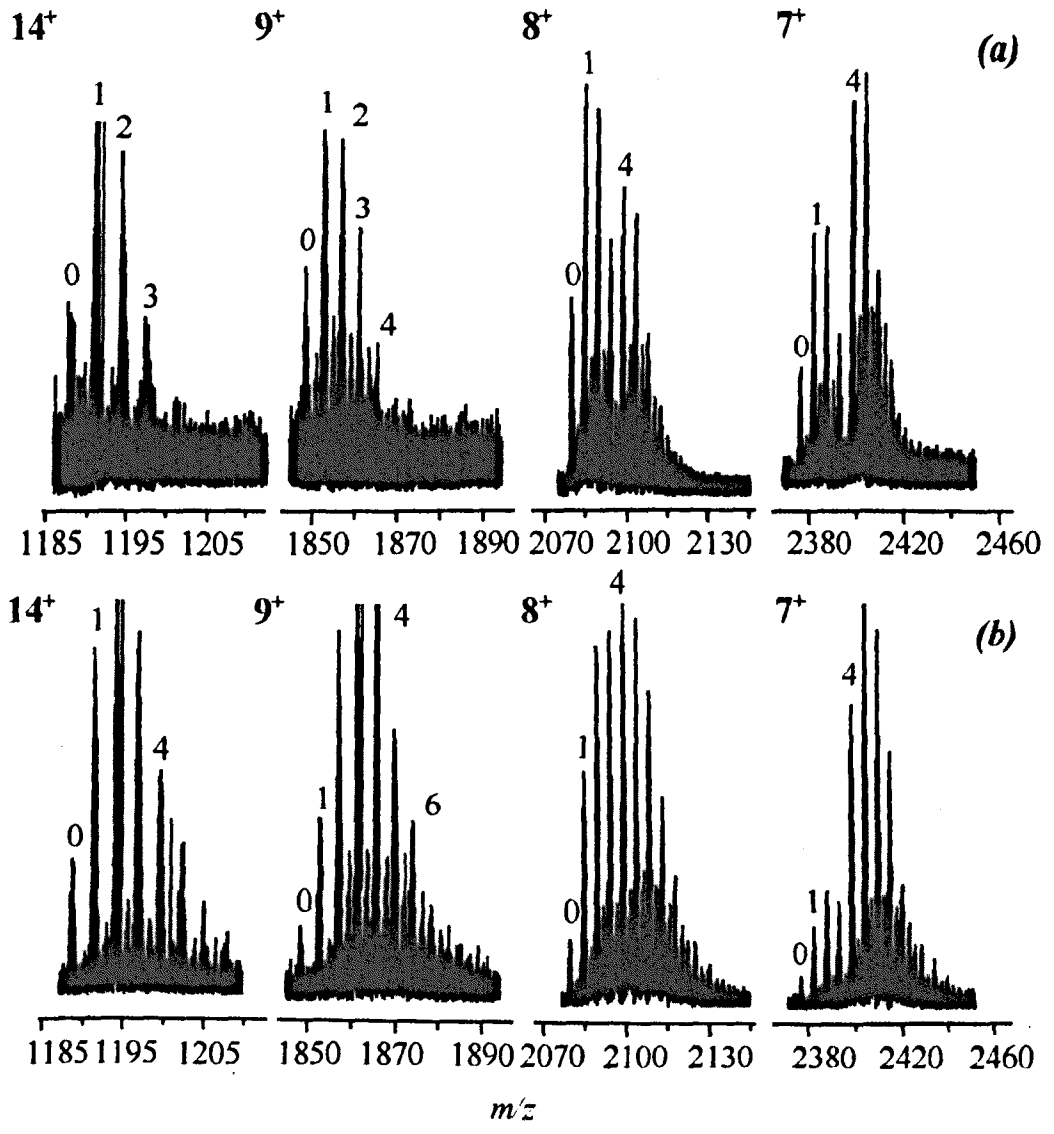

Figure 11: Calmodulin in ammonium acetate (5mM, pH 5.8). Expansions of the relevant charge states at $CaCl_2$ concentrations of (a) 0.1 mM and (b) 1 mM.

The 14^+ and other higher charge states (not shown) had less structure in the adduct peak distribution. This is interpreted as indicative of a more open/ unfolded and therefore unnatural conformation compared with the higher charge states 9^+ to 7^+. Comparison of Figures 11a and 12a show that Mg^{2+} ions, although they bound to calmodulin, did not

produce this structure in the adduct distribution, and thus it is inferred that Mg^{2+} induced no conformational change of calmodulin.

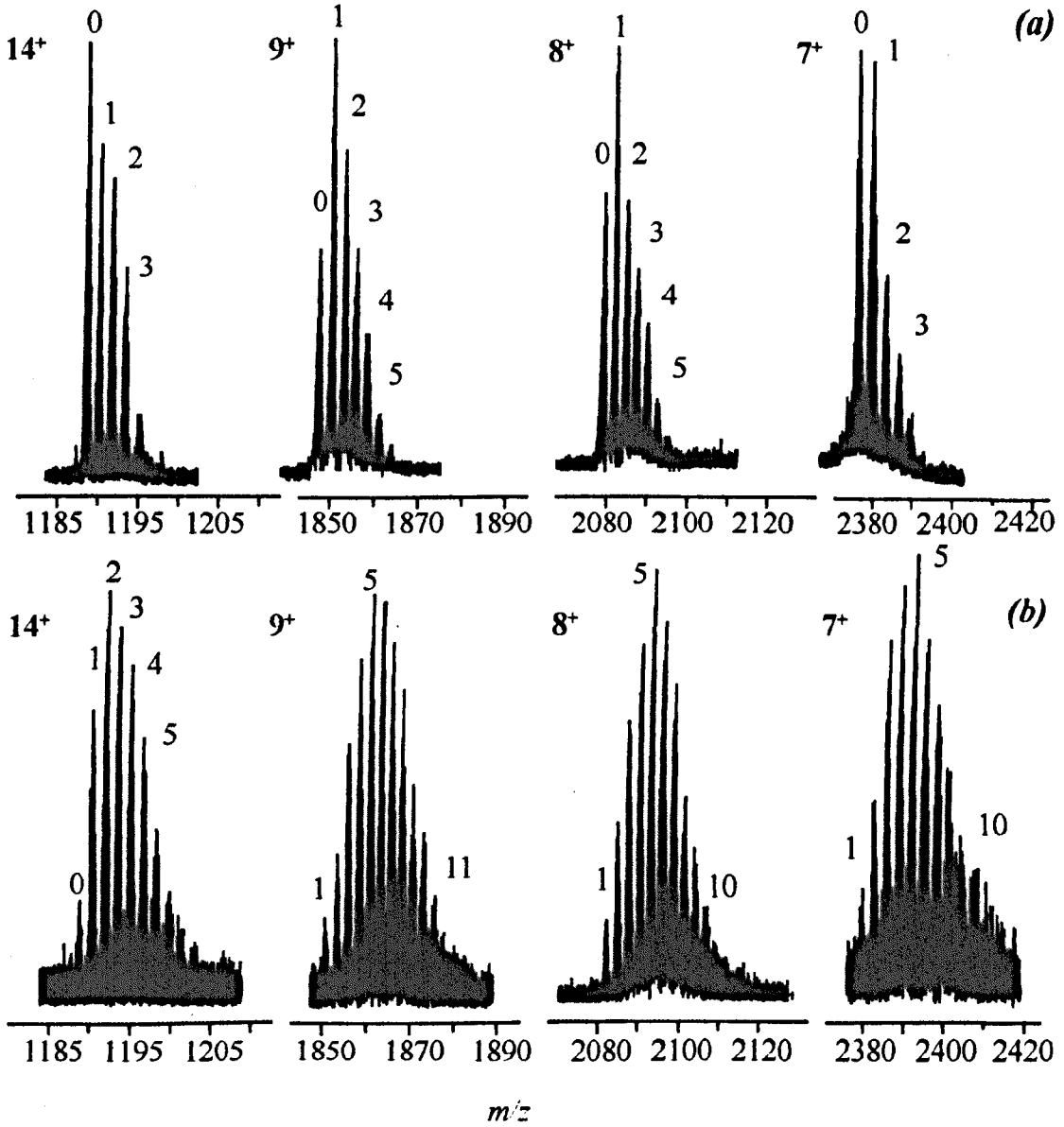

Figure 12: Calmodulin in ammonium acetate (5mM, pH 5.8). Expansions of the relevant charge states at $MgCl_2$ concentrations of (a) 0.1 mM and (b) 1 mM.

5.4 Conclusion

The objective was to study the conformational changes induced by Ca^{2+} ions binding to calmodulin by various methods, including gas and solution phase H/D exchange and the addition of limited amounts of Ca^{2+} ions to the analyte mixture. While providing some interesting results concerning the exchange levels of different charge states for apo-calmodulin, results for the holo-calmodulin were inconclusive. That is, there seemed to be no noticeable calcium-induced conformational change that could be monitored by gas phase H/D exchange. However, both the solution phase H/D exchange studies (section 5.3.2) and the investigation of the effect of Ca^{2+} ions on the molecule ion peak distributions (section 5.3.3) showed evidence of a conformational change in calmodulin as Ca^{2+} ions were added to the protein.

The putative calcium-induced conformational changes observed in section 5.3.3 suggest that FT-ICR, with its superior resolution compared to other mass spectrometry techniques, can be used for the simple analysis of conformational changes induced by metal ions. This straightforward experiment provides complimentary and supporting evidence for the sequential binding of Ca^{2+} ions to calmodulin as postulated by Haiech *et al* [25]and Klotz *et al*[26].

Solution phase H/D exchange with longer reaction times (cf. gas phase H/D exchange) suggests a conformational change in calmodulin on binding Ca^{2+} ions. In these particular experiments it was limited to the observation of a change in the conformation on binding the fourth and final calcium ion. These experiments differ from those conducted in the gas phase in that no change in the conformation of holo-calmodulin was detected. As discussed this may be due to the short reaction delays as compared to the solution phase experiments cf. a maximum of 60 seconds with hours in the solution phase experiments.

Most interesting of all was the conclusion that exchange levels dropped in the gas phase as the charge on the molecule ion increased. This agreed with results provided by McLafferty *et al* on gas phase H/D exchange of cytochrome C. Both results seem to contradict ion mobility measurements that show an increase in protein cross section as charge increases. As has been discussed in section 5.3.1 there could be a variety of explanations for the fact that the exchange levels drop regardless of the increase in the number of exchangeable protons (from the charge itself) with increasing charge, however, the fact that a more diffuse conformer shows less exchange is not so easy to explain. It is possible that intra-molecular bonds such as hydrogen bonds, dipole-dipole and dipole-induced dipole interactions (that result from the high polarity of the functional groups of which the exchangeable hydrogens are a part) may screen potential exchange sites and that this may cause the apparent drop in exchange even as the cross-section increases. Obviously there is an apparent conflict here that is difficult to explain. Campbell *et al* [6] concluded, after studies involving glycine oligomers that "H/D exchange processes involving even simple model peptides are highly complex processes. As a result, any temptation to assign gas-phase structures of biological molecules from H/D exchange results must be approached with caution." The results presented here show that although this type of experiment gives general information on a proteins conformation, there are hidden complexities that at the present time are difficult to explain. A more detailed understanding of the mechanism of gas-phase H/D exchange is needed before unequivocal interpretation of results in terms of conformational changes of proteins is possible.

References

[1] D. L. Smith, Y. Deng, Z. Zhang, *J. Mass Spectrom. 32* (1997) .

[2] V. Katta, B. T. Chait, *Rapid Commun. Mass Spectrom. 5* (1991) 214.

[3] F. Wang, X. J. Tang, *Biochemistry 35* (1996) 4069.

[4] Z. Q. Zhang, D. L. Smith, *Protein Sci. 2* (1993) 522.

[5] Y. Liu, D. L. Smith, *J. Am. Soc. Mass Spectrom. 5* (1994) 19.

[6] S. Campbell, M. T. Rodgers, E. M. Marzluff, J. L. Beauchamp, *J. Am. Chem. Soc. 117* (1995) 12840.

[7] D. Suckau, Y. Shi, S. C. Beu, M. W. Senko, J. P. Quinn, F. M. Wampler, F. W. McLafferty, *Proc. Natl. Acad. Sci. USA. 90* (1993) 790.

[8] T. D. Wood, R. A. Chorush, F. M. Wampler, D. P. Little, P. B. O'Connor, F. W. McLafferty, *Proc. Natl. Acad. Sci. USA. 92* (1995) 2451.

[9] F. W. McLafferty, Z. Guan, U. Haupts, T. D. Wood, N. L. Kelleher, *J. Am. Chem. Soc. 120* (1998) 4732.

[10] E. H. Gur, L. J. Dekoning, N. M. M. Nibbering, *J. Am. Chem. Soc. 6* (1995) 466.

[11] E. Gard, M. K. Green, J. Bregar, C. G. Lebrilla, *J. Am. Soc. Mass Spectrom. 5* (1994) 623.

[12] P. D. Schnier, D. S. Gross, E. R. Williams, *J. Am. Soc. Mass Spectrom. 6* (1995) 1086.

[13] K. B. Shelimov, D. E. Clemmer, R. R. Hudgins, M. F. Jarrold, *J. Am. Chem. Soc. 119* (1997) 2240.

[14] S. J. Valentine, D. E. Clemmer, *J. Am. Chem. Soc. 119* (1997) 3558.

[15] D. E. Clemmer, R. R. Hudgins, M. F. Jarrold, *J. Am. Chem. Soc. 117* (1995) 10141.

[16] R. R. Hudgins, J. Woenckhaus, M. F. Jarrold, *Int. J. Mass Spectrom. Ion Proc. 165/166* (1997) 497.

[17] T. R. Covey, D. J. Douglas, *J. Am. Soc. Mass Spectrom. 4* (1193) 616.

[18] B. A. Collings, D. J. Douglas, *J. Am. Chem. Soc. 118* (1996) 4488.

[19] K. A. Cox, R. K. Julian, R. G. Cooks, R. E. Kaiser, *J. Am. Soc. Mass Spectrom. 5* (1994) 127.

[20] P. A. Sullivan, J. Axelsson, S. Altmann, A. P. Quist, B. U. R. Sunqvist, C. T. Reimann, *J. Am. Soc. Mass Spectrom. 7* (1996) 329.

[21] S. J. Valentine, A. E. Counterman, D. E. Clemmer, *J. Am. Soc. Mass Spectrom. 8* (1997) 954.

[22] O. Nemirovskiy, D. E. Giblin, M. L. Gross, *J. Am. Soc. Mass Spectrom. 10* (1990) 711.

[23] T. D. Veenstra, A. J. Tomlinson, L. Benson, R. Kumar, S. Naylor, *J. Am. Soc. Mass. Spectrom. 9* (1998) 580.

[24] P. Hu, Q. Z. Ye, J. A. Loo, *Anal. Chem. 66* (1994) 4190.

[25] J. Haiech, C. B. Klee, J. Demailee, *Biochemistry 20* (1981) 3890.

[26] I. M. Klotz, *Q. Rev. Biophys 18* (1985) 227.

6.0 Conclusion

It has been shown that the combination of electrospray ionisation with Fourier transform ion cyclotron resonance mass spectrometry facilitates the acquisition quickly and easily of accurate information on the primary, secondary and even tertiary structure of biological molecules. Each chapter has involved a separate examination of some part of a proteins structure or function, from the most elementary results involving charge state distribution which provides information on the proteins general conformation to examination in more detail of the same feature using gas phase hydrogen/ deuterium exchange. In all cases the superior resolution and sensitivity of FT-ICR mass spectrometry has proved beyond doubt its exceptional utility for these types of studies.

The superior resolution has been of specific use in the analysis of metal ion and peptide binding to target proteins such as papain and calmodulin. Resolution greater than 70,000 FWHM in broad mass-range spectra was obtainable in most cases presented here . This allowed the unequivocal assignment of each individual metal ion peak present in spectra of calmodulin and also provided evidence that for every calcium ion binding to calmodulin there was a concurrent loss of two hydrogen ions. This was proven simply by the difference between the accurate mass of calmodulin alone compared to calcium loaded calmodulin, the increase in mass was 38.064 instead of the expected 40.08, a difference of two hydrogens.

At the same time the consequences of ligand binding (in this case RS20) to calmodulin was evaluated, with the effect of the complex formation on calcium uptake monitored by simply varying the ratios of calmodulin to both the calcium ion and the ligand. The superior resolution and accuracy of FT-ICR allowed the assignment of the numerous peaks present in each of the spectra, something that would be unachievable on an instrument with lower resolution. (see section 4.3.3). From these spectra it was possible to confirm

the binding of RS20 to calmodulin in the presence and absence of calcium, (the first mass spectrometric evidence of apo-calmodulin binding a peptide (section 4.3.3.1, Figure18). It was also confirmed that calcium loaded calmodulin favours a 1:1:4 calmodulin: RS20: calcium stoichiometry and demonstrates a greater affinity for calcium in the presence of the peptide. From the same spectra it is possible that there is a conformational change on addition of calcium ions to the analyte solution evidenced by the shift in the charge state distribution in the ESI mass spectra. This change would be from a more open structure (high charge states) to a more compact structure (low charge states), see Figures 18, 21 and 22, chapter 4. At the same time it can be seen that after the four primary binding sites are filled the auxiliary sites present in calmodulin are gradually filled, deduced from the sudden appearance of species such as $[C+P+6Ca]^{7+}$ in the spectra (section 4.3.3.2, Figures 21 and 22).

The addition of Mg^{2+} ions to the analyte solution and their effect on calmodulin could also be evaluated with the result that RS20 did in fact bind to the protein when doped with magnesium ions but with a different ratio, typically of the order 1:1:1 or 1:1:2 calmodulin: RS20: magnesium (section 4.3.3.3, Figure 23).

Similar results were achieved for the cysteine protease papain and its peptide inhibitors. In these cases the expected non-covalent bond between protein and inhibitor was seen to be retained in the gas phase, and the resolution and accuracy of the FT-ICR technique along with the ability to easily implement simple capillary-skimmer collision induced dissociation, allowed the evaluation of the relative binding strengths of the different inhibitors (section 4.2.2). With the conclusion that the tri-peptide KAA binds more strongly to the active site than the tetra-peptide GGYR. Complimentary studies using circular dichroism supported confirmed these conclusions.

As to the conformational studies of calmodulin, FT-ICR mass spectrometry again provided more detailed information than other mass spectrometry techniques, especially where the calcium ion concentration in the analyte solution was varied to provide information on the proposed sequence of calcium binding and thus the activation mechanism of calmodulin by Ca^{2+} ions. Due to the high resolution obtainable, the splitting of the individual charge state distributions was monitored at various Ca^{2+} and Mg^{2+} ion concentrations. This provided valuable evidence for the sequential binding of four Ca^{2+} ions to calmodulin. A complex of the form [Cam+4Ca^{2+}] predominates, in agreement with calcium activated calmodulin and the sequential mechanism of Haiech *et al* [1]and Klotz *et al.* [2], with [Cam+Ca^{2+}], [Cam+2Ca^{2+}] and [Cam+3Ca^{2+}] molecule ion peaks being transitory. Mg^{2+} ions on the other hand, showed no significant change in the distribution of the adducts in each charge state at either high or low concentrations. A comparison of Figures 11 and 12 (section 5.3.3) show that the adduct distribution in each of the charge states for the $MgCl_2$ doped analyte solutions showed unchanged "bell" shaped distributions compared to the splitting observed in the lower charge states (corresponding to the natural conformation of calmodulin) in the $CaCl_2$ doped solutions. Thus, Ca^{2+} ions alone affect activation of calmodulin as postulated by Haiech *et al* [1]and Klotz *et al.* [2]

Solution phase H/D experiments concerning holo-calmodulin showed a conformational change in the protein as Ca^{2+} ions were added unlike similar results obtained in the gas phase. This may be due to the short reaction delay available for calmodulin and the reagent in the gas phase compared to that available in solution and maybe the possibility that the conformational change is very small. A more discriminant reagent gas[3] such as D_2O may help in future with this investigation.

As to the observation of a drop in exchange level as the charge increased on calmodulin, a more thorough knowledge of the mechanism of H/D exchange in the gas phase is needed before a definite conclusion can be made. An increase in cross-section is expected with increasing charge, if only due to coulomb repulsion, yet the opposite is observed in these and others [4-6]experiments. Possible explanations may include intra-molecular bonds preventing otherwise exchangeable protons from reacting with the deuterating reagent or the fact that charge solvation may obscure exchangeable sites. The lack of knowledge concerning the chemistry and conformation of a protein molecule ion in the gas phase limits the interpretation of these results at the present time.

References

[1] J. Haiech, C. B. Klee, J. Demailee, *Biochemistry 20* (1981) 3890.

[2] I. M. Klotz, *Q. Rev. Biophys 18* (1985) 227.

[3] S. Campbell, M. T. Rodgers, E. M. Marzluff, J. L. Beauchamp, *J. Am. Chem. Soc. 117* (1995) 12840.

[4] D. Suckau, Y. Shi, S. C. Beu, M. W. Senko, J. P. Quinn, F. M. Wampler, F. W. McLafferty, *Proc. Natl. Acad. Sci. USA. 90* (1993) 790.

[5] T. D. Wood, R. A. Chorush, F. M. Wampler, D. P. Little, P. B. O'Connor, F. W. McLafferty, *Proc. Natl. Acad. Sci. USA. 92* (1995) 2451.

[6] F. W. McLafferty, Z. Guan, U. Haupts, T. D. Wood, N. L. Kelleher, *J. Am. Chem. Soc. 120* (1998) 4732.

PUBLICATIONS AND PRESENTATIONS

"Calmodulin-Peptide Interactions: Apocalmodulin Binding To The Myosin Light Chain Kinase Target-Site", T. J. Hill, D. Lafitte, J. I. Wallace, P. J. Derrick, *Submitted to Biochemistry.*

"Comparison Of Calcium, Magnesium And Potassium Binding To Calmodulin By Fourier Transform Ion Cyclotron Resonance Mass Spectrometry", D. Lafitte, T. J. Hill, J. I. Wallace, P. J. Derrick, *In Preparation.*

"Evaluation Of Electrospray Ionisation As A General Tool For The Analysis Of Derivatised Fullerenes", M. P. Barrow, X. Feng, J. I. Wallace, O. V. Botalina, R. Taylor, P. J. Derrick, T. Drewello, *Submitted to Analytical Chemistry.*

"Fourier Transform Ion Cyclotron Resonance Mass Spectrometry At 9.4T: Applications From The Pharmaceutical Industry", A. Organ, D. Bell, D. Tolson, J. I. Wallace, A. J. R. Heck, P. J. Derrick, 45th ASMS Conference on Mass Spectrometry and Allied Topics, 1997.

"Non-Covalent Interactions Of Papain And Its Tetra-Peptide Inhibitor GGYR: Comparison Of FT-ICR And Orthogonal TOF Instrumentation", J. I. Wallace, A. J. Organ, D. Bell, P. J. Derrick, 46th ASMS Conference on Mass Spectrometry and Allied Topics, 1998.

"Calmodulin-Peptide Interactions In The Presence And Absence Of Metal Ions: An FT-ICR MS Approach", T. J. Hill, D. Lafitte, J. I. Wallace, P. J. Derrick, 47th ASMS Conference on Mass Spectrometry and Allied Topics, 1999.

"An Investigation of the snake venom Naja Naja Atra by FT-ICR MS", J. I. Wallace, A. J. Organ, D. Bell, P. J. Derrick, British Mass Spectrometry Society 22nd Annual Meeting, 1996.

"An Investigation Of Biological Molecules By Electrospray Ionisation Fourier Transform Ion Cyclotron Resonance Mass Spectrometry", J. I. Wallace, British Mass Spectrometry Society 23rd Annual Meeting, 1998.

"A Study Into The Deependence Of Mass-Bias Effects On Experimental Conditions In The Electrospray Ionisation Fourier Transform Ion Cyclotron Resonance Mass Spectrometry Analysis Of Polymers", M. Woodward, X. Feng, H. J. Cooper, J. I. Wallace, M. Salisbury, P. J. Derrick, British Mass Spectrometry Society 23rd Annual Meeting, 1998.

"Evaluation Of Electrospray Ionisation As A General Tool For The Analysis Of Derivatised Fullerenes", M. P. Barrow, X. Feng, J. I. Wallace, O. V. Botalina, R. Taylor, P. J. Derrick, T. Drewello, British Mass Spectrometry Society 23rd Annual Meeting, 1998.